

Bridging the Gap – Brainstem Evoked Potential Measurements in Patients with Active Middle Ear Implants

DISSERTATION

zur Erlangung des Doktorgrades der Naturwissenschaften
(Dr. rer. nat.)

der

**Naturwissenschaftlichen Fakultät II
Chemie, Physik und Mathematik**

**der Martin-Luther-Universität
Halle-Wittenberg**

vorgelegt von

**Frau Laura Fröhlich, M. Sc.
geboren am 09.12.1991 in Soest**

Erstgutachter: apl. Prof. Dr. rer. nat. Detlef Reichert
Zweitgutachter: apl. Prof. Dr. rer. nat. Torsten Rahne
Drittgutachter: Prof. Dr.-Ing. Dr. rer. med. Ulrich Hoppe

Tag der öffentlichen Verteidigung: 11.12.2020

Abstract

Active middle ear implants are auditory protheses which are used for hearing rehabilitation in patients who cannot be treated with conventional hearing aids. The Vibrant Soundbridge (VSB) middle ear implant transfers sound to the inner ear as vibrational energy by means of a miniature Floating Mass Transducer (FMT) which is coupled to the ossicles in the middle ear or the round or oval window membrane. The rate of the FMT's vibrational energy dissipation determines the energy transfer to the inner ear. Loss of energy due to insufficient coupling leads to unsatisfactory audiological results with the VSB and therefore to revision surgeries in some cases. Coupling dissipation can be measured psychoacoustically by determining the patients' hearing thresholds during stimulation via the implant and comparing those to the patient's bone conduction hearing thresholds. A feasible method for the objective determination of the coupling dissipation is not yet available but would be highly desirably for intraoperative quality control. To date, the surgeon can only rely on tactile feedback during positioning of the transducer. A few studies have shown that recording of auditory evoked potentials to stimulation by the implant is possible using custom-made experimental set-ups for stimulus transmission but the set-ups lack sufficient calibration. This thesis aimed to develop a feasible method for the objective quantification of FMT coupling dissipation. The problem was approached by two different methods which were evaluated in clinical studies and technical investigations of the set-ups with respect to their input-output functions, signal transmission characteristics, artifacts by electrical crosstalk and other limitations.

The first method was based on the recording of auditory steady-state responses using the recent Samba audio processor programmed to maximum amplification and a MiniTek wireless streamer for signal transmission. The set-up has been shown to be feasible for integrity control, since the method was applicable in all 15 included patients of the clinical study, but not for quantification of coupling dissipation. No significant correlation between the objective thresholds measured in the set-up and the coupling dissipation could be observed except at 4000 Hz. Calibration of the set-up was not possible. Inherent noise of the audio processor which could potentially mask hearing thresholds and limited transmission distance of the wireless streamer were identified as the main technical limitations.

An objective determination of coupling dissipation was possible with the second method by recording VSB evoked auditory brainstem responses using an AP404 audio processor with an insert earphone sound tube attached to its single microphone aperture. Clinical results were collected from intraoperative measurements in a multicenter study including 23 patients with different coupling modalities and at different implant centers. Technical investigations showed that 500 Hz had to be excluded from the analysis due to drawbacks in signal transmission with frequency-specific delay times as well as frequency-dependent output of the set-up. Nevertheless, the method has the potential to quantify the FMT coupling dissipation in patients treated with a VSB. It can help the surgeon in finding the optimal coupling of the transducer and therefore improve quality control in VSB surgery.

Acknowledgements

I can say without doubt that the completion of this thesis would not have been possible without the help and encouragement I have had from my supervisors, colleagues, friends, and family.

In the first place, I would like to express my gratitude to my supervisor Torsten Rahne for continuous support throughout my time as a PhD student. I thank you for your patience, your clear and honest opinions and productive discussions. Your office door was always open whenever I had a question about writing or my research. You allowed me to pursue my ideas freely, guiding me in the right direction whenever it was necessary. With a good sense of humor and determination we have solved many problems during our talks over lunch or coffee.

My sincere thanks also goes to my supervisor Detlef Reichert. You let me develop my own ideas and always helped me whenever I ran into a trouble spot. You were always ready to discuss problems. I have felt supported and encouraged to widen my research from various perspectives. I appreciate our uncomplicated and enriching cooperation and hope to continue this in the future.

Alexander Müller, Oliver Dziemba, Tobias Oberhoffner, Sebastian Hoth, Maria Gadyuchko, thank you for the outstanding collaboration in the multicenter study. My thanks also goes to MED-EL and Hamidreza Mojallal for providing hardware for the clinical studies and organizing study meetings. I would also like to thank Jacob Sahlmann for help with data recording and the research workshop of the Martin Luther University Medical Faculty for support with the design of the experimental implant. In this place, I also want to say thank you to all patients who participated in the clinical studies.

I would like to continue with the interdisciplinary team at the Department of the Department of Otorhinolaryngology, Head and Neck Surgery. I cannot name every single person but I would like to thank everyone for support with my studies. Luise Wagner, you have always helped me with your expertise in the field and made valuable comments. Claudia Hahn, your support as study nurse was a great benefit.

Interdisciplinary collaborations and discussions did always make valuable contributions to my work. I would like to thank the Biomedical Signals and Systems group of the Chalmers University Gothenburg, Sabine Reinfeldt, Bo Håkansson, and Karl-Johan Fredén Jansson, and the Vestibular Research Laboratory at the University of Sydney, Ian Curthoys and Ann Burgess, for support during my PhD.

Technical guidance is essential but I would not have been able to get this far and complete this thesis without the constant support of my family. Mama, Papa, you provided me the opportunity to study and supported me throughout my entire life and education. This accomplishment would not have been possible without you and I am incredibly grateful to have you as my parents. Frank, I am lucky to have you by my side. I would not have

achieved this without your support and continuous encouragement. This was very precious to me and I cannot say how grateful I am. Also, I want to thank my parents in law, Heidi and Ernst, thank you for supporting me where you could.

Finally, I would like to thank Stefan Plontke, Professor and Chairman of the Department of Otorhinolaryngology, Head and Neck Surgery at the University Hospital Halle. I thank you for sharing your immense knowledge in the field, your contribution to this work in particular, your input regarding medical questions, and for critical comments pointing me at different perspectives. This work has been enriched by this interdisciplinary collaboration. Your enthusiasm about research in the field is outstanding and inspired me along the way.

Contents

Abstract	i
Acknowledgements	iii
List of Abbreviations	1
Part 1. Introduction	3
Chapter 1. Basic Principles of Audiology	5
1.1. Physics of Sound	5
1.2. The Auditory System	5
1.3. Hearing Disorders	7
Chapter 2. Diagnostics	9
2.1. Basic Audiometric Principles and Calibration	9
2.2. Psychoacoustics	10
2.3. Auditory Evoked Potentials	11
Chapter 3. The Vibrant Soundbridge Active Middle Ear Implant	15
3.1. Design and Function	15
3.2. Vibroplasty and Couplers	16
3.3. Vibroplasty In Situ Thresholds and Coupling Dissipation	17
3.4. Audio Processors and Fitting Procedure	19
Chapter 4. Current State of Research and Aim of this Thesis	23
4.1. Objective Measures of the Floating Mass Transducer Coupling Dissipation ..	23
4.2. Technical Aspects	25
4.3. Thesis Outline	25
Part 2. Objective Assessment of the Floating Mass Transducer Coupling Dissipation by Recording Auditory Steady-State Responses	27
Chapter 5. Background Information	29
Chapter 6. Materials and Methods	31
6.1. Experimental Set-Up	31
6.2. Participants	32
6.3. Procedures	32
6.4. Data Analyses	33
Chapter 7. Results	35
Chapter 8. Discussion	39
Chapter 9. Conclusions	41

Part 3. Intraoperative Recording of Auditory Brainstem Responses for Determination of Floating Mass Transducer Coupling Dissipation	43
Chapter 10. Background.....	45
Chapter 11. Materials and Methods	47
11.1. Experimental Set-Up	47
11.2. Participants	48
11.3. Procedures	48
11.4. Data Analyses.....	49
Chapter 12. Results	51
Chapter 13. Discussion	57
Chapter 14. Conclusions.....	61
Part 4. Technical Investigation of Active Middle Ear Implant Evoked Auditory Potential Recording	63
Chapter 15. Background.....	65
Chapter 16. Technical Principles of Auditory Steady-State Response Recording Using a Samba Hi Audio Processor and a MiniTek.....	67
16.1. Materials and Methods	67
16.2. Results	68
16.3. Discussion.....	73
16.4. Conclusions	74
Chapter 17. Technical Principles of Auditory Brainstem Response Recordings Using an AP404 Audio Processor with a Sound Tube.....	75
17.1. Materials and Methods	75
17.2. Results	77
17.3. Discussion.....	81
17.4. Conclusions	83
Chapter 18. Investigating the Technical Principles of the Vibrogram	85
18.1. Materials and Methods	85
18.2. Results	86
18.3. Discussion.....	89
18.4. Conclusions	91
Part 5. Discussing the Objective Measurement of the Floating Mass Transducer Coupling Dissipation	93
Part 6. Thesis Conclusions	97
List of Tables	101
List of Figures.....	103
Bibliography	105

List of Abbreviations

SPL: sound pressure level
HL: hearing level
RETSPL: reference equivalent threshold sound pressure level
AC: air conduction
VFL: vibratory force level
RETVFL: reference equivalent threshold vibratory force level
BC: bone conduction
peRETSPL: peak-to-peak reference equivalent threshold sound pressure level
peRETVFL: peak-to-peak reference equivalent threshold vibratory force level
AEP: auditory evoked potential
EEG: electroencephalography
ABR: auditory brainstem response
BERA: brainstem electric response audiometry
CAP: compound action potential
ECochG: electrocochleography
ASSR: auditory steady-state response
AMEI: active middle ear implant
VSF: Vibrant Soundbridge
FMT: Floating Mass Transducer
VORP: vibrating ossicular prosthesis
PORP: partial ossicular replacement prosthesis
TORP: total ossicular replacement prosthesis
LP: long process (ossicular)
SP: short process (ossicular)
RW: round window
OW: oval window
VIB: vibrogram
PTA: pure tone average
DSL I/O: desired sensation level input/output formula
NAL-NL: National Acoustic Laboratories' nonlinear fitting procedure
MPO: maximum power output
VSF-ASSR: Vibrant Soundbridge evoked auditory steady-state response
VSF-ABR: Vibrant Soundbridge evoked auditory brainstem response
VL: voltage level

Part 1

Introduction

CHAPTER 1

Basic Principles of Audiology

1.1. Physics of Sound

Hearing or audition describes the reception of sound by the peripheral auditory system and its perception by the central auditory nervous system. Sound itself is a vibration which propagates through a medium as a mechanical wave of displacement and pressure. Mathematically, this process is described by the solutions of a differential equation, i. e., the wave equation. The disturbances of the medium's parameters propagate in all spatial directions at a fixed speed. In fluids and gases, sound waves travel as longitudinal waves, whereas in solids they are transmitted as both longitudinal and transverse waves (Veit, 1988). The speed of a sound wave c , i. e., the wave's phase velocity, depends on the medium, and is approximately 335 m/s in air and approximately 1000 m/s in bone. However, this measure must not be confounded with the particle velocity ν . The relation between sound pressure p and particle velocity is referred to as the acoustic impedance Z :

$$Z = \frac{p}{\nu}. \quad (1)$$

The acoustic impedance is a measure of the opposition which the medium presents to the acoustic pressure and therefore determines the ratio of the wave's reflected and transmitted amplitude at a boundary surface between two different media. The bigger the difference between the media's acoustic impedances, the higher is the reflected amplitude.

The physical properties to characterize the sound waves are their amplitude, wavelength, and frequency. The frequencies perceptible to humans vary from 16 Hz to 20 kHz (Oliver and Fakler, 2008) and determine the perceived pitch of a sound. However, the loudness of a sound is characterized by the wave's amplitude which is also referred to as the sound pressure. The sound pressure humans can detect ranges from 20 μ Pa close to the hearing threshold to 50 kPa for very loud sounds (Ulrich and Hoffmann, 2011). Due to this wide range of amplitudes the root mean square sound pressure of the sound wave p is usually expressed as the sound pressure level (SPL) L in decibels:

$$L_{\text{dB SPL}} = 20 \cdot \log\left(\frac{p}{p_0}\right) \text{dB SPL}. \quad (2)$$

To logarithmize the sound level the sound pressure p is normed and thus made dimensionless by the reference sound pressure $p_0 = 20 \mu\text{Pa}$ (Bille and Schlegel, 1999) which is approximately the human hearing threshold of a sinusoidal sound at 1000 Hz.

1.2. The Auditory System

The process of hearing is very complex and relies on numerous anatomical structures and physiological processes. The first step is the reception of the mechanical sound waves described in the previous section. The vibrations are detected by the peripheral part of the auditory system and are then perceived by higher centers in the brain in the second step. This is referred to as the central part of the auditory system.

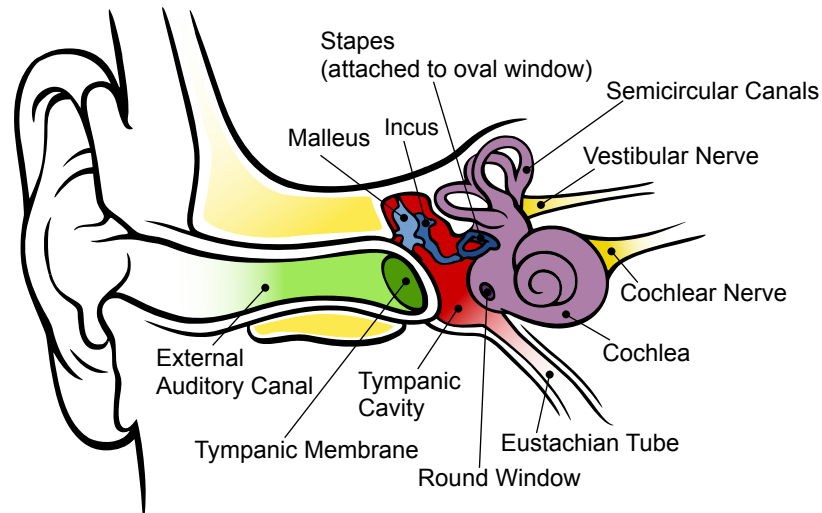


FIGURE 1.1. The image gives an overview of the peripheral auditory system with the outer ear, middle ear, and inner ear.

Source: Chittka and Brockmann (2009), CC BY 2.5, modified

The peripheral system consists of the outer ear, the middle ear, and the inner ear. A simplified diagram of the anatomy is shown in Figure 1.1. When sound hits the outer ear, the sound waves are focused by the pinna acting as a funnel and are then lead through the ear canal to the tympanic membrane. The membrane marks the entrance to the middle ear. As it vibrates according to the air-pressure variations of the incoming sound wave, the signal is transmitted to a chain of ossicles in the middle ear. The first ossicle which is directly connected to the tympanic membrane is the malleus. The malleus transmits the vibrational energy further to the incus which in turn transmits it to the third ossicle of the chain, the stapes. The stapes footplate fits within the so called oval window which is the entrance window to the inner ear, i. e., the cochlea, which is filled with fluids. This transmission of vibrational energy of the air to motion of the cochlear fluids is the most important function of the middle ear. By the interaction of the ossicular chain with the tympanic membrane and the oval window membrane the low impedance of the air is matched to the high impedance of the inner ear fluids (Hall, 2013). Otherwise, about 98 % of the sound wave's energy would be reflected. This way of sound wave transmission from the outer ear through the ear canal and the middle ear is referred to as air conduction (AC) hearing. However, the cochlear can also be stimulated directly by vibrations of the skull which bypass the outer and middle ear. This way of transmitting sound energy to fluid vibrations is called bone conduction (BC) hearing. More details about the physiological, clinical and technical aspects of BC hearing are given in Stenfelt and Goode (2005) and Stenfelt (2011). Once the sound wave's energy is transmitted to the cochlea by either AC or BC the mechanical energy is finally converted into neuronal information based on action potentials. Longitudinally, the cochlear is divided into three sections filled with fluids of different ionic concentrations by the so called Reissner's membrane and the basilar membrane: the scala tympani filled with perilymph, the scala media, filled with endolymph, and the scala vestibuli also filled with perilymph. On the basilar membrane the organ of Corti is located. It contains the functional elements of the inner ear, the hair cells. As the sound waves enter the cochlea, the motion of the cochlear fluids cause the basilar membrane to vibrate

so that the hair cells in the organ of Corti are activated and emit a neurotransmitter which is converted into electrical signals by the afferent neurons innervating the hair cells. The mechanical properties of the basilar membrane change from its base to the apical end so that the amplitude of a traveling wave varies as it moves along the membrane depending on the frequency of the stimulus (Békèsy, 1960). This is called the tonotopy of the basilar membrane. The amplitude is high at the base for high frequencies, while the characteristic place of resonance for the low frequencies is located at the apex.

The processing of the electric signals produced in the neurons innervating the hair cells is done in the central auditory system. The neurons form pathways of nerve fibers which travel from one brain region to the next one. The neurons are grouped in certain centers in the brain which are referred to as nuclei (Hall, 2013). The structures are duplicated on both sides of the brain and nerve fibers crossing from one side to the other allow for communication of the information of both sides. The afferent part of the auditory pathway is shown in Figure 2.1. The neuronal processing begins in the brainstem where the cochlear nucleus is the first site. The pathway continues over the olivary complex and the lateral lemniscus as well as the inferior colliculi (Klinke, 2010). The medial geniculate nucleus is then part of the thalamus. The signals are further processed in the primary auditory cortex as the first region of cerebral cortex to receive auditory input. Each of these centers in the auditory pathway contributes to convert the electrical signals into more and more complex signals in time, frequency and intensity. More detailed information about the neuronal structure and specific functions can be found in Oliver and Fakler (2008) and Klinke (2010).

1.3. Hearing Disorders

As it can be seen from the previous section, the process of hearing and the involved anatomical structures and physiological processes are very complex. Thus, complications in the auditory system leading to hearing disorders can be manifold. Hearing disorders can be classified by their source of origin, i. e., by the location in the auditory system at which the problem occurs. Basically, the different types of hearing disorders are referred to as conductive, sensory, neural or central disorders, depending on the malfunction being located in the outer and/or middle ear, the cochlea, the auditory nerve, or the auditory cortex (Hoth, 1999). An impairment of the outer and/or middle ear leads to an impaired sound conduction and is therefore referred to as a conductive hearing loss. This type of hearing disorder is never associated with complete deafness though, as the inner ear is still functioning so that hearing by BC is still possible. However, the ability to perceive sound is limited, if a malfunction of more central structures occurs. If the cochlea or inner ear itself is affected, the disorder is categorized as an endocochlear or sensory hearing loss. If the auditory nerve is affected, the disorder is referred to as a retrocochlear or neural disorder. The term which describes both these types is sensorineural hearing loss. It can be ranked from slight hearing loss to profound hearing loss or totally deaf. Furthermore, the hearing loss can be temporary or permanent, sudden or progressive and can exist in only one ear (unilateral) or in both ears (bilateral). A combined sensorineural and conductive hearing loss is referred to as mixed hearing loss. The most common form of treatment of sensorineural hearing loss is by hearing aids of which different types exist. Mixed hearing loss, however, is difficult to treat by conventional hearing aids, because the conductive component has to be overcome in addition to the sensorineural component in terms of amplification provided by the device. One special kind of implantable hearing aid which is suitable for the treatment of mixed hearing loss and which is subject to this work is

introduced in Chapter 3. If the amplification which can be reached by hearing aid is no longer sufficient, the cochlear implant is one of the last options to rehabilitate hearing as long as the auditory nerve is still intact. If this is not the case, the only chance to receive acoustic input is by an auditory brainstem implant. If the disorder affects even higher centers in the brain, the processing of auditory input is limited. This is referred to as a central hearing disorder.

CHAPTER 2

Diagnostics

2.1. Basic Audiometric Principles and Calibration

Audiometric test methods are applied to test a person's hearing for certain disorders and to identify the disorder's location with respect to the involved anatomical structures (Hoth, 1999). The results are therefore important for hearing diagnoses and have a great impact on treatment decisions.

One of the most common methods is to measure a person's hearing threshold for different test frequencies. There is a variety of different stimuli which can be used for audiometric testing. The stimuli are generated by an audiometer which feeds alternating currents to headphones for AC testing and to BC transducers for BC testing. Loudspeakers are used for sound field testing, as for example to test a person's hearing with hearing aids.

While the human ear can detect a wide range of sound wave amplitudes, the spectral response is not flat. The softest sound that a person can hear is dependent on the frequency: for the low and very high frequencies, higher sound pressure levels are necessary to attain an auditory sensation as compared to frequencies around 1000 Hz (Lehnhardt and Laszig, 2001). Thus, the graph representing the threshold of normal hearing is curved in terms of dB SPL. For easier interpretation of the results, the thresholds are displayed in terms of dB HL (hearing level, HL). This is done by using correction factors for the softest sound detectable by humans at the specific frequencies. The correction factors are referred to as reference equivalent threshold sound pressure levels (RETSPL) (ISO 389-1:2017). These correspond to the reference point of 0 dB HL as audiometric zero (Hall, 2013) so that a level in dB HL for AC is obtained by subtracting the RETSPL values $L_{\text{dB SPL}}^0$ from the sound pressure levels $L_{\text{dB SPL}}$:

$$L_{\text{dB HL}_{\text{AC}}} = L_{\text{dB SPL}} - L_{\text{dB SPL}}^0. \quad (3)$$

This is similar for BC. However, it has to be considered in this case that the output magnitude is not a sound pressure level but rather a vibratory force level (VFL). As for AC (see Equation (9)), the force level is given in decibels according to the following equation:

$$L_{\text{dB VFL}} = 20 \cdot \log\left(\frac{F}{F_0}\right) \text{dB VFL}. \quad (4)$$

The reference force F_0 is defined to be $1 \mu\text{N}$. The threshold of normal hearing by BC is curved in terms of dB VFL so that correction factors have to be applied in order to obtain hearing levels in dB HL, respectively. These reference equivalent threshold vibratory force levels (RETVFL) $L_{\text{dB OFL}}^0$ (ISO 389-3:2016) are subtracted from the output force levels $L_{\text{dB OFL}}$ to obtain the levels for BC in dB HL:

$$L_{\text{dB HL}_{\text{BC}}} = L_{\text{dB VFL}} - L_{\text{dB VFL}}^0. \quad (5)$$

This approach to indicate hearing thresholds in terms of hearing levels (dB HL) by means of reference equivalent threshold levels for AC and BC hearing is a basis for audiometric

testing. However, the approach is only valid for sinusoidal tones, which are usually used in pure tone audiometry (see Section 2.2). Other audiometric tests require the use of other test signals such as clicks, tone pips, tone bursts or chirps. These are signals of short duration which have very different waveforms and spectra compared to a sine wave. Thus, the physical expression of the magnitude of short duration acoustical signals cannot be sound pressure level (dB SPL) or vibratory force level (dB VFL) as for continuous sinusoidal signals (Jenderka and Fedtke, 2007). Therefore, detailed specifications on the calibration of audiometric test signals of short duration are stated in IEC 60645-3:2007. The standard recommends that the magnitude of these signals should be expressed as peak-to-peak equivalent sound pressure level (dB peSPL) or peak-to-peak equivalent vibratory force level (dB peVFL), respectively. This is the (root mean square) value of the sound pressure or vibratory force level of a long duration sinusoidal signal with the same peak-to-peak sound pressure or vibratory force level as the short duration signal. This provides an objective measure of the stimulus intensity but does not relate to the perceived loudness of a short duration signal which is very different from the subjective loudness which would be perceived of the equivalent stimulus, if it were continuous. To overcome this issue, reference zeros, i. e., peRETSPL and peRETVFL values, were obtained for clicks and certain tone burst stimuli in the same manner as for the sinusoidal signals. The references can be used to transform the levels into hearing levels as described above for AC and BC hearing. The levels are then referred to as normal hearing levels and are indicated in dB nHL. Therefore, there is a direct similarity between the indicated stimulus intensity for short signals in dB nHL and the stimulus intensity of long duration signals in dB HL. The peRETSPL and peRETVFL values for clicks and tone bursts were obtained from studies conducted by Richter and Fedtke (2005) and Fedtke and Richter (2007) and are now specified in ISO 389-6:2007. Other commonly used stimuli are chirp signals of the CE-Chirp stimulus family. However, the reference calibration values peRETSPL and peRETVFL for these specific stimuli are not included in the standard but were obtained in two studies by Fedtke and Hensel (2008) and Gøtsche-Rasmussen et al. (2012). These results are used as references in audiometric testing. Chirp signals are designed to compensate for the cochlear traveling wave delay by delaying the higher frequencies in the stimulus relative to the lower frequencies. The CE-Chirps are available as broadband signals including frequencies between 350 Hz to 11 300 Hz as well as octave-band filtered CE-Chirps with center frequencies 500 Hz, 1000 Hz, 2000 Hz, and 4000 Hz. Detailed information on these signals can be found in Elberling et al. (2007) and Elberling and Don (2010).

2.2. Psychoacoustics

The most frequently applied diagnostic tool is the test of the hearing thresholds at different test frequencies. The thresholds are usually obtained by asking a person about the sensation triggered by an acoustic stimulus. Thus, the results are subjective and the entire auditory system including the sensory organ as well as higher centers in the brain contribute to the results (Hoth, 1999). These tests which relate the perception of sound to an actual physical magnitude, i. e., to a sound pressure or hearing level, are referred to as psychoacoustic methods which require the test persons cooperation and concentration. The relation between the human perception of sound and the physical stimulus follows a logarithmic law called the Weber-Fechner law (Alzheimer, 2008). The hearing threshold is defined as the lowest sound pressure level for AC or the lowest vibratory force level for BC at which the test person responds to hear the test tone on 50% of repeated trials (ISO 8253-1:1989). This corresponds to the turning point of the logarithmic function.

The results of audiometric tests are usually presented in audiograms which include both AC and BC hearing thresholds with the frequency in Hertz on the horizontal logarithmic scale, and a dB HL or dB nHL scale on the vertical axis. The thresholds are then plotted relative to 0 dB HL in such a way that the hearing loss in terms of dB increases downwards (see Figure 3.3 as an example).

2.3. Auditory Evoked Potentials

Besides psychoacoustic tests there are also objective methods available for diagnostics of the auditory system. One of those methods is the use of auditory evoked potentials (AEPs). AEPs are electric potentials of physiologic origin following an acoustic or electric stimulus (Hoth, 2007). The electric potentials are electrophysiologically detected by electroencephalography (EEG) using surface electrodes for signal recording. The acoustic stimuli are presented to a test person via headphones, insert earphones or BC transducers. In order to measure the response signals with a magnitude of tens of microvolts in the noise of spontaneous EEG and muscle activity, some technical aspects have to be considered. These include triggering (stimulus related potential recording), stimulus optimization, acoustic and electric shielding, differential amplification, filtering, artifact reduction, and time domain averaging. Roger and Thornton (2007) provides detailed information on the instrumentation and recording parameters of AEPs.

An attempt to categorize AEPs is by their source of origin. AEPs are generated in the cochlea and compose of many vertex positive and negative peaks usually referred to as waves. They can be further categorized by their peak response latencies which correlate with the different parts of the ascending auditory pathway (see Figure 2.1). The short-latency AEPs have latencies of less than 10 ms and are generated directly from the hair cells in the cochlea and the nuclei in the brainstem. The potentials with latencies from 10 to 50 ms are referred to as middle-latency responses and those with latencies up to 500 ms are referred to as long-latency responses (Eggermont, 2007).

2.3.1. Auditory Brainstem Responses

The short-latency responses, i. e., the auditory brainstem responses (ABRs), are the most commonly recorded AEPs. A typical ABR is illustrated in Figure 2.1. The method is referred to as brainstem electric response audiometry (BERA) accordingly and typically includes a post-stimulus interval of 1 to 12 ms. The ABR peaks are indicated by Roman numerals I to VII, while waves I, III and especially wave V are most reliably recorded. While wave III is generated by the superior olivary complex and wave V by cells in the inferior colliculus, wave I is actually not generated in the brainstem but by the auditory nerve. Thus, wave I is identical to the compound action potential (CAP) of the auditory nerve and can also be measured by placing an electrode near the auditory nerve. This is a different technique referred to as electrocochleography (ECochG). Due to small amplitudes of 100 nV to 0.5 μ V ABRs can only be measured for high synchronous activity in spatially aligned structures. This must be taken into consideration when choosing appropriate stimuli for eliciting the responses. Typical stimuli are clicks and chirps as well as narrowband chirps. Chirps have been shown to result in larger ABR amplitudes compared to clicks and therefore improve signal to noise ratio (Elberling et al., 2007; Dau et al., 2000; Bargaen, 2015). Measuring ABRs is also possible in sleeping or anesthetized subjects as they are independent of vigilance and pharmacological influence. The surface electrodes are typically placed on the left and right mastoid (reference), the hairline or

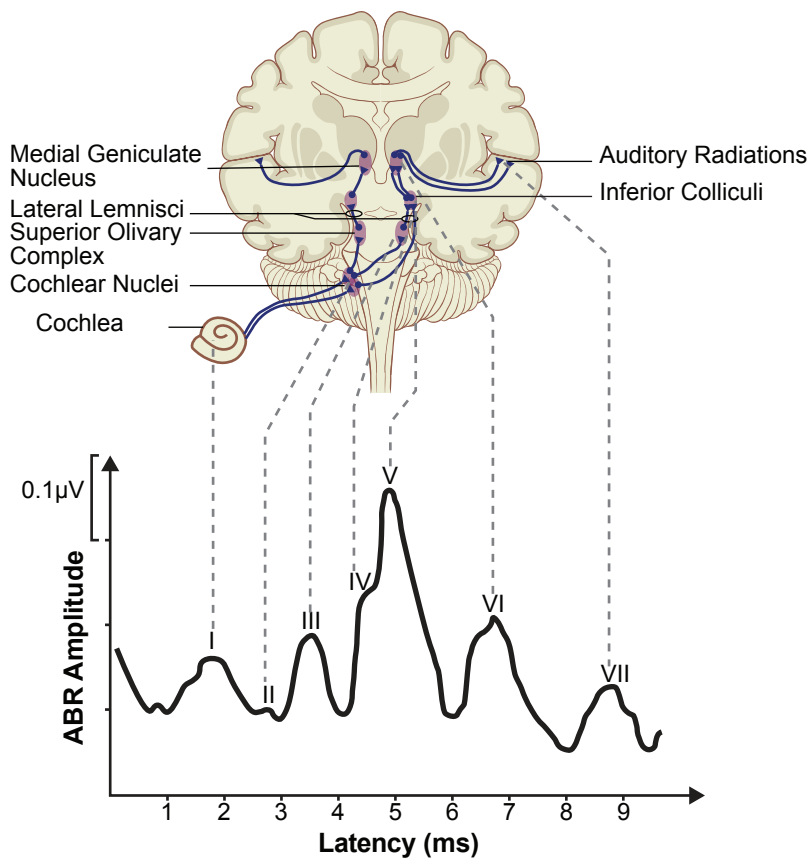


FIGURE 2.1. The upper half of the figure shows the central auditory nervous system pathway and structures. The pathways of only one side are shown. The lower half shows an ABR with waves I to VII. Dashed lines show how the processing of the electrical signals traveling along the central auditory pathway from the cochlea up to the primary auditory cortex (auditory radiations) generates peaks I to VII of the response. Waves I, III and V are most reliably recorded. Wave III is generated by the superior olivary complex, wave V by cells in the inferior colliculus, and wave I is not generated in the brainstem but by the auditory nerve.

Source: Coronal section of human brain from Lynch and Jaffe (2016), CC BY 2.5, modified

vertex (active) and approximately 1 cm below the active electrode (ground). The wave amplitudes decrease with decreasing stimulus intensities while the latencies increase due to increasing cochlear processing. Evaluation of the amplitudes and latencies allows for conclusions about hearing disorders and tumors in the cerebellopontine angle. This evaluation is based on the experience of the examiner who has to visually identify wave V and the response threshold as the stimulus intensity where wave V can just be detected before it disappears for the next lower stimulus intensity. A summary of the parameters of interest and their interpretation in a clinical context is given in Burkard (2007) and Hoth et al. (2015).

2.3.2. Auditory Steady-State Responses

ABRs are transient potentials following an acoustic stimulus. However, when the stimuli are presented at certain stimulation rates, the positive and negative peaks of the transient

responses can overlap and result in a steady-state response, i. e., a waveform which repeats at the same rate as the stimulus (Mühler, 2012). Stimulation rates of 40 Hz and 80 Hz have been shown to be most useful to elicit these auditory steady-state responses (ASSR). In adults, the ASSR is usually measured at stimulation frequencies around 40 Hz. The underlying neural generators of this response are mainly located in the primary auditory cortex, the auditory midbrain and the thalamus. In infants and young children, whose auditory cortices are not yet fully mature, the ASSR is typically measured at frequencies around 80 Hz as these responses are generated primarily by structures in the superior olivary complex, inferior colliculus, and the cochlear nucleus (Korczak et al., 2012). These generators within the auditory brainstem are not affected by age. Several types of broadband and frequency specific stimuli can be used to record the ASSR. The most common types of stimuli are sinusoidal amplitude modulated tones, frequency modulated tones, mixed modulated tones, and repeating sequence gated stimuli (e. g. tone bursts or chirps). It is possible to present multiple stimuli at different carrier frequencies simultaneously, with each stimulus presented at a slightly different modulation/stimulation frequency. With this technique, up to four carrier frequencies in one ear or eight in two ears, typically 500 Hz, 1000 Hz, 2000 Hz, and 4000 Hz, can be presented simultaneously. As the ASSR is following the modulation or presentation frequency, it is composed of discrete frequency components and peaks at the modulation frequencies are present in the EEG amplitude spectrum. Therefore, the responses are usually evaluated in the frequency domain. Usually, the EEG is recorded for several minutes and multiple subsamples of several hundred ms of EEG data are averaged together, since averaging as well as increasing the duration of the data submitted to the Fourier transform decrease the amplitude of the EEG background noise (Picton, 2007). Statistical techniques are then applied to test whether the responses are significantly different from the noise. The two primary techniques are the analysis of phase coherence values and the F test (Korczak et al., 2012). In contrast to BERA, the ASSR is therefore independent of the subjective interpretation of the data by an examiner.

The Vibrant Soundbridge Active Middle Ear Implant

3.1. Design and Function

In some cases hearing rehabilitation can be achieved by surgical treatment or by the use of conventional hearing aids which basically amplify sound to make it audible again for patients suffering from hearing loss. Conventional hearing aids are generally used for a variety of pathologies including sensorineural as well as conductive hearing loss. However, in some cases conventional hearing aids are insufficient. This applies for some patients with conductive and mixed hearing loss where the impaired sound conduction has to be compensated for by additional amplification. This goes along with technical issues such as feedback, sound distortion, and unfavorable conditions for energy transfer. But also patient related issues like recurrent infections or eczema of the auditory canal can make the use of conventional hearing aids impossible in some patients (Zwartenkot et al., 2013). Hearing rehabilitation in these cases is possible and can be advantageous for the patient compared to wearing a conventional hearing aid by the use of active middle ear implants (AMEIs) (Beutner et al., 2018). AMEIs are devices that overcome the issue of sound conduction by directly stimulating the cochlea or vibrating the ossicular chain.

The Vibrant Soundbridge¹ (VSB) is a frequently used semi-implantable AMEI (Beleites et al., 2014). It received the Economic Community (CE) trademark in 1998 (Fisch et al.,

¹MED-EL, Innsbruck, Austria

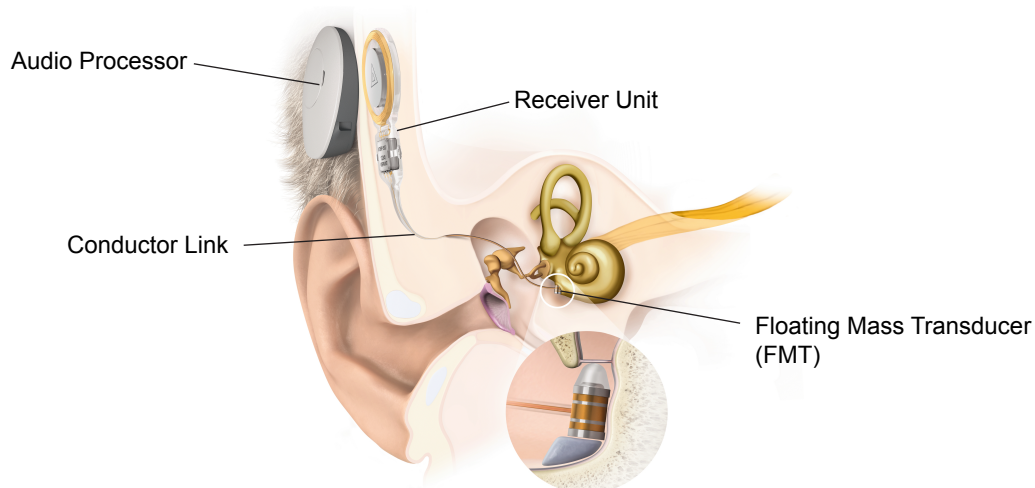


FIGURE 3.1. Schematic view of the VSB in situ, here shown for a round window vibroplasty with the FMT coupled to the round window by means of a RW-Soft-Coupler.

Source: © by MED-EL Elektromedizinische Geräte Deutschland GmbH, printed with permission, modified

2001) and has been used in Europe over the last 20 years. For the United States' market, the VSB was approved in 2000 by the Food and Drug Administration. The system consists of an external and an internal part. Figure 3.1 shows a schematic illustration of the implant in situ. An audio processor, i. e., the external part, is held directly over the implantable part by magnetic attraction. The microphones of the audio processor pick up the sound which is then converted into electrical signals and inductively transmitted to the implant's receiver unit. The signal is demodulated and relayed through a conductor link to a miniature electromagnetic driver called the floating mass transducer (FMT). The implantable part as a whole is referred to as the vibrating ossicular prosthesis (VORP), following the naming of the passive middle ear implants PORP and TORP (partial/total ossicular replacement prosthesis). The FMT consists of a magnet which is placed inside a cylindrical housing and biased by a pair of silicone springs. A pair of oppositely wound coils surrounds the housing. The FMT is only 2.3 mm in height and 1.8 mm in diameter. When the coils receive the electrical signals, varying magnetic fields are generated which interact with the magnetic field of the permanent magnet. This results in inertial vibration of the magnet causing the housing of the FMT to vibrate relative to the magnet. The dual coil floating mass transducer was first described by Geoffrey Ball, who is the inventor of the system (Ball et al., 1999). The FMT is coupled to structures in the middle ear. When airborne sound is converted into mechanical vibration of the FMT, the structures are set into motion which is then perceived by the patient. The former implant was called VORP502 and a right and left (A and B) version existed. In 2014, the new VORP503 was introduced which is now MRI compatible at 1.5 T and fits both ears, as the coupler is attached to the FMT for each patient individually and according to the indication (see following section).

3.2. Vibroplasty and Couplers

After the development of the VSB, the only option to couple the FMT to the middle ear was to crimp it onto the long process of the incus. However, the versatility of the FMT has led to a variety of surgical applications referred to as vibroplasty. For this, a different coupling methods have been developed so that the FMT can now be coupled to the long process (LP) of the incus (Fisch et al., 2001), the short process (SP) of the incus (Mlynski et al., 2015b), the stapes suprastructure, the round window (RW) membrane (Colletti et al., 2006), or the oval window (OW) (Huber et al., 2012; Mlynski et al., 2015a), i. e., the stapes footplate.

Various couplers have been designed for this purpose. The couplers are illustrated in Figure 3.2. The Incus-SP-, Incus-LP-, and Incus-Symphonix-Couplers are used for sensorineural hearing loss, whereas the RW-Soft-, Vibroplasty-CliP-, Vibroplasty-Bell-, Vibroplasty-OW-, and Vibroplasty-RW-Couplers are used for conductive or mixed hearing loss. For the Incus-LP- and the Incus-Symphonix-Coupler two different versions for the right and left ear are available. The other couplers are suitable for both right and left ears.

Since the VSB has been used, several studies have compared the audiological outcomes with those of conventional hearing aids. The results from these studies differed, most likely due to major differences in the study designs and patients cohorts. Generally, the AMEI seems to be at least as effective as an external conventional hearing aid (Butler et al., 2013) with improvement in patient satisfaction due to better sound quality, less feedback and occlusion (Snik and Cremers, 2001; Tysome et al., 2011). Looking more specifically at patients with down-sloping high frequency hearing loss, the VSB can improve speech intelligibility in quiet and especially in noise when compared to a conventional hearing aid (Todt et al., 2002; Uziel et al., 2003; Truy et al., 2008; Boeheim et al., 2010; Lee et al.,

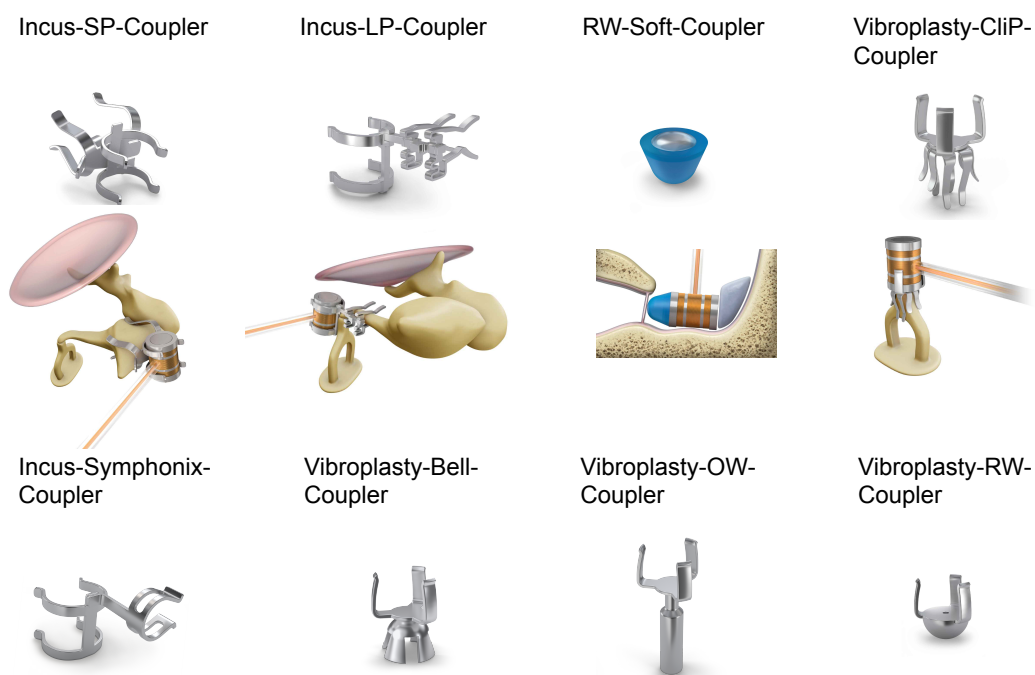


FIGURE 3.2. Schematic view of the available vibroplasty couplers (and their position in situ).

Source: © by MED-EL Elektromedizinische Geräte Deutschland GmbH, printed with permission, modified

2017). With the development of the new couplers the inclusion criteria expanded from the original sensorineural hearing loss to conductive and mixed hearing loss as well as malformations (Beltrame et al., 2009; Mlynski et al., 2010; Colletti et al., 2006; Huber et al., 2012; Rahne et al., 2020, in press). In these cases, the direct drive stimulation overcomes the patients conductive hearing loss and provides a more efficient sound transfer than can be achieved with conventional hearing aids (Rahne and Plontke, 2016; Rahne, 2019).

3.3. Vibroplasty In Situ Thresholds and Coupling Dissipation

In order for the VSB's full potential benefits in terms of direct energy transfer to the inner ear by direct drive stimulation to take effect, the FMT has to be coupled to the desired middle ear structure in a way that no mechanical vibration energy is lost. In case of optimal coupling of the FMT to the middle ear structure, the energy is transferred from the FMT to the inner ear without loss.

The effectiveness of actuator coupling to the cochlea can be measured and quantified by vibroplasty in situ thresholds which are obtained psychoacoustically while the patient is being stimulated via the implant. For this, the external audio processor is connected to a computer. The VSB fitting software Symfit within Connexx software² is used to set the audio processor to defined gain and compression parameters during the measurement. These parameters meet the calibration of the decibel scale by the vibrogram function of the manufacturer. The vibroplasty in situ thresholds are then obtained psychoacoustically as in ordinary pure tone audiometry for frequencies between 500 Hz and 6000 Hz. Due to

²Sivantos GmbH under Trademark License of Siemens AGs, Erlangen, Germany

the underlying calibration of the manufacturer the thresholds are also often referred to as vibrogram (VIB) thresholds. The thresholds measured in this procedure are comparable to HL. However, the underlying calibration procedure is not published by the manufacturer and the unit of VIB thresholds as displayed in the fitting software is dB and not dBHL or dB nHL. It is known from various studies that the vibrogram thresholds are strongly correlated to the BC thresholds and to the audiological outcome with the VSB middle ear implant so that the vibrogram is a widely used outcome measure (Canale et al., 2014; Mlynski et al., 2015b; Wang et al., 2016; Park et al., 2017; Lee et al., 2017). Vibrogram threshold measurements have become a tool to assess the effectiveness of FMT vibration energy transfer to the cochlea in clinical routine (Marino et al., 2015; Müller et al., 2017; Todt, 2019). For optimal coupling, the vibroplasty in situ stimuli become audible at the patient’s individual hearing thresholds, the BC thresholds, and therefore correspond to the sensorineural hearing loss. There is a consensus among audiologists that the difference between the vibrogram and BC thresholds is a measure for the loss of energy due to insufficient coupling and that it should be measured as outcome measure for quality control and long term stability with the implant. Müller et al. (2017) reported that good word recognition scores could less likely be achieved in VSB patients, if this difference was larger (worse) than 20 dB.

The term *coupling efficiency* was often used to describe the relation between vibrogram and BC thresholds indicating the effectiveness of energy transfer from the FMT to the cochlear (Marino et al., 2015; Müller et al., 2017; Geiger et al., 2019). However, the term *efficiency* is normally used as a technical or physical term describing the energy conversion efficiency as the ratio between input and output energy (in %). The term *coupling efficiency* in the context of audiological outcome in patients treated with a VSB refers to the ratio between the energy that is needed to achieve hearing with the implant and the energy needed to achieve hearing by BC. In terms of dB this can be expressed as a difference, i. e., the difference between the vibrogram and BC thresholds. However, in this case large differences are associated with poor coupling, i. e., poor energy transmission, whereas high *efficiency* (100 %) is usually associated with good energy transmission. Thus, the term *coupling efficiency* is a counterintuitive concept in the context of audiological outcome in VSB patients. Alternative terms such as *effectiveness* or *efficacy*, are used when referring to a goal or mission, e. g. when testing new medications. Therefore, the term *coupling dissipation* will be used in this thesis to describe the loss of vibrational energy for poor coupling of the FMT. Energy *dissipation* refers to the conversion of mechanical energy into another form, e. g. heat, and is often used in thermodynamics. It is therefore more precise than *energy loss* as it considers the principle of energy conservation, i. e., energy is not lost but converted. The term is also applied in electronics to describe current flow through an electrical resistance (Joule heating) or in acoustics to describe acoustic attenuation or absorption (Dunn et al., 2015). In the case of the FMT vibrations, it is likely a frictional dissipation of mechanical energy leading to attenuation. Using the term *coupling dissipation* is also applicable to consider the associated outcome, since poor coupling is associated with a large amount of energy loss, i. e., large *coupling dissipation*, and good coupling is reflected by little loss of energy, i. e., little *coupling dissipation*.

Thus, the coupling dissipation is calculated as

$$\text{coupling dissipation (dB)} = \text{VIB} - \text{BC} \quad (6)$$

as a frequency specific measure. However, it can also be calculated as an average difference between the BC and vibrogram thresholds. The pure tone averages (PTAs) from the BC and vibrogram thresholds at 500 Hz, 1000 Hz, 2000 Hz, and 4000 Hz are usually used

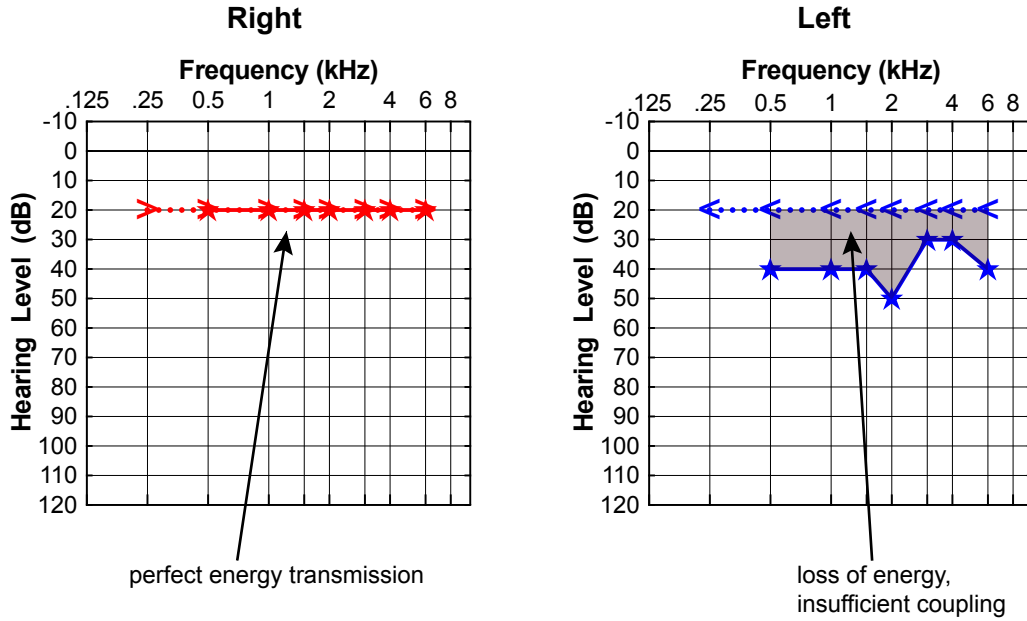


FIGURE 3.3. Vibrogram of a fictitious patient. BC thresholds are illustrated by left or right pointing arrows and dashed lines as in a typical clinical audiogram. Vibrogram thresholds are illustrated as stars. On the right side, the coupling is perfect, i. e., the vibrogram thresholds correspond to the BC thresholds. On the left side, the vibrogram thresholds are increased compared to the BC thresholds which reflects a coupling dissipation quantified by the difference between the thresholds.

$(4\text{PTA}_{\text{BC}}, 4\text{PTA}_{\text{VIB}})$:

$$4\text{PTA coupling dissipation (dB)} = 4\text{PTA}_{\text{VIB}} - 4\text{PTA}_{\text{BC}}. \quad (7)$$

The concept is illustrated in Figure 3.3. The vibrogram of a fictitious patient with bilateral BC thresholds at 20 dB HL is shown in a typical audiogram plot. The vibrogram thresholds on the right side correspond to the BC thresholds at all test frequencies and thus reflect perfect energy transmission with a coupling dissipation of 0 dB. On the left, the vibrogram thresholds are increased compared to the BC thresholds. For example, at 1000 Hz, the coupling dissipation is 40 dB – 20 dB = 20 dB (see Equation (6)). In practice, this loss of energy has to be overcome by the system in terms that more amplification is needed to reach the hearing threshold, comparable to the situation of using conventional hearing aids for treatment of conductive hearing loss. In patients who just meet the inclusion criteria of the VSB, poor coupling can therefore result in insufficient dynamic range, i. e., the maximum output is just slightly higher than the patient’s vibrogram threshold so that tones just become audible with the implant but will never be perceived at normal loudness.

3.4. Audio Processors and Fitting Procedure

Frequency specific gain, i. e., the amount of amplification applied to an input signal, is calculated in hearing aids based on the desired sensation level input/output formula (DSL I/O) (Cornelisse et al., 1995) or the National Acoustic Laboratories’ nonlinear fitting procedure, version 1 (NAL-NL1) (Byrne et al., 2001) or NAL-NL2 (Keidser et al., 2011) gain prescription rule.

The DSL I/O and NAL-NL procedures are both commonly used in hearing aid fitting but are based on different principles and formulae. The first NAL procedure was published by Byrne and Tonisson (1976) and was updated several times since then. The aim of the NAL-NL procedure is to maximize speech intelligibility while keeping the overall loudness close to normal loudness and thus equalizing rather than normalizing loudness of speech bands. This reflects the philosophy behind the approach that intelligibility is maximized when all speech bands have the same loudness. The speech intelligibility is predicted by the speech intelligibility index which was modified to take the reduced performance due to hearing loss into account. This is used with a loudness model in a complex optimization process. The required gain is calculated for each 1/3 octave band and each input level. The gain is dependent on the average at 500 Hz, 1000 Hz, and 2000 Hz as well as the absolute input level (Ulrich and Hoffmann, 2011). In the DSL I/O approach, the relation between the input level of a signal and its output level produced by a hearing aid are described in a series of device-independent mathematical equations (Cornelisse et al., 1995). The aim is to fit the complete signal's input dynamic range into the residual dynamic range of a hearing impaired person by applying amplification and compression (Ulrich and Hoffmann, 2011). Behind this is the philosophy that speech intelligibility is maximized when all speech bands are audible and comfortably loud (loudness normalization). A desired amplification (sensation level) is calculated for each frequency and each hearing loss. The input dynamic range is divided into three regions: the linear gain region, the compression region and the output limitation region. Linear gain is applied for input signals below the compression threshold (knee point). For input signals equal to or greater than a maximum input level, the output is limited. In between these limits, compression is applied to the input signal. At the knee point, a signal's input level is amplified to the hearing impaired person's threshold. The maximum output is limited to the person's upper limit of comfort. Since acclimatization to hearing aids usually requires some time, different acclimatization levels can be chosen in the fitting process. These acclimatization levels use different compression settings to give the hearing impaired patient time to adjust to the aided condition.

For the VSB, the intensity of the FMT's mechanical vibrations which determines the output and perceived loudness by the patient can be adjusted by an audiologist to the patient's hearing loss. This is done during fitting sessions in order to optimize the patient's hearing with the VSB. Taking the coupling dissipation into account, the vibrogram thresholds usually serve as a basis for this fitting procedure, i. e., as a basis for the amount of frequency specific amplification needed. Nowadays, the vibrogram is used in the fitting software to calculate the frequency specific individual dynamic range and to create a precise first fit based on the DSL I/O or NAL-NL prescription rule. Since the prescription rules were designed for the fitting of conventional hearing aids, the vibrogram thresholds are declared as AC thresholds in the VSB fitting software. However, in contrast to conventional hearing aids, the energy is directly transferred to the inner ear by the means of the FMT in VSB patients. Thus, the DSL I/O prescription rule was slightly modified for acclimatization levels 1, 2, and 3 to take the different way of energy transmission into account. Acclimatization level 4 was not modified. Documentation of this modification by the manufacturer was not published and is therefore not available in detail.

The first fit procedure and vibrogram measurement is available in the current audio processor *Samba* and the previous version *Amadé* but not the first generation audio processor *AP404*. Additionally, there are two different versions of the recent *Samba* and the previous *Amadé* audio processors – a *Lo* and a *Hi* version. The maximum power output (MPO) of a *Samba* or *Amadé Lo* is 90 dB HL at maximum gain and 90 dB SPL

input. For a Samba and Amadé Hi, the MPO is 110 dB HL. However, in practice the MPO of the system is not only dependent on the audio processor's output but also on the implant's output. While the MPO of acoustic devices is measured on ear simulators, calibration devices have not been developed for middle ear implants. Therefore, VSB MPO measurements were performed in patients as sound pressure measurements in the ear canal. The MPO of the VSB system was found to be variable between 65 dB HL and 88 dB HL (Snik et al., 2004; Zwartenkot et al., 2014). The variability is caused by varying coupling dissipation among patients which is another factor contributing to the MPO in practice.

Current State of Research and Aim of this Thesis

4.1. Objective Measures of the Floating Mass Transducer Coupling Dissipation

Vibrogram thresholds should be measured for clinical and audiological monitoring as well as for audio processor fitting purposes in all VSB patients. The procedure of measuring the vibrogram thresholds requires the patients' vigilance and cooperation so that they cannot be measured in some disabled patients or in general anesthesia during the implant surgery. However, especially intraoperative measurements would be highly desirable, because they could provide an important feedback for the surgeon helping in finding the optimal position of the FMT or the FMT-coupler assembly. So far, this is only accomplished by tactile feedback and the surgeon's experience. Objective measures of the coupling dissipation could reduce the risk of revision surgeries due to insufficient coupling and unsatisfactory audiological outcome. The data on revision rates due to insufficient FMT coupling, vary between 3.4 % (Brkic et al., 2019), 8.7 % (Zwartenkot et al., 2016), 9.5 % (Skarzynski et al., 2014), and up to 15.6 % (Schraven et al., 2016). Spiegel et al. (2020) investigated long-term stability of different coupling sites and reported revision rates of 20 % in patients with RW vibroplasty without specifying the indication for revision surgery.

The use of objective measurements in the VSB has been investigated in a few studies which show that the recording of auditory evoked potentials originating from direct stimulation by the implanted transducer is possible. The studies have utilized custom made set-ups for stimulation and recording of the responses. However, most of the studies are lacking sufficient absolute calibration of the custom designed procedure and set-up so that to date there is no objective method for the absolute and quantitative assessment of FMT coupling dissipation relative to the BC thresholds.

Verhaegen et al. (2010) conducted intraoperative ASSR measurements on four patients with mixed hearing loss to optimize the positioning of the FMT. Acoustic output was conveyed by the plastic tube of an insert earphone glued to the opening of an AP404 audio processor's microphone. The audio processor was programmed to a linear input/output level function with an amplification of 20 dB. The set-up was calibrated by measuring the audio processor's output as a function of the acoustic input. However, the study did not aim to quantify the coupling dissipation relative to the BC thresholds but rather to do relative comparisons of ASSR thresholds with a certain coupling compared to another coupling.

Radeloff et al. (2011) recorded CAPs in response to stimulation via the VSB system during revision surgery in three patients. The set-up was similar as in the study by Verhaegen et al. (2010), as the stimuli were delivered to the microphone aperture of an AP404 audio processor via a plastic tube of an insert earphone. Calibration was performed by programming the amplification of the audio processor individually for each patient according to the audiogram without information about whether AC or BC thresholds were

used as a reference. With the individual amplification according to the patient's hearing loss, the authors anticipated a threshold near 0 dB HL for good coupling. However, in 2010 the measurement of vibrogram thresholds was not available yet so that this method of calibration could not be proven to be sufficient.

A similar approach was followed by Mandala et al. (2011) who measured CAPs in 14 children undergoing RW vibroplasty. The set-up was utilizing the AP404 audio processor with an attached sound tube as well. However, in this study the gain of the audio processor was set to 0 dB. CAPs were measured before and after optimization of the FMT positioning in the RW niche with significantly lower ECoChG thresholds after the optimization procedure. Again, no direct conclusions about coupling dissipation could be drawn, as the vibrogram measurement was not available yet.

CAPs were also recorded intraoperatively during the positioning of the VSB's FMT in 13 patients with moderate to severe conductive and mixed hearing loss by Colletti et al. (2012). In that study, the FMT coupling was modified relative to the recorded thresholds and amplitudes. A set-up in which an AP404 audio processor was connected directly to the recording system was used but no more details were reported about the type of connection. The amplification of the audio processor was set to 0 dB and compression was deactivated so that the output was linear. No information was provided whether calibration of the set-up was performed. Postoperative audiological results were compared to those of a group without intraoperative monitoring but no absolute quantification of coupling dissipation was derived in that study.

In a study by Cebulla et al. (2017), ABRs were recorded intraoperatively in 12 VSB patients by using the most recent generation Samba audio processor and a wireless streamer (MiniTek¹) for signal transmission. An optimized chirp stimulus was designed to compensate for the frequency dependent time delays of the signal chain. Here, an estimation of the calibration of the signals was performed in already implanted patients by comparing sound field thresholds and thresholds by stimulation using the wireless streamer. The most recent study by Geiger et al. (2019) utilized the optimized chirp stimulus and set-up including the calibration procedure described in the earlier study by Cebulla et al. (2017) to measure intraoperative ABRs in 30 VSB patients. A significant correlation was found between the intraoperative ABR thresholds and the BC thresholds but not between the ABR and vibrogram thresholds. Differences between the intraoperative ABR and the vibrogram as well as between the BC thresholds and the vibrogram were significant while the difference between BC and intraoperative ABR threshold was not. The missing relation between the intraoperative ABR and vibrogram thresholds implies missing relation between the intraoperative ABR and the coupling dissipation so that quantification of coupling dissipation with this set-up is not possible.

Ghoncheh et al. (2020) developed another custom made set-up based on an AP404 audio processor, i. e., a radiofrequency link to transmit calibrated stimuli to the FMT of a BC implant. A precision driver device determines the distance between the transmitter coil and the receiver coil in the implant and compensates for transmission loss in this set-up. The authors did not perform clinical experimental measurements in patients or in AMEIs but proposed that the method would also be applicable in AMEI.

In summary, it has been shown that the use of objective measures such as ECoChG, ASSR, and ABR to stimulation by an implanted VSB is possible. However, most measurements were only relative and did not aim at an absolute calibration. Attempts of calibration were described by Verhaegen et al. (2010), Cebulla et al. (2017), and Radeloff et al. (2011)

¹Siemens, Erlangen, Germany

who programmed the audio processor according to the patients audiogram. Nevertheless, a calibrated reliable procedure quantifying the absolute coupling dissipation is still not available to date.

4.2. Technical Aspects

Despite the consensus about the importance of vibrogram measurements and their role in quantification of coupling dissipation, until today there is no technical paper available about the underlying calibration values or the technical background of this tool. Differences between vibrogram thresholds measured with Samba Hi and Samba Lo audio processors are sometimes observed in patients during clinical routine measurements. However, the vibrogram serves as the basis for all attempts of (objective) determination of coupling dissipation and should therefore be specified with respect to its technical properties.

Along with missing information on the technical background of the vibrogram itself, the experimental set-ups utilized in former studies for objective quantification of coupling dissipation lack the investigation of possible technical limitations of these set-ups and resulting consequences for the AMEI evoked potential measurements. Only Cebulla et al. (2017) considered the stimulus transmission in their set-up and designed an optimized stimulus for ABR measurements compensating for the frequency specific time delay in their signal chain consisting of the MiniTek, the Samba audio processor and the FMT itself. No other aspects were reported.

4.3. Thesis Outline

The results in the literature and clinical importance of vibrogram measurements for determination of coupling dissipation indicate that objective measurements of the vibrogram thresholds would be highly desirable. This would allow for clinical monitoring also in non-cooperative patients and especially for intraoperative measurements of coupling dissipation in order to help the surgeon in the process of coupling the FMT during vibroplasty surgery. This could further increase quality assurance and reduce the number of revision surgeries. While the current research is limited to intraoperative measurements and lacks calibration and investigation of the technical properties of the experimental set-ups, from a clinical and audiological stand point there is a need for a feasible and objective method for assessing and quantifying the absolute FMT coupling dissipation in terms of dB and relative to the BC thresholds. Thus, the aim of this thesis was to address the problem of the objective measurement of coupling dissipation by investigating a feasible method to measure AEPs during stimulation via the implant and calibrate the set-up so that the thresholds can be used to objectively quantify the FMT coupling dissipation in terms of dB.

To approach this problem, two different methods were developed and investigated in two prospective clinical experimental studies. In the first study, the current Samba audio processor with fixed amplification parameters and linear output was used and the stimuli were transmitted wirelessly using the MiniTek wireless streamer. Calibration was approached indirectly in this study by measuring VSB evoked ASSR thresholds in the described set-up in patients already implanted with a VSB and comparing the obtained thresholds to the actual vibrogram thresholds to derive calibration factors.

The investigation of the second method was carried out in a multicenter study in which the author of this thesis was the principal investigator. In this study, the calibration was approached directly by using the former AP404 audio processor with a sound tube

adapter glued to the audio processor's single microphone aperture so that calibrated stimuli were directly delivered to the audio processor by insert earphones. The frequency specific amplification was programmed according to the patients BC hearing thresholds and the output was linear. ABRs were recorded intraoperatively in patients who received a VSB.

Both methods were examined for their technical properties in detail in a third study. The stimulus transmission characteristics and limitations of both approaches were considered and compared. The basis for the calculation of coupling dissipation, the vibrogram measurement, was technically investigated as part of the third study as well with respect to linearity, output for different types of audio processors, influence of skin flap thickness and output limitation.

These three studies are outlined in Parts 2, 3, and 4 of this thesis with each part including short background information as well as the materials and methods, results, discussion, and conclusions of each study. In Part 5, the results from the two different approaches to objectively determine the coupling dissipation are compared and discussed with respect to their clinical results and technical properties. Accordingly, the conclusion in Part 6 is referring to the problem of objective determination of FMT coupling dissipation in general and is based on the results from all three studies .

All thresholds measured to stimulation via the VSB, i. e., VSB evoked AEPs, will be referred to in dB nHL according to the unit of the stimulus intensities (short duration stimuli) in the AEP measurement system at which a response is recorded. The true stimulus intensities at audio processor level and at the FMT are unknown and have to be determined in the calibration of the set-ups (the clinical studies). The VSB evoked AEPs will be referred to as *VSB-ABRs*, if ABRs (BERAs) are measured, and as *VSB-ASSRs*, if ASSRs are measured, respectively. Vibrogram thresholds will be referred to in dB as it is depicted by the manufacturer in the software applied for vibrogram measurements. The scale can be assumed to be a HL equivalent scale (dB eqHL) but as explained earlier there is no documentation about the calibration of the vibrogram.

Part 2

Objective Assessment of the Floating Mass Transducer Coupling Dissipation by Recording Auditory Steady-State Responses

CHAPTER 5

Background Information

As was introduced in Section 4.1, the coupling dissipation of the FMT should be measured routinely for audiological monitoring in all patients treated with a VSB middle ear implant. However, objective measures of the coupling dissipation, which are necessary in some disabled or non-cooperative patients and especially intraoperatively to monitor surgical outcome and avoid revision surgeries, are not available yet and have only been investigated in a few studies. These studies show the feasibility of VSB evoked AEPs.

Most studies used the AP404 audio processor with only one microphone and the plastic tube of an insert earphone glued to it to deliver the stimuli (Verhaegen et al., 2010; Radloff et al., 2011) or even a direct connection to the recording system (Colletti et al., 2012). However, the measurement of the psychoacoustic vibrogram thresholds only became available later on and cannot be conducted with the AP404 audio processor. The most recent available equipment, i. e., a Samba audio processor and the MiniTek wireless streamer for signal transmission, was used by Geiger et al. (2019) but the set-up could not be calibrated in this study, as no significant correlation between the VSB evoked ABR and vibrogram thresholds was observed.

The following chapters describe the first approach to use the most recent available Samba audio processor and the MiniTek streamer to record VSB evoked ASSR and calibrate the set-up. Using the Samba Hi audio processor with fixed amplification parameters, calibration was approached by comparing the obtained VSB-ASSR thresholds in implanted patients to the psychoacoustic vibrogram thresholds and deriving calibration factors. This study was conducted as a prospective experimental study at the Department of Otorhinolaryngology, Head and Neck Surgery at the University Hospital Halle.

Materials and Methods

6.1. Experimental Set-Up

The experimental set-up for the recording of VSB evoked ASSRs is illustrated in Figure 6.1. The Eclipse EP25¹ was used for stimulation and recording of the evoked potentials. The system includes an ASSR module allowing for automated analysis of the ASSR. A MiniTek² wireless streamer was connected to the insert earphone output and transmitted the stimuli wirelessly to a Samba Hi³ audio processor. The audio processor was programmed to maximum amplification with a flat amplitude transfer function. The output limitation and compression settings were deactivated and special options (wind noise reduction, sound smoothing, feedback stopper, speech enhancement features) were disabled. The stimuli were then converted by the audio processor into electrical signals and inductively sent to the implanted VORP (see Chapter 3).

The ASSRs were recorded in a two-channel set-up using Neuroline 720⁴ surface electrodes. The skin was prepared to provide impedances of 5 k Ω or less and the electrodes were placed on the left and right mastoids (reference), the hairline (active) and approximately 1 cm below the active electrode (ground).

For stimulation, octave band CE-Chirps of 500 Hz, 1000 Hz, 2000 Hz, and 4000 Hz were presented simultaneously at 40 Hz stimulation frequency. The analysis time to detect a significant response was six minutes. The EEG signal was sampled at 30 kHz with an A/D resolution of 16 bit. The responses were automatically analyzed by the ASSR module in the frequency domain by modified q -sample uniform scores tests (Cebulla et al., 2006). The false pass probability was set to 1%. The artifact rejection level was set to 40 μ V.

¹Interacoustics A/S, Middelfart, Denmark

²Siemens, Erlangen, Germany

³MED-EL, Innsbruck, Austria

⁴Ambu A/S, Ballerup, Denmark

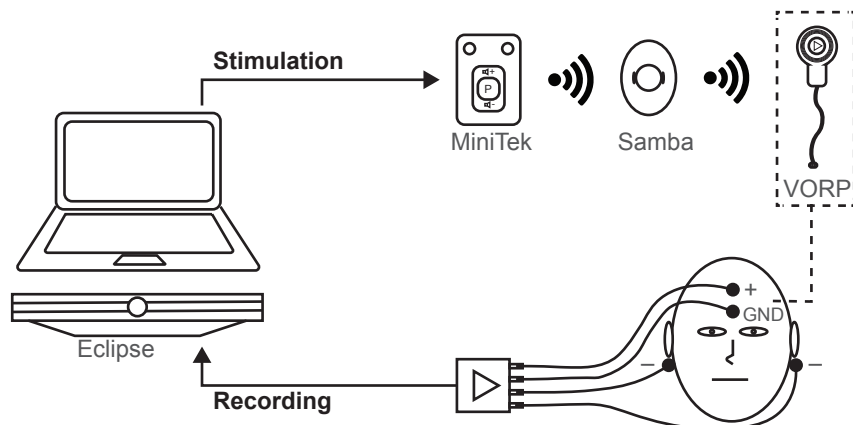


FIGURE 6.1. Experimental set-up to measure ASSR thresholds during stimulation by the implanted VORP using the Eclipse EP25 for stimulation and recording. ASSRs were recorded in a two-channel set-up with the reference electrodes (-) on the left and right mastoids, the active (+) electrode at the hairline and the ground (GND) electrode approximately 1 cm below the active electrode. Narrowband CE-Chirp Stimuli of 500 Hz, 1000 Hz, 2000 Hz, and 4000 Hz were transmitted to the Samba Hi audio processor by the MiniTek wireless streamer.

6.2. Participants

The participants in this study were patients of the University Hospital Halle who had received a VSB middle ear implant (VORP type 503 or 502 A,B), and had experience with the implant for a minimum of 6 months. Patients were included between 18 and 80 years of age. Besides chronic hearing loss due to various causes, the participants did not have any acute ear problems during the time of testing.

Written informed consent was obtained from all patients before inclusion to the study. The study protocol was reviewed and approved by the ethics committee of the Medical Faculty and the University Hospital Halle (approval number: 2017-56).

6.3. Procedures

Air Conduction and Bone Conduction Thresholds

Pure tone AC and BC thresholds were measured as psychoacoustical thresholds with an AT900⁵ clinical audiometer, using HDA 200 or HDA 300⁶ circumaural headphones for AC and a KH70⁷ transducer for BC testing.

Vibrogram Thresholds

The patient's vibrogram thresholds were measured psychoacoustically in the clinical routine procedure as described in Section 3.3 using the Symfit fitting software within Connexx software. Thresholds were measured at 500 Hz, 1000 Hz, 2000 Hz, and 4000 Hz.

⁵Auritec, Hamburg, Germany

⁶Sennheiser electronic, Wedemark, Germany

⁷Präcitronic, Dresden, Germany

VSB Evoked ASSR Thresholds

The objective thresholds during stimulation by the implanted FMT were measured by ASSR in the set-up described in Section 6.1 (VSB-ASSR thresholds). During the threshold measurements, the patients were in supine position on a patient couch and were instructed to close their eyes and relax, moving as little as possible. The starting stimulus intensity was determined by loudness scaling in order to avoid stimulus intensities which are uncomfortably loud. The stimulus intensity at which the patient responded to hear the stimuli at a comfortable level was set as the starting intensity. When a significant response was detected, the stimulus intensity was further reduced in steps of 5 dB until no response could be detected anymore. stimulus intensity with negative responses were repeated twice to avoid false negative results.

Subjective VSB Evoked Thresholds in the Experimental Set-Up

For verification of the obtained VSB-ASSR thresholds, the thresholds in the experimental set-up were additionally measured as psychoacoustical thresholds by asking the patients when the stimulus became audible. For this, the ASSR stimuli at 500 Hz, 1000 Hz, 2000 Hz, and 4000 Hz were presented separately. These thresholds will be referred to as VSB-ASSR_{subj.} thresholds in the following.

6.4. Data Analyses

The pure tone averages for AC and BC hearing ($4PTA_{AC}$, $4PTA_{BC}$) were calculated from the thresholds at 500 Hz, 1000 Hz, 2000 Hz, and 4000 Hz. Statistical analyses were performed using SPSS Statistics software⁸. A confidence level of 95% or above was considered significant ($p < 0.05$).

To test for normal distribution of the data, the Kolmogorov-Smirnov test was applied. It revealed that the following threshold distributions deviated significantly from normality: the vibrogram thresholds at 1000 Hz ($D(15) = 0.234$, $p < 0.05$), the VSB-ASSR_{subj.} thresholds at 1000 Hz ($D(15) = 0.238$, $p < 0.05$), 2000 Hz ($D(15) = 0.354$, $p < 0.05$), and 4000 Hz ($D(15) = 0.276$, $p < 0.05$), as well as the VSB-ASSR thresholds at 500 Hz ($D(15) = 0.291$, $p < 0.05$), 1000 Hz ($D(15) = 0.255$, $p < 0.05$), 2000 Hz ($D(15) = 0.235$, $p < 0.05$), and 4000 Hz ($D(15) = 0.25$, $p < 0.05$). Thus, the Wilcoxon Signed-Rank test was applied to test for significant differences between thresholds. The relationship between thresholds was analyzed by linear regression. Spearman's correlation coefficient was computed to test for significant correlations. The calibration, i. e., the correlation between the VSB-ASSR and the vibrogram thresholds was derived from the equation describing the linear regression, if applicable.

⁸version 25, IBM, Armonk, NY, USA

CHAPTER 7

Results

Fifteen patients (six male and nine female) participated in the study. The mean age was 58.7 years (SD: 9.3 years), the youngest participant was 44 and the oldest was 74 years old. All recruited patients had a mixed hearing loss, i. e., a combination of conductive and sensorineural hearing loss, and had been treated with a VSB middle ear implant for at least six months. Details about the implant types, the vibroplasty types, and the couplers are summarized in Table 7.1. The $4PTA_{BC}$ was 40.2 dB HL (SD: 10.6 dB HL) and the $4PTA_{AC}$ was 63.2 dB HL (SD: 12.6 dB HL). Ten patients had been implanted with a VORP502 and five patients with a VORP503. Various couplers and coupling positions, i. e., vibroplasty types, had been applied in the study participants.

The measurements could be successfully conducted in all 15 patients according to the protocol. In no case did the procedure have to be interrupted or cancelled. The obtained BC, vibrogram, VSB-ASSR_{subj.}, and VSB-ASSR thresholds are shown in Figure 7.1. The data which were not normally distributed are illustrated in gray. It was observed that the BC thresholds of the patients were distributed normally. The vibrogram thresholds were normally distributed as well except at the FMT's resonance frequency at 1000 Hz. However, the distributions of thresholds measured in the experimental set-up, i. e., the

TABLE 7.1. Characterization of study participants by age, affected side, couplers, vibroplasty types, and implanted VORP

Patient ID	Gender	Age (years)	Ear	Coupler	Vibroplasty	Implant VORP
1	M	72	R	Vibroplasty-CliP	PORP	502
2	M	50	R	Vibroplasty-OW	TORP OW	502
3	F	56	R	Incus-LP	Incus	502
4	F	50	R	Incus-Symphonix	Stapes	503
5	F	66	L	Direct (no coupler)	Stapes	502
6	M	53	L	Vibroplasty-CliP	PORP	503
7	F	47	R	Direct (no coupler)	Stapes	502
8	F	72	R	Direct (no coupler)	Stapes	502
9	F	74	R	Vibroplasty-CliP	Stapes	502
10	F	61	R	Direct (no coupler)	RW	502
11	M	44	L	Direct + Soft CliP reinforcement*	Incus	502
12	M	59	R	Vibroplasty-CliP	PORP	503
13	M	61	L	Incus-SP	Incus	503
14	F	65	R	Direct (no coupler)	Stapes	502
15	F	51	L	RW-Soft	RW	503

*Clip from a Soft CliP-Stapes-Prosthesis with piston detached, see Mlynski et al. (2015a).

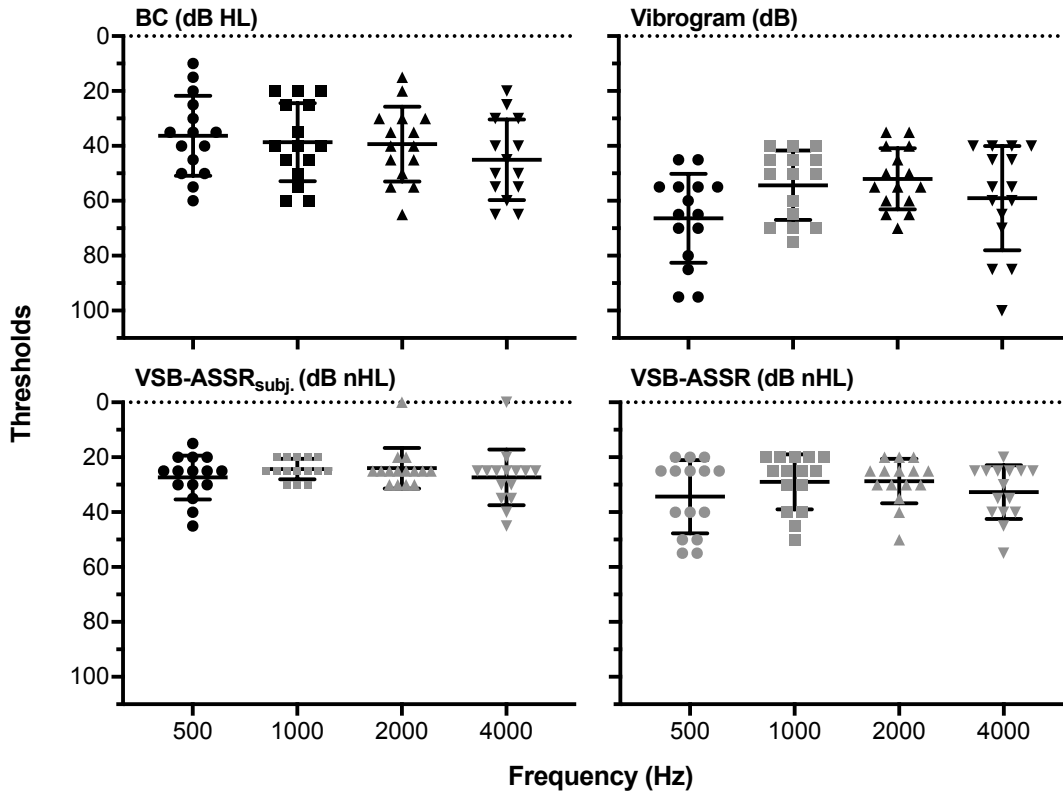


FIGURE 7.1. BC, vibrogram, VSB-ASSR_{subj.}, and VSB-ASSR thresholds at 500 Hz, 1000 Hz, 2000 Hz, and 4000 Hz. Each data point represents the threshold of a single patient ($n = 15$). The horizontal lines indicate the means and standard deviations. Data distributions deviating significantly from normality are illustrated in gray.

VSB-ASSR_{subj.} and the VSB-ASSR thresholds, mostly deviated significantly from normality and accumulated between 20 and 40 dB nHL.

Figure 7.2 shows the relation between the VSB-ASSR_{subj.} and the objectively determined VSB-ASSR in a scatter plot. There was a mean difference between the VSB-ASSR and VSB-ASSR_{subj.} of 7.0 dB (SD: 8.8 dB) at 500 Hz, 4.7 dB (SD: 7.9 dB) at 1000 Hz, 4.7 dB (SD: 9.9 dB) at 2000 Hz, and 5.3 dB (SD: 7.4 dB) at 4000 Hz. It was revealed by the Wilcoxon Signed-Rank test that the VSB-ASSR_{subj.} thresholds were significantly lower than the VSB-ASSR thresholds at 500 Hz ($T = 5.25$, $p < 0.05$, $r = -0.45$), 1000 Hz ($T = 2$, $p < 0.05$, $r = -0.37$), and 4000 Hz ($T = 3.5$, $p < 0.05$, $r = -0.46$) with the effect sizes r indicating a medium effect. The Spearman correlation identified significant correlations between the VSB-ASSR_{subj.} and VSB-ASSR thresholds at 500 Hz ($r_s(15) = 0.665$, $p < 0.05$), 1000 Hz ($r_s(15) = 0.767$, $p < 0.05$), and 4000 Hz ($r_s(15) = 0.802$, $p < 0.05$).

The relation between the vibrogram and the VSB-ASSR specifying possible calibration factors is illustrated in a scatter plot in Figure 7.3. The VSB-ASSR were lower than the vibrogram thresholds for all except one patient. For this patient, the VSB-ASSR_{subj.} was still lower than the vibrogram thresholds. During the ASSR threshold measurement the patient was very strained. At 1000 Hz and 2000 Hz, the VSB-ASSR thresholds showed no dependence on the vibrogram thresholds and were approximately constant. At 500 Hz and 4000 Hz, the VSB-ASSR increased with increasing vibrogram thresholds. The Spearman

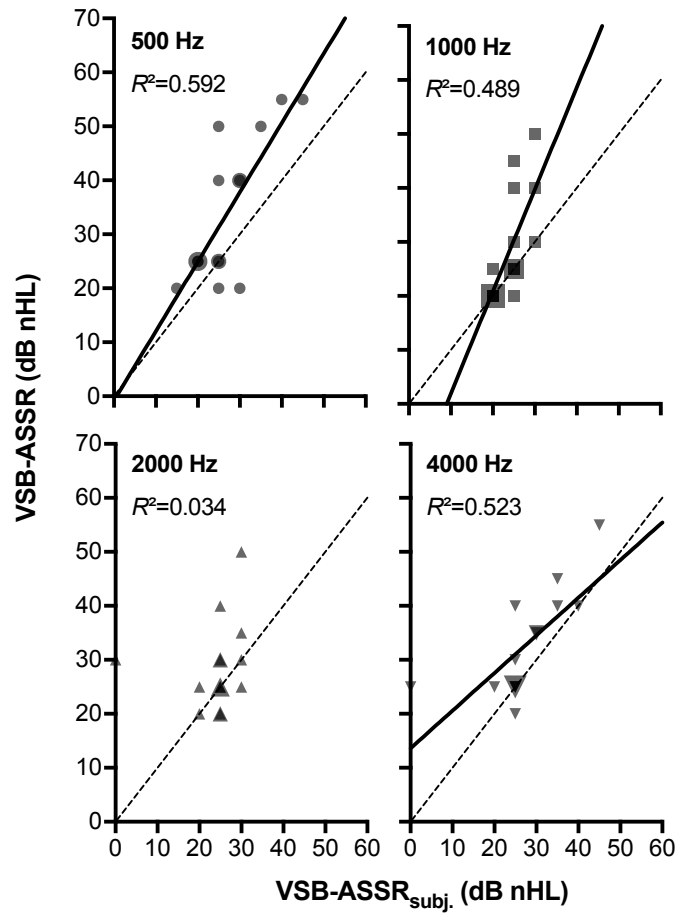


FIGURE 7.2. Relation between VSB-ASSR_{subj.} and VSB-ASSR thresholds at 500 Hz, 1000 Hz, 2000 Hz, and 4000 Hz. Each data point represents the threshold of a single patient ($n = 15$). Overlapping data points are illustrated darker and larger. The dashed line is the line of equal thresholds. Significant correlations between the VSB-ASSR_{subj.} and VSB-ASSR thresholds were identified by the Spearman correlation at 500 Hz, 1000 Hz, and 4000 Hz. The linear regression of the data is shown by the solid black line and the coefficient of determination R^2 is noted on the graph.

correlation identified a significant correlation at 4000 Hz, ($r_s(15) = 0.575$, $p < 0.05$), while no significant correlation was observed at 500 Hz, 1000 Hz, and 2000 Hz. Thus, a calibration factor could be derived at 4000 Hz but not for the other test frequencies. The relation between the VSB-ASSR and the vibrogram thresholds at 4000 Hz derived from the equation describing the linear regression was

$$\text{Vibrogram (dB)} = 1.3 \cdot \text{VSB-ASSR} + 15.5, \quad (8)$$

with a slope of 1.3 ± 0.4 dB/dB nHL and an intercept at 15.5 ± 13.3 dB nHL.

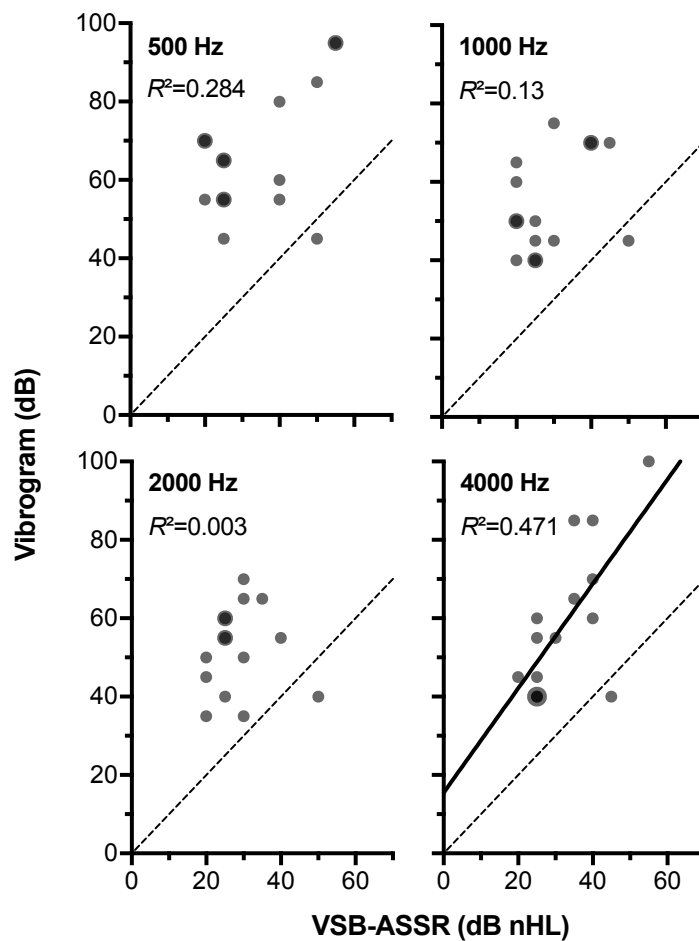


FIGURE 7.3. Relation between vibrogram and VSB-ASSR thresholds at 500 Hz, 1000 Hz, 2000 Hz, and 4000 Hz. Each data point represents the threshold of a single patient ($n = 15$). Overlapping data points are illustrated darker and larger. The dashed line is the line of equal thresholds. A significant correlation between the VSB-ASSR_{subj.} and VSB-ASSR thresholds was identified by the Spearman correlation at 4000 Hz. The linear regression of the data is shown by the solid black line and the coefficient of determination R^2 is noted on the graph.

CHAPTER 8

Discussion

The methodological key point of the study was the measurement of objective thresholds during stimulation via the VSB using ASSR and psychoacoustic vibrogram thresholds in patients implanted with a VSB for at least six months. Calibration of the set-up should be derived by the relation between the VSB-ASSR and the vibrogram thresholds. Thereby, it might be possible to calculate the vibrogram thresholds from the VSB-ASSR thresholds in those patients where vibrograms are not measurable for various reasons.

The VSB-ASSR thresholds were obtained in this study for all test frequencies in all 15 patients. Thus, the described set-up using the Eclipse ASSR module with the Samba Hi audio processor and the MiniTek for wireless stimulus transmission is generally feasible to measure ASSRs during stimulation via the implanted VSB. Both the VORP502 and the VORP503 implant types and various couplers and vibroplasty types were investigated in the study.

However, the only significant correlation between the vibrogram and the VSB-ASSR thresholds was at 4000 Hz. Thus, the calibration of the described method could only be derived at 4000 Hz but not at 500 Hz, 1000 Hz, and 2000 Hz. In practice, the vibrogram thresholds can therefore only be calculated from the VSB-ASSR thresholds with this method for 4000 Hz according to Equation (8) but not for the other test frequencies.

The correlation between the VSB-ASSR and the VSB-ASSR_{subj.} thresholds was statistically significant except at 2000 Hz, which supports the conclusion of the general feasibility of the method. The average VSB-ASSR threshold was between 4.7 and 7 dB higher than the average VSB-ASSR_{subj.} threshold. Despite statistical significance of these absolute differences between the thresholds at 500 Hz, 1000 Hz, and 4000 Hz, the differences were small and in agreement with the literature on the accuracy of ASSR measurements and the difference between the objective and psychoacoustic thresholds (Ozdek et al., 2010; Herdman and Stapells, 2009). Thus, the objective VSB-ASSR thresholds reflect the psychoacoustic thresholds, i. e., the VSB-ASSR_{subj.} thresholds, in the experimental set-up so that the objective data cannot be the result of false positive responses, e. g. due to electrical artifacts.

The BC and the vibrogram thresholds were normally distributed except for the vibrogram thresholds at 1000 Hz indicating a representative study sample. The FMT's resonance frequency is approximately 1000 Hz which causes the vibrogram data to deviate from normal distribution at this frequency. However, it was observed that the VSB-ASSR and the VSB-ASSR_{subj.} threshold data obtained in the experimental set-up deviated from normal distribution at most test frequencies and accumulated between 20 and 40 dB nHL indicating possible limitations of the method's dynamic range.

VSB evoked ASSR thresholds have only been measured before in the study by Verhaegen et al. (2010) who described a detailed calibration procedure but the study did not aim to

quantify the coupling dissipation relative to the BC thresholds and only relative measurements were performed. The set-up used in their study was very different from the set-up utilized here. The set-up used in this study was also used in the study by Geiger et al. (2019). However, Geiger et al. (2019) recorded VSB-ABRs. The recording of VSB-ASSR thresholds with this set-up has not been reported in the literature before. Unlike the results from this study, the data in the study by Geiger et al. (2019) were normally distributed. However, the programming of the audio processor was not exactly specified in that study making a detailed comparison of the data impossible.

The missing correlation between the vibrogram and the VSB-ASSR thresholds is closely related to the observed data distribution in this study which hints that there could be technical limitations of the equipment used in the experimental set-up making a calibration of the set-up impossible.

The lower limit of the method, i. e., approximately 20 dB nHL, could be caused by the inherent noise of the Samba Hi audio processor. The inherent noise would result in masking of the responses in those patients with BC and vibrogram thresholds close to 20 dB nHL. To test this hypothesis, the study needs to be repeated using a Samba Lo audio processor for which the inherent noise is significantly lower. Unfortunately, technical data about the magnitude of the inherent noise and the difference between the input-output function of the Samba Hi and Lo audio processors are not available. Another aspect that has to be considered in the context of a lower and upper limit is the audio processor's input-output function in general. In the Samba Hi in this study the output limitation and compression were deactivated for linear input-output behavior but the actual input-output function is unknown and only available to the manufacturer. Besides the audio processor also the MiniTek's transmission characteristics have to be taken into account. Output limitation could result in the upper limit. The MiniTek is a wireless streamer which is normally used by patients for audio streaming, i. e., listening to music or watching television. Thus, the device is a commercially available consumer article not originally intended to produce linear output for research applications.

CHAPTER 9

Conclusions

The applied method has been shown to be feasible to measure objective thresholds during stimulation via an implanted VSB for different implant, coupler, and vibroplasty types. It was not feasible to quantify the absolute coupling dissipation with respect to the BC thresholds as initially intended. There was no significant correlation between the vibrogram and the VSB-ASSR thresholds from which the calibration could be derived. Therefore, in its current version the method can only be used as an integrity test or for relative evaluations comparing one coupling method to another during implantation surgery.

In order to solve the problem of calibration and be able to finally quantify the absolute coupling dissipation, other methods have to be investigated. One solution could be a direct input to the audio processor which is calibrated similar to the audiogram and could be connected to an ABR system providing the trigger for stimulation. This solution would possibly come along with additional software and would have to be provided by the manufacturer.

Another approach could be to refer back to former equipment and follow the ideas of Verhaegen et al. (2010) and Radloff et al. (2011) to use a type 404 audio processor programmed to compensate for the patient's sensorineural hearing loss (BC thresholds) with a sound tube attached to its single microphone aperture. The relation between the thresholds measured in this set-up and the BC and vibrogram thresholds would need to be evaluated for calibration.

Part 3

Intraoperative Recording of Auditory Brainstem Responses for Determination of Floating Mass Transducer Coupling Dissipation

CHAPTER 10

Background

The results from the first study show that the recording of VSB evoked ASSRs using a Samba Hi audio processor and a MiniTek wireless streamer for signal transmission is possible but that this set-up could not be calibrated as intended. It was assumed that this is due to technical limitations of the equipment.

Thus, the problem of objective determination of the FMT coupling dissipation was addressed in another study. The problem of calibration was approached by using an AP404 audio processor with the sound tube of an insert earphone connected to the processor's single microphone as it was already introduced by Verhaegen et al. (2010) and Radeloff et al. (2011). Calibrated stimuli were delivered directly to the microphone. To compensate for the patients's sensorineural hearing loss, the audio processor's amplification was adjusted according to the patient's BC hearing thresholds. Thus, amplification should be sufficient for each patient to make a tone audible at a certain stimulus intensity, if the coupling is optimal. This stimulus intensity would be the calibration stimulus intensity or calibration VSB-ABR threshold corresponding to 0 dB coupling dissipation. Accordingly, the VSB-ABR threshold measured in the described set-up should increase with increasing coupling dissipation by the amount of coupling dissipation in dB. In order to identify the threshold for optimal coupling and certain degrees of coupling dissipation, normative data have to be recorded. The stimulus intensity at the audio processor's microphone membrane is close to the calibrated dB nHL scale of the ABR stimulus intensity. However, the exact stimulus intensity is assumed to be slightly higher, because the cavity of the microphone aperture is smaller than the 2 cm³ cavity of an acoustic coupler (artificial ear) which is normally used for the calibration of AC stimuli. However, preliminary investigations indicate that calibration errors in the signal chain cancel so that the VSB-ABR threshold for perfect coupling is 0 dB nHL (corresponding calibration VSB-ABR threshold) (Fröhlich et al., 2019). Thus, the VSB-ABR threshold would directly indicate the magnitude of coupling dissipation, e. g. a VSB-ABR threshold of 10 dB nHL would correspond to a coupling dissipation of 10 dB.

The objective of this study was to compare the intraoperative VSB evoked ABR thresholds to the postoperative coupling dissipation as the reference standard to evaluate the agreement between the two methods. The feasibility of the VSB evoked ABRs to predict the FMT coupling dissipation was evaluated in a series of patients with different coupling modalities in multiple implant centers.

The multicenter prospective experimental study was conducted with the Department of Otorhinolaryngology, Head and Neck Surgery at the University Hospital Halle as the leading investigation center. The other participating centers were:

- ORL Department Friedrichshain Clinic, Vivantes Hearing Center, Berlin
- Department of Oto-Rhino-Laryngology, Head and Neck Surgery "Otto Körner", Rostock University Medical Center, Rostock

- Department of Otorhinolaryngology, Head & Neck Surgery, University Medicine of Greifswald, Greifswald
- Department of Otorhinolaryngology, Institute of Phoniatriy/Pedaudiology, Jena University Hospital, Friedrich-Schiller-University Jena, Jena
- Department of ENT, University of Heidelberg, Heidelberg.

Materials and Methods

11.1. Experimental Set-Up

Figure 11.1 illustrates the experimental set-up of the study which was used for the recording of the VSB evoked auditory potentials. BERA was performed with the Eclipse EP25. ER-3A¹ insert earphones were connected to the insert earphone output. The sound tube of the earphones was connected to an AP404² audio processor with a sound tube adapter glued to its microphone aperture. The frequency specific amplification of the audio processor was programmed according to the patient's preoperative BC thresholds using the DSL I/O fitting formula and acclimatization level 4. The output limitation and compression were deactivated and all special options (microphone noise reduction, channel coupling, active digital signal processing) were disabled. The audio processor converted the acoustical stimuli into electrical signals driving the implanted FMT.

The ABRs were recorded in a two-channel set-up. Neuroline 720 surface electrodes were used for recording of the potentials. The skin was prepared to provide impedances of 5 k Ω or less. The electrodes were placed on the hairline (active) and approximately 1 cm below

¹3M, St. Paul, MS, USA

²MED-EL, Innsbruck, Austria

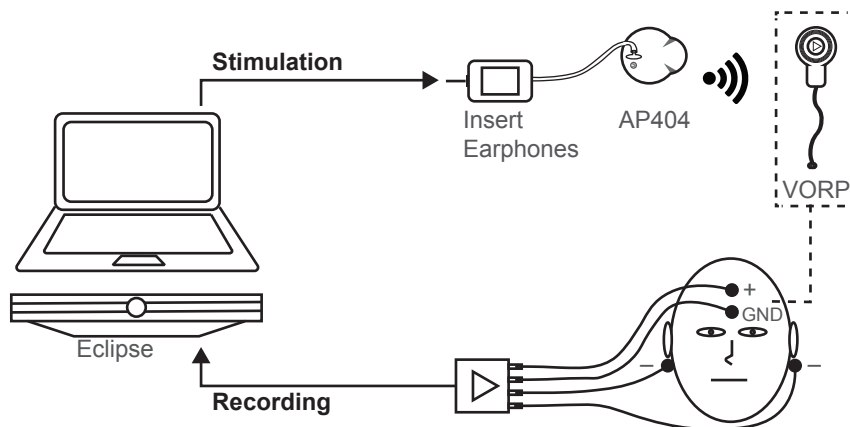


FIGURE 11.1. Experimental set-up to measure ABR thresholds during stimulation by the implanted VORP using the Eclipse EP25 for stimulation and recording. ABRs were recorded in a two-channel set-up with the reference electrodes (-) on the left and right mastoids, the active (+) electrode at the hairline and the ground (GND) electrode approximately 1 cm below the active electrode. For intraoperative recordings, the ipsilateral reference electrode was placed on the neck instead of the mastoid. Broadband CE-Chirp stimuli were delivered to the AP404 audio processor by an insert earphone sound tube connected to the processor's microphone aperture by a sound tube adapter.

this electrode (ground). For postoperative recordings, the reference electrodes were placed on the left and right mastoids. For intraoperative recordings, the reference electrodes were placed on the contralateral mastoid and the ipsilateral neck to provide adequate distance to the surgical field.

Broadband CE-Chirps of alternating polarity were presented at 49.1 Hz. The EEG signal was sampled at 30 kHz with an A/D resolution of 16 bit. A bandpass filter of 33 to 1500 Hz was applied and the responses to at least 1000 stimuli for intraoperative recordings and at least 2000 stimuli for postoperative recordings were averaged. The recording was terminated earlier, if the residual noise was below 40 nV. The artifact rejection level was set to 40 μ V.

11.2. Participants

The participants of this study were patients of the participating study centers who were scheduled for hearing rehabilitation with the VSB implant or VSB revision surgery. Thus, the participants met the clinical and audiological inclusion criteria of the manufacturer (absence of active middle ear infections; ability to get benefit from amplification; ear anatomy allows FMT positioning; stable BC thresholds ≤ 45 dB HL at 500 Hz, ≤ 50 dB HL at 1000 Hz, ≤ 55 dB HL at 1500 Hz, and ≤ 65 dB HL at 2000 Hz, 3000 Hz, and 4000 Hz). Patients were included at 18 years or older. Patients suffering from retro-cochlear, or central auditory disorders as well as patients suffering from an emotional disorder that would interfere with the ability to perform the psychoacoustic tests were excluded from the study. If postoperative BC thresholds deteriorated by more than 10 dB compared to preoperative BC thresholds, the patients were excluded from the study as well.

Before inclusion to the study, written informed consent was obtained from all participants. The multicenter study was approved by the ethics committee of the Medical Faculty and the University Hospital Halle (approval number: 2018-34). The other participating centers collected the data based on a study contract or ethical approval by their local ethics committees based on the approval in Halle.

11.3. Procedures

Preoperative

Pure tone AC and BC thresholds were measured preoperatively as psychoacoustic thresholds (preoperative AC and BC). The clinical routine audiometers and transducers (circumaural headphones and bone conduction transducers) were used at each study center.

Intraoperative

During surgery, after positioning of the FMT and during or shortly after wound closure, the ABR thresholds were measured using the experimental set-up described in Section 11.1 (intraoperative VSB-ABR). The recording electrodes were positioned before the beginning of the surgery and before draping of the surgical field. During the threshold measurements the anesthesiologist was instructed to keep the patient's level of anesthesia constant as during the rest of the surgery to prevent the patient from moving which would cause muscle artifacts in the ipsilateral electrode placed on the neck. The ABR measurement was started at a stimulus intensity of 30 dB nHL and wave V was identified. The stimulus intensity was then decreased in steps of 10 dB until no response was detected followed by another increase

of the intensity by 5 dB until the visible threshold was reached (descending/ascending -10 dB/ $+5$ dB). For reproducibility, the responses at threshold were recorded twice.

Postoperative

Four to six weeks after surgery, the pure tone AC and BC thresholds were measured in the same manner as before surgery (postoperative AC and BC).

After postoperative pure tone audiometry, the initial audio processor fitting was conducted and the patient's vibrogram thresholds were measured as psychoacoustic thresholds using the Symfit fitting software within Connexx software and standard clinical procedure (see Section 3.3). For the vibrogram measurements, a Samba Lo audio processor was used to reduce the risk of threshold masking by inherent noise.

The ABR measurement during stimulation via the implant was repeated using the same experimental set-up and procedure as intraoperatively (postoperative VSB-ABR). The audio processor setting was the same as well, i. e., the amplification was programmed according to the preoperative BC thresholds.

11.4. Data Analyses

Descriptive statistics were used for reporting demographic and baseline characteristics. The preoperative and postoperative AC and BC thresholds were calculated as pure tone averages at 500 Hz, 1000 Hz, 2000 Hz, and 4000 Hz ($4PTA_{BC}$, $4PTA_{AC}$).

The PTA coupling dissipation was calculated for each patient from the difference between the vibrogram and postoperative BC thresholds and was compared to the intraoperative VSB-ABR thresholds by a Bland-Altman analysis. The differences of the two measures – coupling dissipation as difference between vibrogram and BC thresholds as the gold standard and the intraoperative VSB-ABR – were plotted against the averages of the two measures. The limits of agreement defined as the mean difference plus and minus 1.96 times the standard deviation of the differences were calculated and compared to the maximum allowed difference between the two techniques. The maximum allowed difference was set to ± 10 dB. If the measurement error between the two methods exceeded this tolerance level in more than 5% of the study population, the two methods could not be considered equivalent. Limits of agreement not exceeding this maximum allowed difference were considered to be not clinically important implying agreement between the methods so that they could be used interchangeably. Further, the VSB-ABR method was analyzed for systematic bias, proportional error, and variation depending on the magnitude of the measurements. The mean of the difference was compared to 0 (no difference between the two methods) by a one sample t -test to detect statistically significant bias. The level of significance was set to $p < 0.05$. SPSS Statistics software was used for all statistical analyses.

Outliers in the Bland-Altman plot were identified as data points where the difference exceeded the ± 10 dB maximum allowed difference. For these patients, the postoperative VSB-ABR threshold was compared to the coupling dissipation (the difference between vibrogram threshold measured at the time when the postoperative VSB-ABR was obtained and the postoperative BC thresholds) to evaluate whether a change of coupling dissipation from the time of the intraoperative VSB-ABR measurement to the time of the vibrogram measurement caused the discrepancy.

An analysis of the effect of coupler on the agreement between the two measures was performed qualitatively by plotting the PTA coupling dissipation as function of the intraoperative VSB-ABRs and scanning the data for clusters with respect to a certain type of coupler.

CHAPTER 12

Results

Intraoperative measurements were performed in a total of 30 patients. Seven patients had to be excluded from the analysis, six due to deterioration of the postoperative BC thresholds by more than 10 dB, and one due to a calcified round window which was observed intraoperatively. Thus, 23 patients were included in the study and the final data analysis.

The mean age of the included patients was 56.6 years (SD: 12.5 years) years, the youngest participant was 33, the oldest was 81 years old. Thirteen patients were male, ten were female. In 15 patients, the left ear was implanted and in eight patients the right ear was implanted. The mean preoperative $4PTA_{BC}$ threshold of the participants was 36.4 dB HL (SD: 9.9 dB HL), the mean preoperative $4PTA_{AC}$ threshold was >69.8 dB HL (SD: 18.0 dB HL). In some patients the thresholds exceeded the measurement limit of the audiometer ($>$). With implantation of the VSB, six patients received a CliP-, three an SP-, one an LP-, two a RW-, two a RW-Soft- (one on the stapes footplate), five an OW-, and one a Symphonix-Coupler modified for placement on the stapes suprastructure. No coupler was used with the FMT placed directly in the RW niche ($n = 2$) or with a small piece of cartilage between the FMT and the RW ($n = 1$). The patients' characteristics are summarized in Table 12.1.

Intraoperatively, the VSB-ABR was measured in all patients. The measurement duration was approximately 10 minutes, respectively. VSB-ABR thresholds could be obtained in all but one patient (ID 6) where no potentials could be recorded. The threshold for this patient was marked as >30 dB nHL. The VSB-ABR response thresholds of the other 22 patients were between 0 and 20 dB nHL. The mean intraoperative VSB-ABR threshold was 9.8 dB nHL (SD: 6.7 dB nHL). Figure 12.1 shows the intraoperative VSB-ABR of patient 5 as an example. Postoperatively, the VSB-ABR was measured in 19 patients. VSB-ABR thresholds were obtained in 16 patients. In the other three patients, artifacts interfered with the responses so that response thresholds could not be determined.

The mean postoperative $4PTA_{BC}$ threshold of the participants was 35.8 dB HL (SD: 10.0 dB HL). AC thresholds were measured postoperatively in 16 patients. In seven patients, the auditory canal was surgically obliterated. The mean postoperative $4PTA_{AC}$ threshold was >70.3 dB HL (SD: 13.3 dB HL). The pre- and postoperative BC thresholds of all included patients are shown in Figure 12.2. All postoperative BC thresholds of the included patients were within a ± 10 dB range of the preoperative BC thresholds. The vibrogram thresholds could be measured in all 23 patients and the mean was 52.4 dB (SD: 12.6 dB). Thus, the mean $4PTA$ coupling dissipation was 16.6 dB (SD: 8.7 dB). For patient 6, where no intraoperative VSB-ABR threshold could be measured (marked as >30 dB nHL), the coupling dissipation was 36.7 dB. The frequency specific coupling dissipation for all individual patients is illustrated in Figure 12.3, showing scatterplots of the vibrogram thresholds and the postoperative BC thresholds at 500 Hz, 1000 Hz, 2000 Hz, and 4000 Hz. At 500 Hz, the mean frequency specific coupling dissipation was 30.9 dB (SD:

TABLE 12.1. Characterization of study participants by age, affected side, couplers, vibroplasty types, and hearing thresholds.

Patient ID	Gender	Age (years)	Ear	Coupler	Vibroplasty	BC 4PTA (dB HL)	AC
1	M	50	L	RW-Soft	RW	23.75	58.75
2	F	56	R	Vibroplasty-CliP	PORP	25.00	51.25
3	M	51	L	Direct (no coupler)	OW	27.50	56.25
4	M	53	L	Vibroplasty-CliP	PORP	43.75	60.00
5	M	60	L	Incus-Smphonix	Stapes	43.75	76.25
6	F	39	R	Vibroplasty-OW	TORP	33.75	45.00
7	F	39	L	Incus-SP	Incus	42.50	51.25
8	F	51	L	Direct (no coupler, cartilage)	RW	43.75	98.75
9	F	34	R	Incus-SP	Incus	18.75	73.75
10	F	33	R	Vibroplasty-RW	RW	37.50	76.25
11	M	72	L	Vibroplasty-CliP	PORP	25.00	65.00
12	M	67	L	Direct (no coupler)	RW	47.50	>85.00
13	M	59	L	Incus-SP	Incus	41.25	53.75
14	F	58	R	Vibroplasty-OW	TORP	38.75	57.50
15	M	60	L	Vibroplasty-OW	Incus	43.75	81.25
16	M	81	L	Vibroplasty-CliP	PORP	40.00	80.00
17	F	52	L	Vibroplasty-CliP	PORP	12.50	57.50
18	M	67	L	Vibroplasty-OW	TORP	42.50	82.50
19	M	67	L	Vibroplasty-OW	TORP	33.75	55.00
20	F	59	R	Incus-LP	Incus	43.75	46.25
21	M	77	R	RW-Soft	OW	40.00	101.25
22	M	55	R	Vibroplasty-CliP	PORP	37.50	90.00
23	F	60	L	Vibroplasty-RW	RW	51.25	>102.50

12.4 dB), at 1000 Hz it was 15.0 dB (SD: 10.7 dB), at 2000 Hz it was 7.6 dB (SD: 11.4 dB), and at 4000 Hz it was 12.8 dB (SD: 10.1 dB). The scatterplots and the standard deviations of mean coupling dissipation show that the largest variation was at 500 Hz.

Based on the results of a technical examination of the experimental set-up showing a significant delay in signal transmission at 500 Hz (see Chapter 17 later in this thesis) as well as the broad distribution of coupling dissipation at 500 Hz, the pure tone average at 1000 Hz, 2000 Hz, and 4000 Hz (3PTA) was used for all further analyses.

Figure 12.4 panel A shows the 3PTA coupling dissipation as function of the intraoperative VSB-ABR thresholds for all included patients. The 3PTA coupling dissipation was between 0 dB and 15 dB for 18 patients (78%). In three patients (13%), the 3PTA coupling dissipation was higher (worse) than 20 dB and in two patients (9%) it was lower (better) than 0 dB. Accordingly, the results of these five patients exceeded the ± 10 dB limits where the 3PTA coupling dissipation was better or worse than the intraoperative VSB-ABR by more than 10 dB. The data are shown in a Bland-Altman plot in Figure 12.4 panel B. The Bland-Altman analysis showed a mean difference between the intraoperative VSB-ABR thresholds and the 3PTA coupling dissipation of 1.6 dB (SD: 8.4 dB). This mean was not statistically different from 0 ($t(22) = 0.905$, $p = 0.375$), i. e., no statistically significant absolute systematic bias was observed. The limits of agreement were 18.2 dB and -15.0 dB. Thus, the limits of agreement exceeded the maximum allowed difference of 10 dB. A proportional error could not be observed, i. e., the difference between the intraoperative

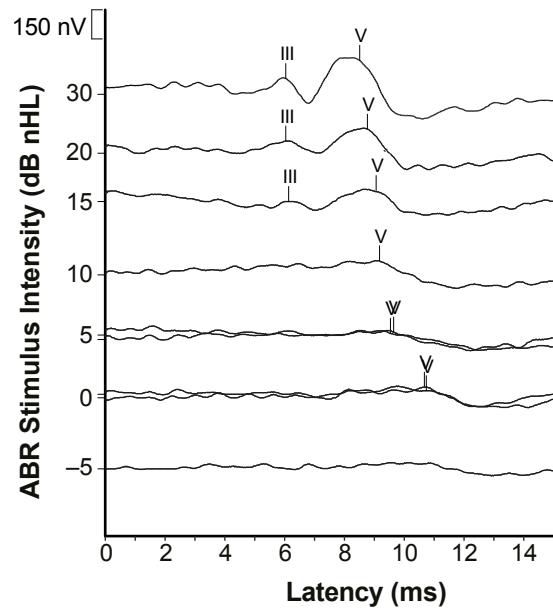


FIGURE 12.1. Example for an intraoperative VSB-ABR (patient 5). Waves III and V are marked. Measurements at 5 and 0 dB nHL ABR stimulus intensity were repeated twice. The VSB-ABR threshold, i. e., the lowest ABR stimulus intensity at which wave V could be detected, was at 0 dB nHL.

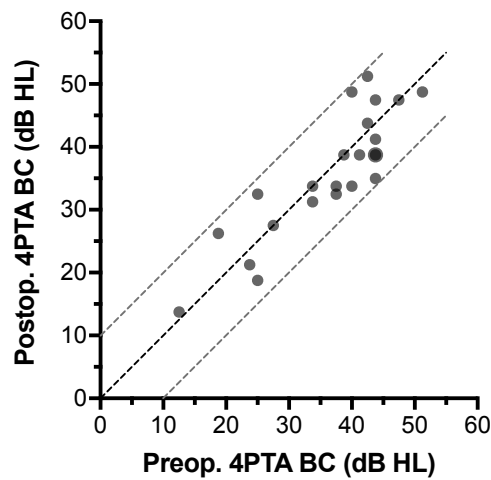


FIGURE 12.2. Comparison of pre- and postoperative 4PTA_{BC} thresholds. Each data point represents the thresholds of a single patient ($n = 23$). The dashed lines represent the line of equal thresholds as well as the ± 10 dB deviations (gray). Overlapping data points are illustrated darker and larger.

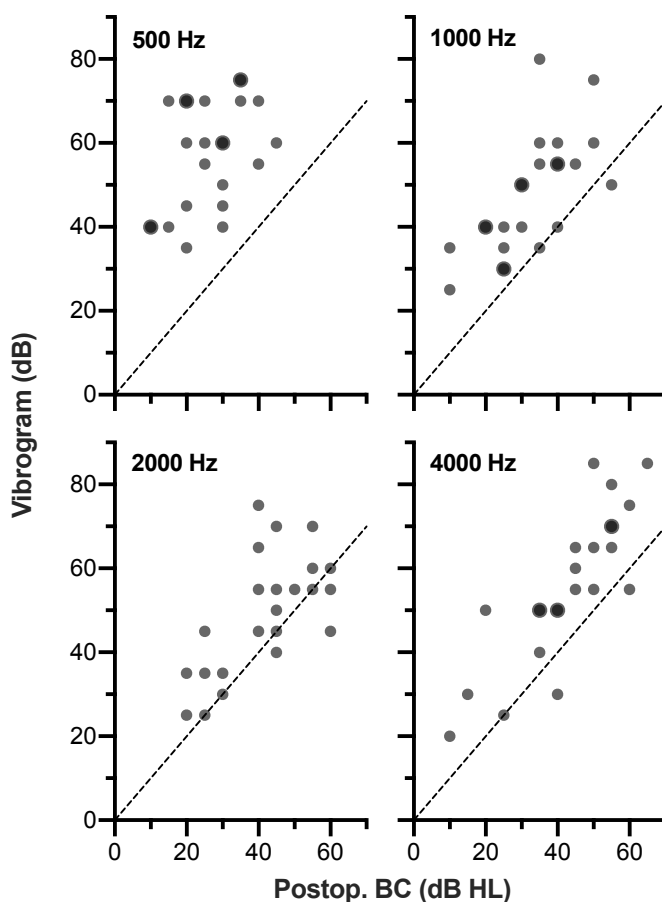


FIGURE 12.3. Vibrogram thresholds plotted against the postoperative BC thresholds for 500 Hz, 1000 Hz, 2000 Hz, and 4000 Hz showing the frequency specific coupling dissipation of the included patients. Each data point represents the thresholds of a single patient ($n = 23$). The dashed lines are the lines of equal thresholds, i. e., perfect coupling. Overlapping data points are illustrated darker and larger. The largest variation of coupling dissipation was observed at 500 Hz.

VSB-ABR and 3PTA coupling dissipation was independent of the magnitude of the two measures.

The outliers, where the intraoperative VSB-ABR was lower (better) (patients 11, 20, and 22) and where it was higher (worse) (patients 7, and 10) than the 3PTA coupling dissipation by more than 10 dB, were identified. The analysis of the postoperatively measured VSB-ABR revealed that the difference between the postoperative VSB-ABR threshold and the 3PTA coupling dissipation reduced to 3.33 dB and -1.67 dB for patients 10 and 11. For patients 20 and 22, the difference remained unchanged, as the postoperative VSB-ABR was equal to the intraoperative VSB-ABR. The postoperative VSB-ABR was not measured in patient 7.

The 3PTA coupling dissipation as function of the intraoperative VSB-ABR thresholds are shown with respect to the coupler in Figure 12.5. The distribution of the data did not show clustering for certain couplers. In patients with OW-couplers, the agreement between

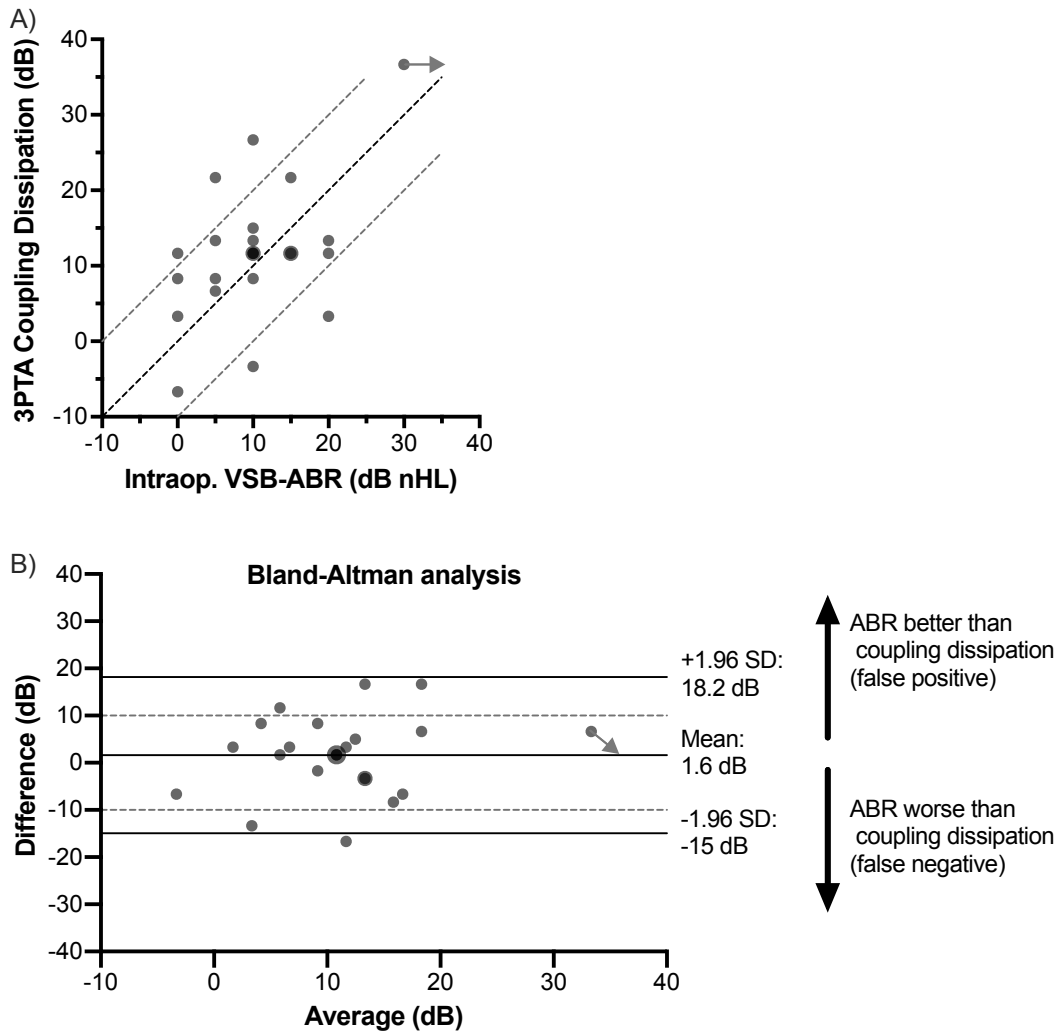


FIGURE 12.4. Analysis of the intraoperative VSB-ABR thresholds in relation to the 3PTA (1000 Hz, 2000 Hz, and 4000 Hz) coupling dissipation for all included patients. Each data point represents the thresholds of a single patient ($n = 23$). Two data points are overlapping and are illustrated darker and larger. For the patient where no response threshold of the intraoperative VSB-ABR measurement could be detected, the data point is marked by an arrow (assumed threshold >30 dB). A) 3PTA coupling dissipation as function of the intraoperative VSB-ABR thresholds. The dashed lines are the line of equal thresholds as well as the ± 10 dB deviations (gray). B) Bland-Altman analysis showing the differences of the 3PTA coupling dissipation and the intraoperative VSB-ABR thresholds against the averages. The solid horizontal lines show the mean of the differences and the limits of agreement. The gray dashed lines show the ± 10 dB maximum allowed difference between the two measures.

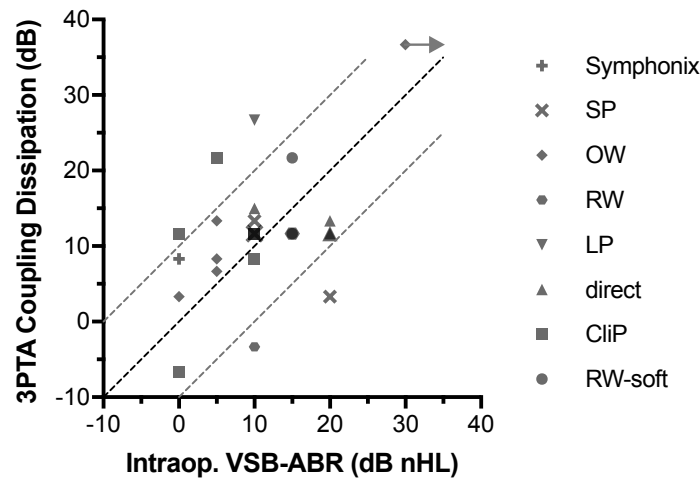


FIGURE 12.5. 3PTA (1000 Hz, 2000 Hz, and 4000 Hz) coupling dissipation as function of the intraoperative VSB-ABR thresholds for all included patients, stratified by coupler. Each data point represents the thresholds of a single patient ($n = 23$). Overlapping data points are two CliP- and one SP-coupler at 10 dB nHL/11.67 dB, one RW- and one RW-Soft-coupler at 15 dB nHL/11.67 dB, and two with direct coupling at 20 dB nHL/11.67 dB. For the patient where no response threshold of the intraoperative VSB-ABR measurement could be detected, the data point is marked by an arrow (assumed threshold >30 dB). The dashed lines are the line of equal thresholds as well as the ± 10 dB deviations (gray).

3PTA coupling dissipation and intraoperative VSB-ABR was most accurate, differences were within ± 10 dB.

CHAPTER 13

Discussion

The results showed that the experimental set-up was feasible for measuring intraoperative ABR to stimulation via the VSB (intraoperative VSB-ABR). This was shown for a series of patients with different coupling modalities and at different implant centers. VSB-ABR response thresholds could be measured in all except one patient where the intraoperative VSB-ABR was assumed to be >30 dB nHL. Postoperatively, the 3PTA coupling dissipation was 36.7 dB in this patient.

In a Bland-Altman analysis, the intraoperative VSB-ABR as the new method was compared to the 3PTA coupling dissipation determined from the difference between the vibrogram and BC thresholds as the gold standard. The analysis revealed no statistically significant bias. The mean difference was 1.6 dB and within measuring accuracy. A proportional error could also be excluded, as the VSB-ABR method was independent of the magnitude of measures. However, the limits of agreement exceeded the maximum allowed difference of ± 10 dB which was defined as the difference which is not clinically important. This indicates that the methods would not agree by an acceptable amount. A possible explanation for discrepancies between the methods is that the 3PTA coupling dissipation could have changed between the time of the intraoperative VSB-ABR measurement and the postoperative vibrogram measurement which is the basis for the calculation of coupling dissipation. This could have occurred during wound closure or in the healing process and would show that the discrepancy was not due to a false positive/or negative result by the VSB-ABR method itself. After identifying the five outliers, the postoperative VSB-ABR threshold was analyzed to test this hypothesis. The postoperative VSB-ABR should be in line with the 3PTA coupling dissipation, as it was recorded at the same time as the vibrogram thresholds. This was true for two of these patients, while in the other two patients the postoperative VSB-ABR was equal to the intraoperative VSB-ABR, so that the difference between VSB-ABR and 3PTA coupling dissipation of more than ± 10 dB remained unchanged. In the other patient, the postoperative VSB-ABR recording was not conducted. Therefore, the hypothesis could not be conclusively confirmed with three patients where the deviation by more than ± 10 dB cannot be explained but could be identified as a potential explanation in two patients.

Comparing the results of this study with respect to agreement between 3PTA coupling dissipation as a psychoacoustic measure and the VSB-ABR to the consistency of ABR and psychoacoustic thresholds reported in other studies revealed similar variations between thresholds. ABRs have been shown to be feasible for threshold estimation and consistency with psychoacoustic thresholds has been shown by significant correlations. Cho et al. (2015) reported correlation coefficients between 0.43 at 500 Hz and 0.74 at 2000 Hz for CE-Chirps and between 0.45 at 1000 Hz and 0.70 at 2000 Hz and 3000 Hz for clicks. The low correlation coefficients indicate wide data spread. Predictions of psychoacoustic thresholds from ABR thresholds were also observed to vary with the degree of hearing loss. Gorga et al. (2006) found differences between ABR and behavioral thresholds between -40 dB to 20 dB with ABR thresholds overestimating psychoacoustic thresholds in cases of normal hearing and

underestimating psychoacoustic thresholds in hearing impaired subjects. McCreery et al. (2015) reported differences between ABR and psychoacoustic thresholds ranging between -40 dB to 20 dB with a mean difference of -1.2 dB. This is comparable to the results in our study with a small mean difference but several data points with deviations of more than 10 dB. The results from the literature show that ABR is a predictor for psychoacoustic thresholds but that discrepancies between ABR and psychoacoustic thresholds can occur so that the methods cannot be used interchangeably. The VSB-ABR in our study has been shown to be a predictor for 3PTA coupling dissipation but variations occurred. A dependence of the difference between thresholds on the magnitude of thresholds, i. e., a proportional error, as described by Gorga et al. (2006) and McCreery et al. (2015) was not observed in our study but data points for weak and insufficient coupling were rare and the problem was more complex due to applied audio processor amplification and the experimental signal chain in general. A more detailed and final analysis of the relation requires more data for optimal but especially for insufficient coupling.

Agreement between the intraoperative VSB-ABR thresholds with the 3PTA coupling dissipation is assumed to be due to programming of the audio processor to the patients' BC thresholds, therefore compensating for the hearing loss, and the use of calibrated stimuli with insert earphones. However, the calibration of air conducted stimuli is normally conducted by measuring the sound pressure level in an acoustic coupler with a 2 cm^3 cavity and specified shape (artificial ear). The microphone aperture of the audio processor does not correspond to an acoustic coupler. The cavity is smaller, so that the sound pressure level at the microphone membrane is potentially higher than at a tympanic membrane in a human subject. However, it seems likely that a coincidental cancellation of calibration errors occurred so that the signal at FMT level was in line with the ABR stimulation level in the stimulation system. Thus, it is also a coincidence that the VSB-ABR thresholds were in line with the 3PTA coupling dissipation and can be considered as a direct indicator for the magnitude of coupling dissipation with a VSB-ABR thresholds of 0 dB nHL corresponding to optimal coupling.

The analysis of VSB-ABR amplitudes and latencies was not the objective of the study. However, the example in Figure 12.1 shows that the wave V latency was at approximately 8.5 ms, increasing to 11 ms close to the threshold. This is delayed compared to the wave V latency to acoustic stimulation in normal hearing subjects. The delay is probably caused by the stimulation set-up (see technical investigations in Chapter 17). Unlike in this example, wave III could not be detected in every patient. Thus, the investigation of amplitudes, latencies, and wave morphology, especially with respect to the coupling dissipation, coupler, and vibroplasty type, should be performed in future studies.

The stability of the BC thresholds is a key prerequisite for the method applied in this study. The intraoperative VSB-ABR threshold would be expected to be enhanced, if the BC thresholds deteriorated during surgery and the AP404 was programmed according to a better threshold not compensating for the hearing loss, accordingly. False-negative results could occur. An intraoperative measurement of BC thresholds by ASSR or ABR could be conducted in this case. It has been shown in several studies though, that objective measurements, especially ASSR, of BC thresholds are difficult in hearing impaired patients because high stimulation levels are necessary and artifacts from the BC transducer interfere with the AEPs (Small and Stapells, 2004; Picton and John, 2004; Gorga et al., 2004; Swanepoel et al., 2008; Brooke et al., 2009) . However, the stability of BC thresholds is a key prerequisite in any method aiming to quantify coupling dissipation as this is a measure with respect to BC thresholds.

The thresholds at 500 Hz had to be excluded from the analysis due to delay in signal transmission (compare Section 17.3) and the broad distribution of coupling dissipation at this frequency. Therefore, the described method was not feasible to determine the coupling dissipation at 500 Hz and alternative stimuli have to be used as was suggested by Cebulla et al. (2017). The method used in this study was therefore applicable to determine the 3PTA coupling dissipation at 1000 Hz, 2000 Hz, and 4000 Hz but not at 500 Hz. However, the coupling at 500 Hz is often insufficient especially in RW vibroplasty so that determination of coupling dissipation at this frequency would be highly desirable and alternative stimuli specific to this method need to be developed.

While the method was fast, robust (simple mechanical set-up with approved medical devices), and easy to conduct for any audiologist, the missing telemetry function was a potential pitfall. In the current set-up, the investigator does not receive any feedback about proper signal transmission of the audio processor to the implant as it is known in other devices with a specific intraoperative test software, e. g. in cochlear implants. This requires optimal positioning of the audio processor over the implant, preferably by the surgeon, so that signal transmission and auditory stimulation via the implant is provided. Otherwise, this can lead to false negative outcome. Other technical drawbacks of the set-up are discussed in Chapter 17.

CHAPTER 14

Conclusions

This is the first study to describe a method applicable to determine the magnitude of coupling dissipation in VSB patients. The method was evaluated in a multicenter study, collecting data of patients with various coupling modalities. Intraoperative ABRs were recorded to stimulation by the implanted FMT, driving the implant by a modified audio processor programmed to the patient's BC thresholds and fitted with insert earphone sound tubes attached to its microphone. The response thresholds recorded in this set-up have been shown to be in agreement with the 3PTA (1000 Hz, 2000 Hz, and 4000 Hz) coupling dissipation within the general measurement accuracy of ABRs to predict psychoacoustic thresholds. The method can help the surgeon to find the optimal position of the transducer or the transducer-coupler assembly to provide an optimal surgical basis for good postoperative audiological results. Therefore, the method has the potential to improve intraoperative quality control so that revision surgeries in VSB patients due to insufficient coupling could be avoided.

Since the determination of coupling dissipation at 500 Hz requires alternative stimuli, a chirp stimulus specific for the described experimental set-up – corresponding to the VSB-Chirp described for their set-up by Cebulla et al. (2017) – needs to be developed and evaluated in future studies. Further, a feedback about proper connection and thus signal transmission of the audio processor to the implant needs to be included as a technical improvement in a future set-up. An influence of coupler could not be observed in the qualitative analysis in this study. However, a quantitative and statistical analysis requires a larger study cohort.

Part 4

Technical Investigation of Active Middle Ear Implant Evoked Auditory Potential Recording

Background

The results from the two previous studies dealing with the problem of objective quantification of the absolute coupling dissipation in patients treated with a VSB have shown that the development of a feasible method is not trivial. As there is no commercially available solution, experimental set-ups have to be utilized to solve the problem of stimulation via the implant. Two different approaches have been introduced in the previous parts: the recording of ASSRs using a Samba Hi and wireless MiniTek streamer for stimulation and the recording of ABRs using an AP404 audio processor with the sound tube of an insert earphone attached to the microphone for signal transmission. In order to investigate the underlying technical limitations and specifications of these two set-ups as well as the technical background of the vibrogram measurement, several technical examinations were conducted.

The results from the first study revealed that there could be technical limitations in using a Samba Hi and a MiniTek for stimulation when recording VSB evoked ASSRs. It was assumed that lower and upper limits caused the VSB-ASSR thresholds to accumulate between 20 and 40 dB nHL. Thus, the input-output function of the set-up was examined. Additionally, the distance of the wireless signal transmission was recorded for various positions of Samba and MiniTek. The influence of potential false positive results was investigated by displaying the electrical artifacts of Samba and MiniTek using a patient simulator and simulating an ASSR measurement while reording false positive responses.

The input-output function of the AP404 audio processor with the attached sound tube was examined, accordingly. As the audio processor was programmed individually for each patient, the input-output function was analyzed for different amplification settings. The signal transmission of the AP404 with the sound tube was measured in a two channel set-up with an oscilloscope. The artifacts resulting from electrical crosstalk were also displayed using a patient simulator. To test the feasibility of automated analysis, an ASSR measurement was simulated to look for possible false positive responses.

The vibrogram is the basis for the assessment of the VSB's coupling dissipation. Even though there is no literature available about the underlying technical principles and its calibration, it has been shown to be strongly correlated with audiological outcome (Müller et al., 2017). Thus, it is a consensus, that coupling dissipation is quantified as the difference between the vibrogram and the BC thresholds. Therefore, the vibrogram serves as the basis for the calibration in both studies presented in this thesis. Since the technical principles are unknown, some aspects were analyzed in technical examinations. The linearity of the vibrogram was verified by displaying the signal on an oscilloscope. Also the influence of the skin flap thickness, i. e., the distance between the transmission and receiver coil, was measured in this course. To check for differences between the Samba Hi and Samba Lo audio processors, the processors' vibrogram input-output functions were recorded with an oscilloscope. The inherent noise of the Samba Hi and Samba Lo audio processors was

estimated by a qualitative noise measurement of the processors' output for the vibrogram setting.

The objective of the technical examination of the experimental set-ups for the recording of ASSRs or ABRs in VSB patients was to put the results of the clinical studies in a technical context and identify technical limitations

Technical Principles of Auditory Steady-State Response Recording Using a Samba Hi Audio Processor and a MiniTek

16.1. Materials and Methods

16.1.1. Input-Output Function

To measure the input-output function and thus the signal transmission of the Samba Hi audio processor and the MiniTek, an implant-in-the-box¹ was used for signal recording. The implant-in-the-box was connected to an Infinii Vision 2000 X-Series oscilloscope². The Samba Hi audio processor was programmed as during the study (amplification was maximal and output limitation and compression settings were deactivated) and was placed on the implant-in-the-box. The MiniTek was connected to the Eclipse by the insert earphone output. For stimulation, the ASSR module was used and octave band 500 Hz, 1000 Hz, 2000 Hz, and 4000 Hz CE-Chirps were presented at 40 Hz stimulation frequency as in the clinical study. The amplitude of the transmitted signal was recorded for ASSR stimulus intensities between 0 and 100 dB nHL in steps of 5 dB for all stimulation frequencies. The voltage (V) were converted into voltage levels (VL) in dB (dB VL) by the following equation:

$$L_{\text{dB VL}} = 20 \cdot \log\left(\frac{V}{V_0}\right) \text{dB VL}, \quad (9)$$

with the reference voltage $V_0 = 1 \mu\text{V}$.

16.1.2. Transmission Distance

Using the same set-up as for the recording of the input-output function (see Section 16.1.1), the transmission distances of the wireless signal transmission were recorded. This was done for various orientations of the Samba Hi and the MiniTek relative to each other. The MiniTek was positioned with the flat side down for the first two measurements, resting on the long edge for the next two measurements, and resting on the short edge for the last two measurements with the Samba rotated by 90° in one plane, respectively (see schematic illustrations of orientations in Figure 16.3). The amplitude of the transmitted ASSR stimuli was measured on the oscilloscope for increasing distances between the two devices.

¹AP adapter, MED-EL, Innsbruck, Austria

²Keysight Technologies, Santa Rosa, CL, USA

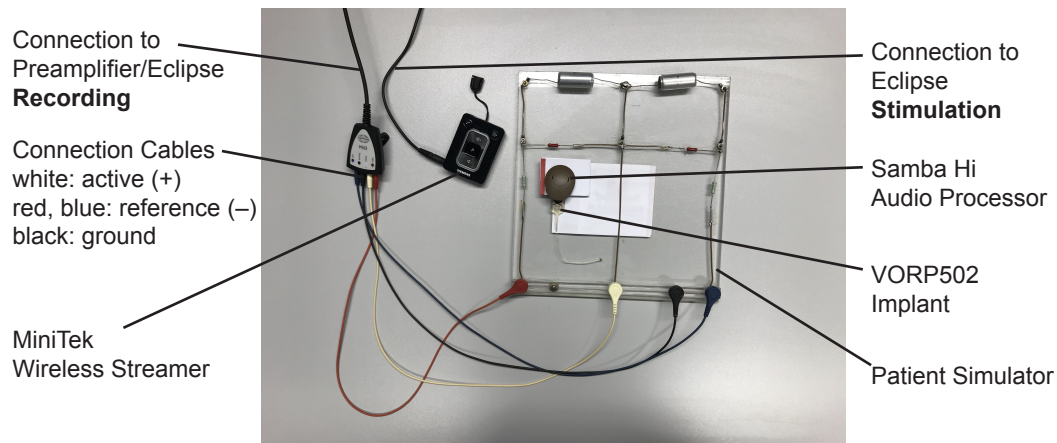


FIGURE 16.1. Experimental set-up for visualization of artifacts from Samba Hi and MiniTek. The Samba Hi was placed over a VORP502 implant which was positioned on a patient simulator. Stimulation signals were transmitted wirelessly by the MiniTek connected to the Eclipse. The artifacts were measured in an ABR recording.

16.1.3. Artifacts

To visualize the artifacts arising from electrical crosstalk of the Samba Hi audio processor, the MiniTek and the implanted VORP during an AEP recording, a patient simulator (Mühler et al., 2014; Hoth and Lenarz, 1994) was used. The Samba Hi audio processor was placed on a VORP502 implant which was positioned on the patient simulator (see Figure 16.1). A stack of paper as non-conductive material was placed between the transmitter and receiver coil, i.e., between the audio processor and the VORP. The distance between transmitter and receiver coil was approximately 0.4 mm. For stimulation, the narrowband 500 Hz, 1000 Hz, 2000 Hz, and 4000 Hz CE-Chirps were transmitted by the MiniTek wireless streamer connected to the Eclipse at 30 Hz stimulation frequency and various stimulus intensities. An ABR was recorded to display the artifacts. The responses to at least 2000 stimuli were averaged.

In order to investigate the influence of the recorded artifacts on the VSB-ASSRs, an ASSR measurement was also conducted in the described set-up. The procedure and all settings were the same as in the clinical study and negative responses were recorded twice. False positive responses were displayed in an audiogram.

16.2. Results

16.2.1. Input-Output Function

The output level from Samba Hi and MiniTek measured with the implant-in-the-box on an oscilloscope is illustrated as a function of ASSR stimulus intensity in Figure 16.2 for the 500 Hz, 1000 Hz, 2000 Hz, and 4000 Hz CE-Chirps. The output level could only be measured for ASSR stimulus intensities of 30 dB nHL and higher due to the signal noise. Up to 55 dB nHL, the output level increased linearly with increasing ASSR stimulus intensities with a slope of 1 dB VL/1 dB nHL. However, for ASSR stimulus intensities above 55 dB nHL, the output level no longer increased but saturated at approximately 187 dB VL.

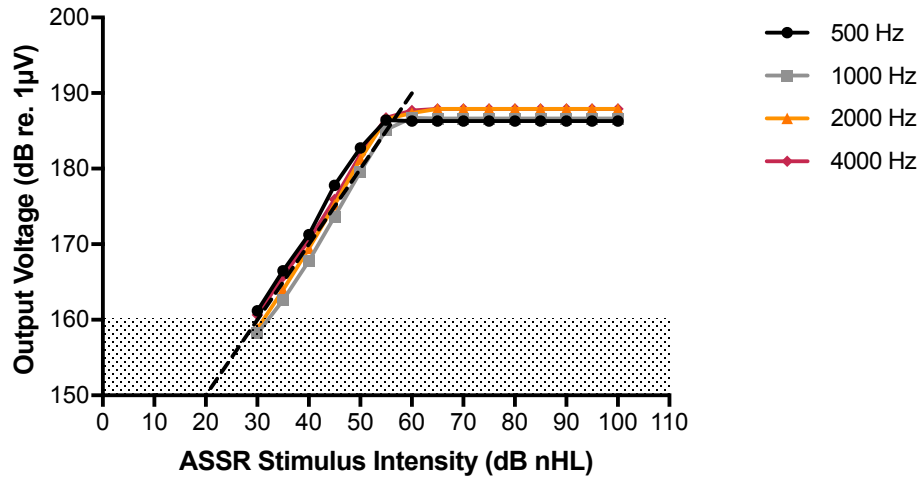


FIGURE 16.2. Output level from Samba Hi and MiniTek measured with an implant-in-the-box as a function of ASSR stimulus intensity. The stimuli were narrowband 500 Hz, 1000 Hz, 2000 Hz, and 4000 Hz CE-Chirps. The dashed black line illustrates a linear function with a slope of 1 dB VL/1 dB nHL. The dotted area represents the noise floor. The output level saturated for ASSR stimulus intensities above 55 dB nHL.

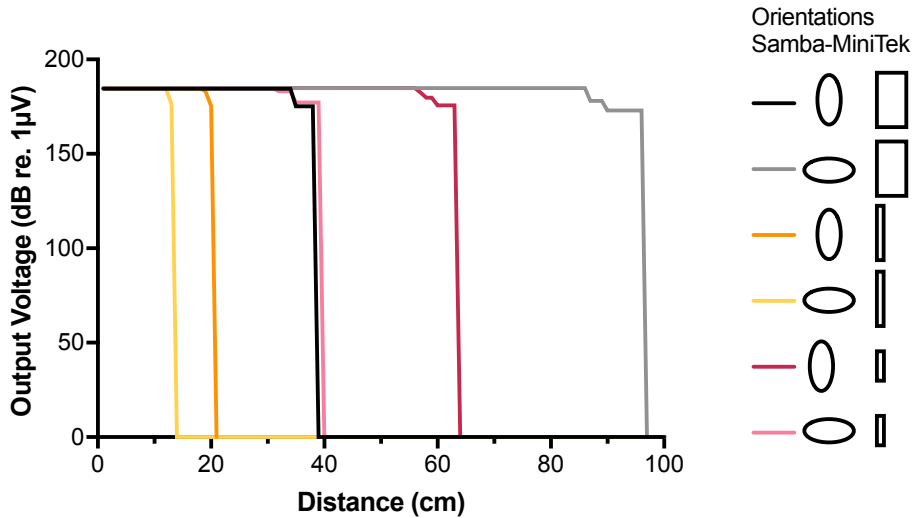


FIGURE 16.3. Wireless signal transmission distances for the MiniTek to the Samba Hi audio processor. Signals were measured with the implant-in-the-box on an oscilloscope for various orientations between the Samba and MiniTek relative to each other. The orientations are depicted by schematic illustrations (view from the top). The MiniTek was positioned with the flat side down for the first two measurements, resting on the long edge for the next two measurements, and resting on the short edge for the last two measurements with the Samba rotated by 90° in one plane, respectively. The transmission distance varied significantly depending on spacial orientation between the devices.

The input-output function was equal for all frequencies. The maximum output difference was 4.2 dB between 500 Hz and 1000 Hz at an ASSR stimulus intensity of 45 dB nHL.

16.2.2. Transmission Distance

The transmission distance of the wireless transmission from the MiniTek to the Samba Hi audio processor is illustrated in Figure 16.3. The transmission distance varied significantly for the different spacial orientations of the devices relative to each other. The shortest transmission distance was only 13 cm while the longest distance was 96 cm. Before disappearing completely, the signal was reduced in amplitude in most cases.

16.2.3. Artifacts

In Figure 16.4 the artifacts arising from electrical crosstalk of the set-up including the Samba Hi audio processor, the MiniTek and the implanted VORP are visualized. The artifact morphology and threshold was dependent on stimulus frequency. The lowest threshold at 45 dB nHL stimulus intensity was observed for the 500 Hz CE-Chirp. The artifact morphology was burst-like. The highest artifact threshold was 60 dB nHL for 1000 Hz. For 2000 Hz and 4000 Hz, the threshold was 55 dB nHL.

The ASSR measurement on the patient simulator showed false positive ASSR thresholds caused by the artifacts at 55 dB nHL ASSR stimulus intensity for all frequencies (see Figure 16.5).

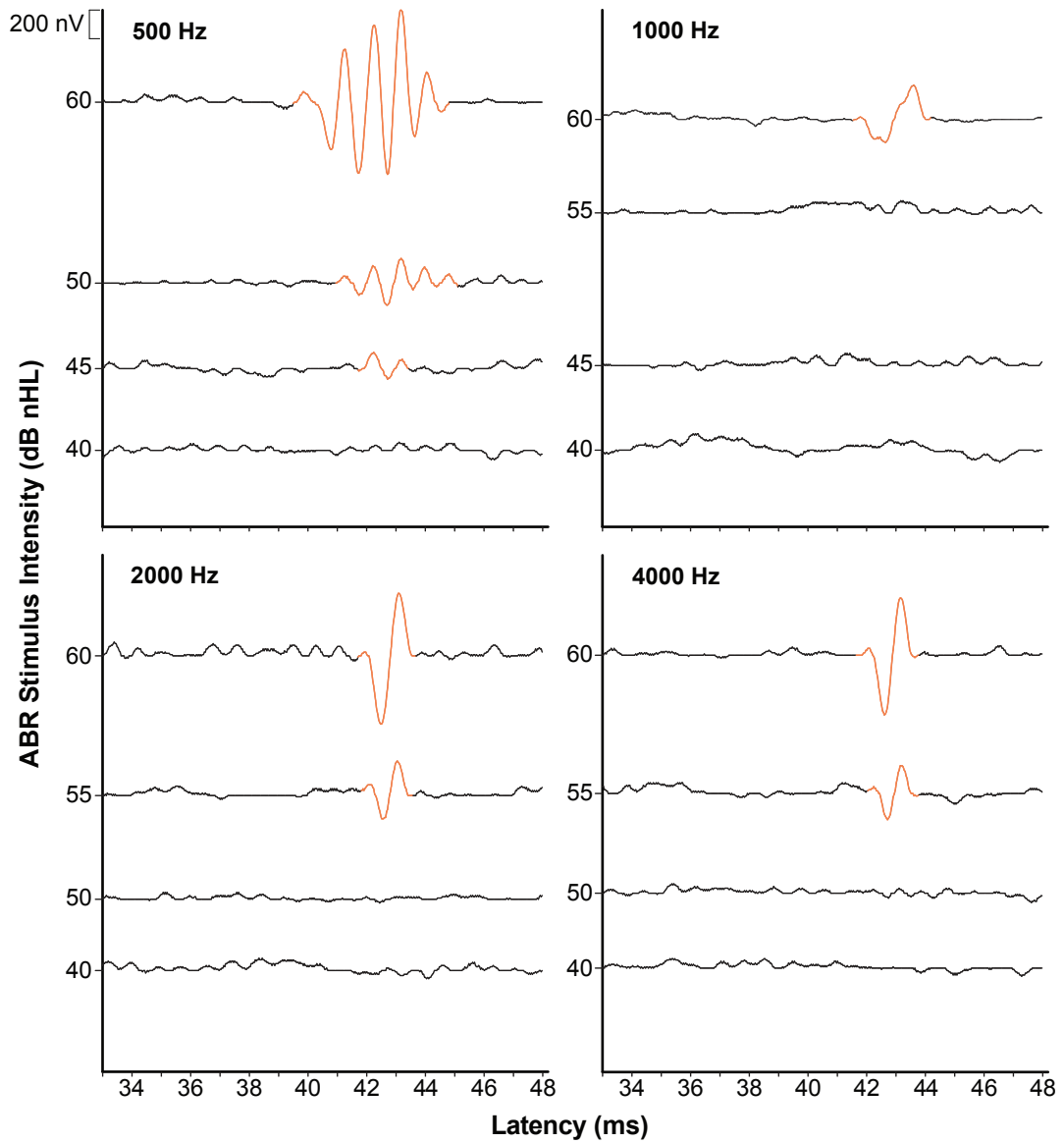


FIGURE 16.4. Electrical artifacts in the set-up with Samba Hi and MiniTek measured on a patient simulator. The artifacts are orange colored.

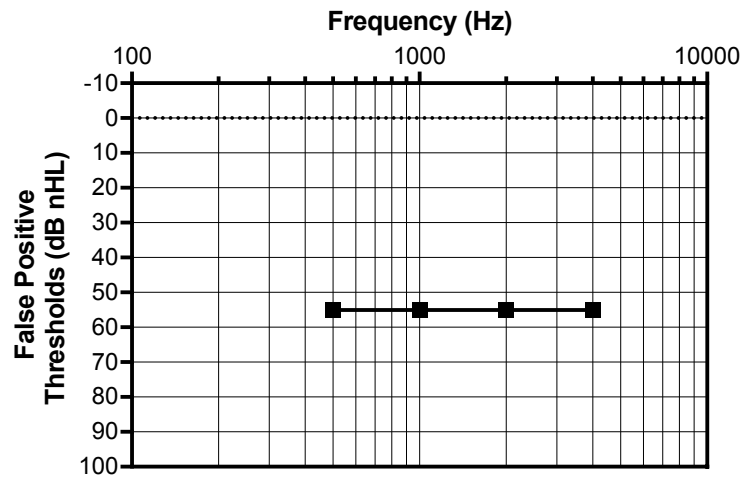


FIGURE 16.5. False positive ASSR thresholds by Samba Hi and MiniTek measured on a patient simulator.

16.3. Discussion

The measurement of the input-output function revealed linear behavior and equal output levels for all test frequencies and a limited dynamic range, since the voltage level did not increase for ASSR stimulus intensities above 55 dB nHL. For stimulus intensities below 30 dB nHL, the output level could not be measured due to signal noise. Thus, it remains unknown, if there is also a lower limit to the dynamic range. Further, it cannot be distinguished whether the limitation is attributed to the audio processor itself or to the transmission of the wireless streamer. However, this information is not crucial for the set-up. In practice, the limitation of the dynamic range has to be considered during objective measures of the VSB-ASSR thresholds introduced in Part 2. It was observed in the study that the VSB-ASSR_{subj.} and VSB-ASSR thresholds accumulated between 20 dB nHL and 40 dB nHL and it was assumed that this points at a technical limitation of the method. However, the upper limit was found to be 55 dB nHL stimulus intensity by the input-output function. Thus, the accumulation of the data to the upper limit cannot be explained by the dynamic range of technical equipment. Looking at the accumulation towards the lower limit of 20 dB nHL though, this could be attributed to the inherent noise of the audio processor resulting in masking of thresholds below 20 dB nHL stimulus intensity. However, this has to be investigated in another set-up (see Chapter 18). With the trend of the vibrogram thresholds being considerably higher than the VSB-ASSR (compare Figure 7.1 and Equation (8)) this could be a key point in identifying the reasons for the data accumulation and the failing calibration approach of this method.

The transmission distance has been shown to vary over a great range and to be strongly dependent on the spacial orientation between the audio processor and the MiniTek. For the measurement of VSB-ASSR thresholds the MiniTek has to be positioned very closely to the audio processor, i. e., to the patients head in order to avoid signal loss. Advantages of wireless signal transmission are therefore not applicable.

The delay caused by the signal chain consisting of the Samba Hi and MiniTek was measured in a study by Cebulla et al. (2017) who used the same experimental set-up. The total time delay of the set-up is more than 40 ms. Cebulla et al. (2017) showed that the delay was also frequency-dependent with the maximum delay at low frequencies. Thus, the CE-Chirp was transmitted at the FMT as a click-like stimulus. To compensate for the frequency specific delay and create a CE-Chirp equivalent stimulus for use with the described set-up they measured the delay for tone bursts and created a new VSB optimized chirp stimulus. However, narrowband CE-Chirps were used in the clinical study in this thesis. It must be assumed that the delay times within this frequency band are affected as well (longer delay for low frequencies) but the delay is without consequences for VSB-ASSR measurements. The analysis of the VSB-ASSRs was done in the frequency domain by modified q -sample uniform scores tests (Cebulla et al., 2006) which are therefore not affected by the delay. Phase coherence values which would be affected by the delay were not analyzed in the clinical study to detect significant responses. While the use of chirp stimuli has been shown to lead to larger ABR amplitudes and therefore improve signal to noise ratio, this would also improve the ASSR but is not crucial. For the recording of transient potentials as in ABR measurements, however, the delay would be crucial. Due to the very long delay of more than 40 ms and a typical ABR recording window of 15 ms the responses to one stimulus would be transferred into one of the following recording windows. This would have to be considered when reading the latencies. Alternatively, the stimulation frequency would have to be adjusted according to the delay in order to read the latencies as usual.

The technical investigations have also shown that the recording of ASSRs in VSB patients using the Samba Hi and MiniTek is affected by artifacts arising from electrical crosstalk of the implanted VORP and the stimulation chain. The artifacts are misinterpreted by the recording system and lead to false positive VSB-ASSR thresholds at 55 dB nHL. This coincides with the maximum stimulus intensity before saturation occurred in the input-output function. Therefore, the maximum ASSR stimulus intensity which should be tested is 50 dB nHL. Considering the significant correlation found in the study at 4000 Hz, the vibrogram threshold would be estimated to be 82 dB for a 50 dB nHL VSB-ASSR threshold, according to Equation (8). The method is therefore limited to estimate vibrogram thresholds up to 82 dB at 4000 Hz. Considering the indication criteria for the VSB implant with a maximum BC threshold of 65 dB HL, the method is limited to evaluate the coupling dissipation up to $82 \text{ dB} - 65 \text{ dB} = 17 \text{ dB}$ at this frequency. Since a coupling dissipation higher (worse) than 20 dB has been shown to be insufficient for achieving appropriate word recognition scores (Müller et al., 2017), the method’s dynamic range is actually sufficient to estimate the coupling dissipation for an acceptable range.

A limitation of the experimental set-up used in this study for the recording of the artifacts is the constant and small distance between the transmitter and receiver coil in the audio processor and the VORP. In patients, the distance is realized by the skin thickness which is variable. The energy transmission from the transmitter to the receiver coil is dependent on several factors such as coil spacing and coil geometry (Hochmair, 1984). The design of radio frequency links as inductively coupled coils for data and power transmission has to consider voltage gain, power efficiency, bandwidth and other factors so that different types of radio frequency links have been designed (Taghavi et al., 2012b,a). Thus, the artifact threshold measured in this study and possibly also the artifact morphology can change with varying skin flap thickness. However, the data can serve as a predictor for artifacts and allow for the objective visualization of artifacts enabling the comparison to other possible set-ups. The patient simulator itself is most likely to have a greater influence on the results than the parameters of the two coupled coils (transmitter and receiver).

16.4. Conclusions

The results of these technical investigations support the general feasibility of using a Samba Hi audio processor and a MiniTek for signal transmission in VSB evoked auditory potential measurements. The limitation of the dynamic range observed from the clinical study data could not be explained by technical limitations of the set-up directly. However, the technical details of the set-up have been shown to be essential for interpretation of the clinical study results and for avoiding methodological pitfalls. It was found by input-output function and artifact measurements that the method is not feasible to measure VSB-ASSR thresholds above 50 dB nHL due to potential recording of false positive results. During the AEP recording, the MiniTek should be in very close distance to the Samba Hi audio processor to avoid signal interruption. Moreover, due to a long signal delay of 45 ms the set-up is rather feasible for ASSR measurements but not for ABR recordings to avoid confusion with response latencies.

Technical Principles of Auditory Brainstem Response Recordings Using an AP404 Audio Processor with a Sound Tube

17.1. Materials and Methods

17.1.1. Input-Output Function

The input-output function of the AP404 audio processor with the ER-3A sound tube attached to its microphone aperture were measured with the implant-in-the-box connected to an Infinii Vision 200 X-Series oscilloscope as described for the previous study (see Chapter 16). By the Eclipse ABR module octave band 500 Hz, 1000 Hz, 2000 Hz, and 4000 Hz CE-Chirps as well as the broadband CE-Chirp were presented at 49.1 Hz stimulation frequency as in the clinical study. The sound tube of the ER-3A insert earphones was connected to the AP404 audio processor's microphone sound tube adapter glued to its microphone aperture. For ABR stimulus intensities between 0 and 100 dB nHL the transmitted voltage level was recorded in steps of 5 dB for all stimulation frequencies. The input-output function was measured for two different settings. First, the AP404 audio processor was programmed to BC thresholds of 40 dB HL and the input-output function for all frequencies was measured. In the second recording, the audio processor's amplification was varied by programming the AP404 to BC thresholds of 0 dB HL, 20 dB HL, and 40 dB HL to consider different audio processor amplification settings in the clinical study. The broadband CE-Chirp was the stimulation signal in this recording.

17.1.2. Signal Transmission

To measure the signal transmission through the complete signal chain (ER-3A insert earphones with sound tube, AP404, FMT), an experimental implant was used. A VORP502 implant was modified by cutting the FMT and soldering connecting cables to the demodulator (see Figure 17.1). The audio processor was programmed to 0 dB HL BC thresholds and placed over the experimental implant which was connected to the oscilloscope. The stimulation in the Eclipse was set to bilateral simultaneous stimulation at 70 dB nHL and a stimulation frequency of 49.1 Hz. The free insert earphone output was used to display the original stimulation signal on the oscilloscope. The input signal and signal at FMT were recorded for tone bursts of 500 Hz, 1000 Hz, 2000 Hz, and 4000 Hz, as well as the broadband CE-Chirp.

17.1.3. Artifacts

The artifacts arising from electrical crosstalk during ABR measurements in VSB patients using an AP404 audio processor with an attached sound tube for signal transmission were displayed using the patient simulator and same set-up as described in Chapter 16. An ABR

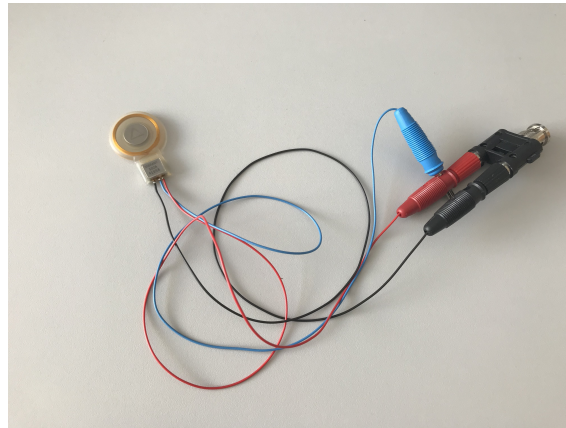


FIGURE 17.1. Experimental implant for the recording of transmitted signals. Connecting cables were soldered to the implant's demodulator.

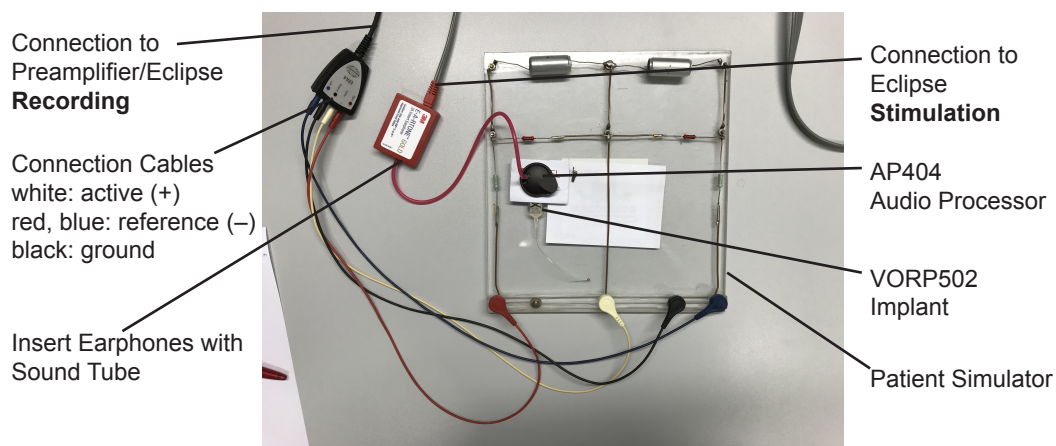


FIGURE 17.2. Experimental set-up for visualization of artifacts from the AP404 audio processor with an insert earphone sound tube. The type 404 audio processor was placed over a VORP502 implant which was positioned on a patient simulator. Stimulation signals were transmitted through the sound tube of an ER-3A insert earphone to the processor's microphone. The artifacts were measured in an ABR recording.

was recorded with the Eclipse using the same protocol as during the clinical study. 500 Hz, 1000 Hz, 2000 Hz, and 4000 Hz CE-Chirps were presented for various stimulus intensities. The responses were averaged to at least 2000 stimuli. To identify the maximum possible artifact, the AP404 was programmed to maximum amplification for this recording.

In addition to displaying the artifacts, the feasibility of the set-up for use in ASSR recordings was investigated. An ASSR was recorded from the patient simulator to 40 Hz stimulation with 500 Hz, 1000 Hz, 2000 Hz, and 4000 Hz CE-Chirps. The frequencies were presented simultaneously and negative responses were recorded twice. The false positive threshold results were displayed in an audiogram.

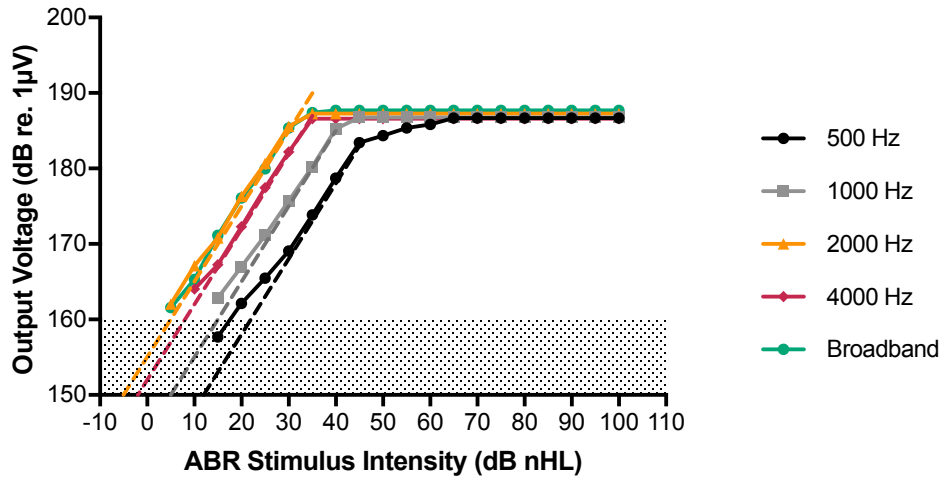


FIGURE 17.3. Output level from the AP404 audio processor with an insert earphone sound tube measured with the implant-in-the-box as a function of ABR stimulus intensity. The stimuli were narrowband 500 Hz, 1000 Hz, 2000 Hz, and 4000 Hz CE-Chirps as well as the broadband CE-Chirp. The dashed lines illustrate linear functions with a slope of 1 dB VL/1 dB nHL. The dotted area represents the noise floor. The output level was frequency dependent following a high-pass characteristic. Saturation of the output level occurred frequency dependent between 35 dB nHL and 55 dB nHL ABR stimulus intensities.

17.2. Results

17.2.1. Input-Output Function

Figure 17.3 shows the output voltage level of the AP404 with the attached sound tube as a function of ABR stimulus intensity for 500 Hz, 1000 Hz, 2000 Hz, and 4000 Hz CE-Chirps as well as the broadband CE-Chirp. Due to signal noise, the output level could only be obtained for ABR stimulus intensities higher than 15 dB nHL for 500 Hz and 1000 Hz, higher than 10 dB nHL for 2000 Hz, and higher than 10 dB nHL for 4000 Hz and the broadband CE-Chirp. For all stimuli, the output voltage increased linearly with increasing ABR stimulus intensities but saturated at approximately 187 dB V. However, the input-output function was frequency dependent following a high-pass characteristic. Therefore, the broadband CE-Chirp data basically reflected the data of the 4000 Hz CE-Chirp. Saturation was reached for ABR stimulus intensities of 45 dB nHL at 500 Hz, 40 dB nHL at 1000 Hz, and 35 dB nHL at 2000 Hz, 1000 Hz and the broadband CE-Chirp. The output difference at 30 dB nHL ABR stimulus intensity was approximately 7 dB between 500 Hz and 1000 Hz, 10 dB between 1000 Hz and 2000 Hz, and 3 dB between 2000 Hz and 4000 Hz as well as the broadband CE-Chirp.

The input-output function for different audio processor amplification settings, i. e., different BC hearing thresholds and thus different degrees of hearing loss, is illustrated in Figure 17.4 for the broadband CE-Chirp stimulus. Both the saturation level as well as the ABR stimulus intensity at which saturation occurred were dependent on the audio processor amplification level. For the settings corresponding to BC thresholds of 40 dB nHL, saturation at 187 dB V was reached at 35 dB nHL ABR stimulus intensity (compare results reported above). Due to signal noise, the output level for settings corresponding to BC thresholds of 0 dB nHL and 20 dB nHL could only be obtained for ABR stimulus intensities higher than 30 dB nHL and

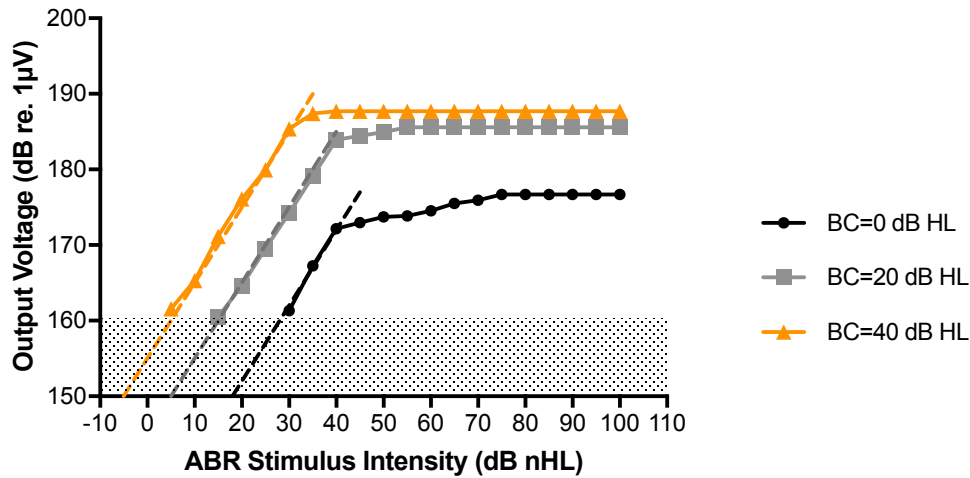


FIGURE 17.4. Output level from the AP404 audio processor with an insert earphone sound tube measured with the implant-in-the-box as a function of ABR stimulus intensity for different audio processor amplification settings (BC hearing thresholds). The stimulus was the broadband CE-Chirp. The dashed lines illustrate linear functions with a slope of 1 dB VL/1 dB nHL. The dotted area represents the noise floor. The maximum output levels and saturation stimulus intensities varied with underlying BC thresholds.

15 dB nHL, respectively. For programming of the AP404 to 20 dB nHL BC thresholds, the output level saturated at approximately 186 dB V for ABR stimulus intensities of 40 dB nHL and higher. For underlying BC thresholds of 0 dB nHL, the output level saturated between 172 dB V and 176 dB V for ABR stimulus intensities of 40 dB nHL and higher. At 30 dB nHL ABR stimulus intensity, the offset between the output voltage for 0 dB nHL BC threshold amplification and 20 dB nHL BC threshold amplification was approximately 13 dB, between 20 dB nHL BC threshold amplification and 40 dB nHL BC threshold amplification it was approximately 11 dB.

17.2.2. Signal Transmission

Figure 17.5 shows the signal transmission of the complete signal chain consisting of the ER-3A insert earphones with the sound tube attached to the AP404 and the FMT. Panel A shows the frequency specific transmission for tone bursts. The transmission delay varied with frequency. The largest delay was 7.58 ms at 500 Hz, the shortest delay was 2.02 ms at 4000 Hz. The time delay function is illustrated in panel B. The transmitted signals were burst-like at 500 Hz and 1000 Hz and resembled the original signals. At 2000 Hz and 4000 Hz, the quality deteriorated so that the transmitted signal at 4000 Hz was no longer burst-like. The effects resulted in a click-like transmission of the broadband CE-Chirp at the FMT as can be seen in panel C.

17.2.3. Artifacts

The artifacts caused by electrical crosstalk from the set-up including an AP404 with an insert earphone's sound tube connected to the audio processor's microphone and the VORP are shown in Figure 17.6. The morphology and threshold of the artifacts varied with stimulus frequencies. For 500 Hz, 2000 Hz, and 4000 Hz, the artifact could be detected for ABR stimulus intensities down to 0 dB nHL. While the artifact's amplitude stayed

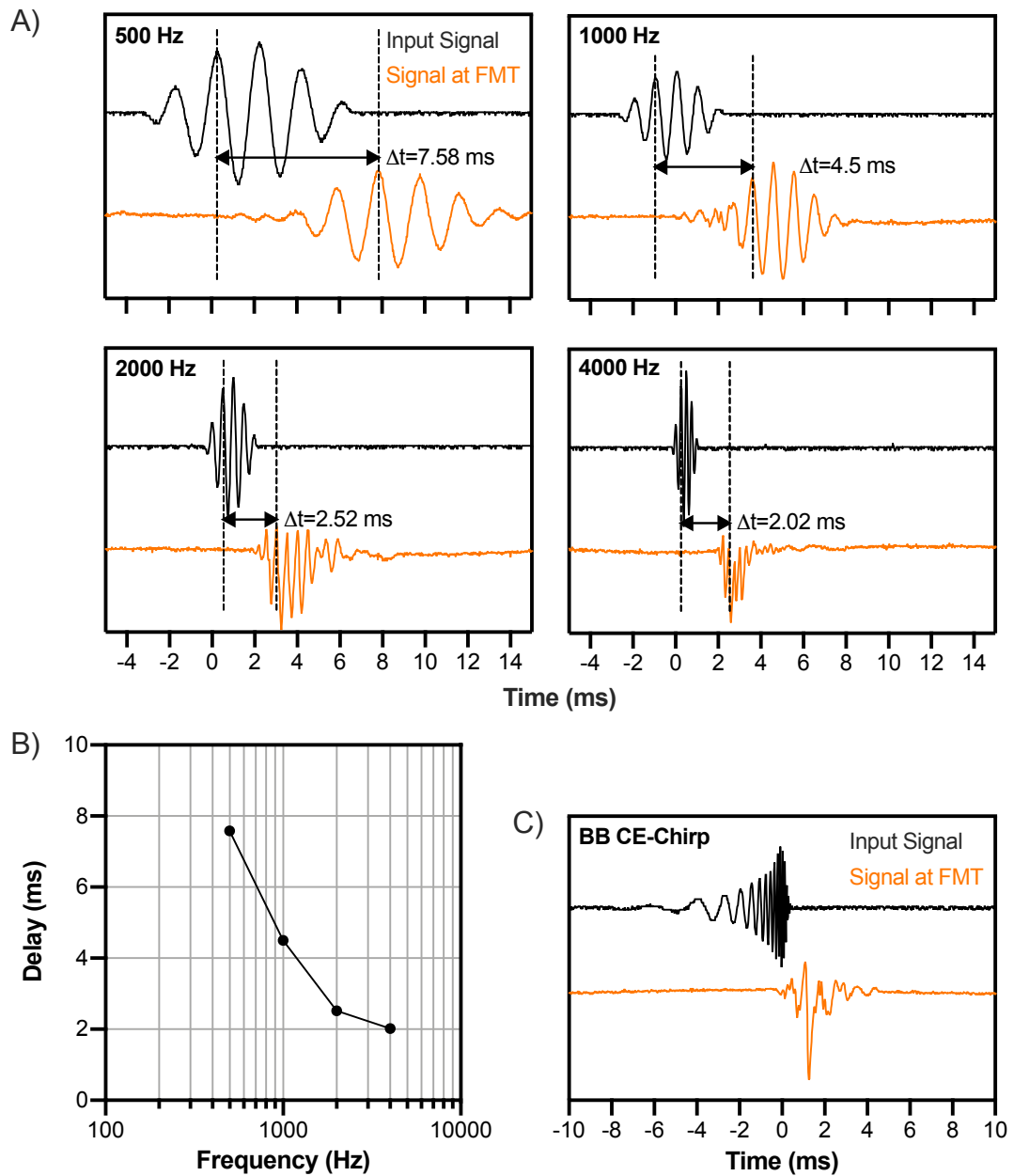


FIGURE 17.5. Signal transmission of the complete signal chain (ER-3A insert earphone with sound tube, AP404, and FMT) measured with an experimental implant. A) Temporal waveforms of 500 Hz, 1000 Hz, 2000 Hz, and 4000 Hz tone bursts. The back line shows the original signal, the orange line shows the signal at the FMT. B) Frequency specific delay time function for transmitted tone-bursts. C) Transmission of the broadband CE-Chirp emerging as a click-like stimulus at the FMT.

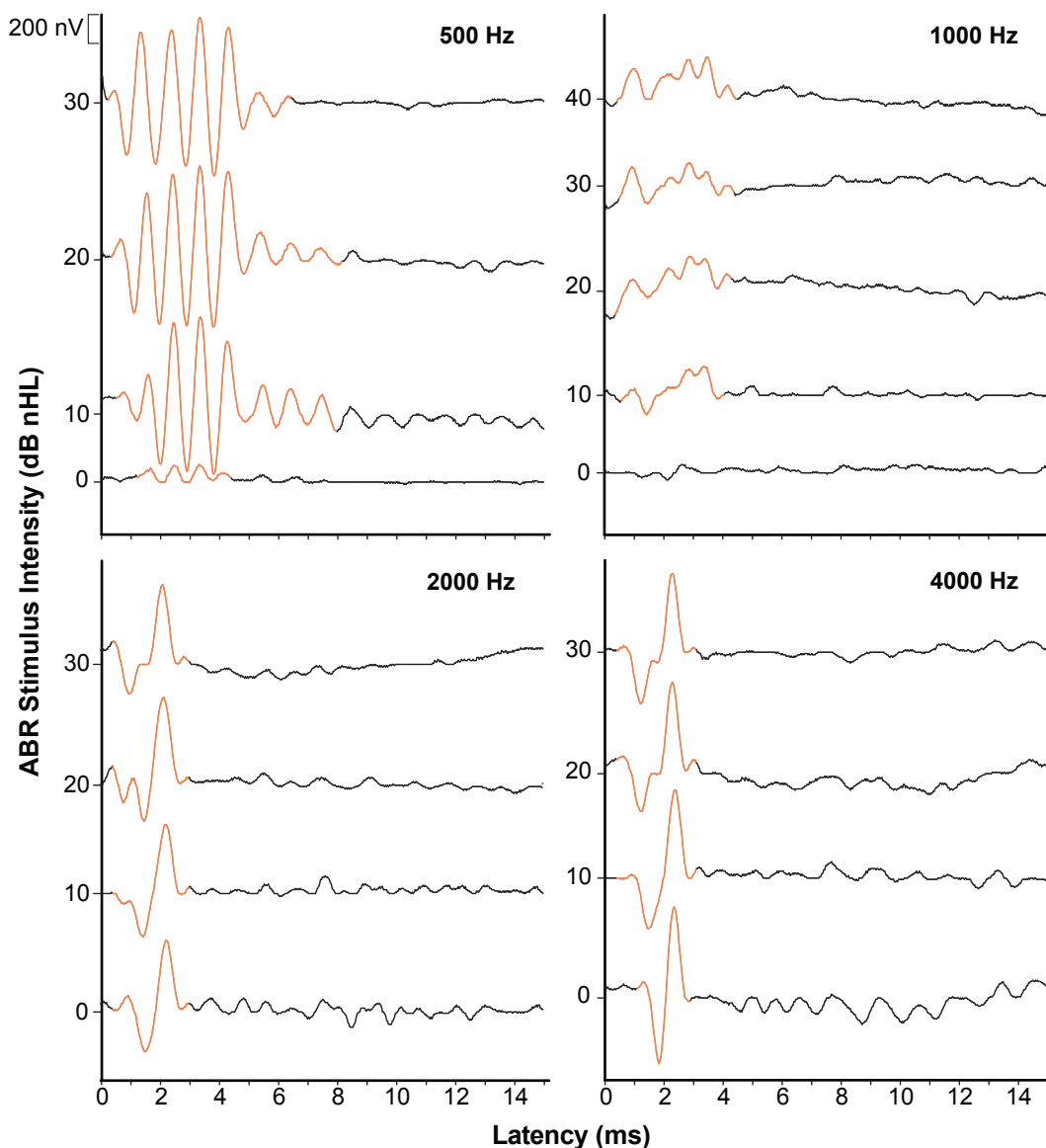


FIGURE 17.6. Electrical artifacts in the set-up with the AP404 audio processor with an insert earphone sound tube attached to its microphone measured on a patient simulator. The artifacts are orange colored.

approximately constant for 2000 Hz and 4000 Hz, it was reduced for 500 Hz at 0 dB nHL. For 1000 Hz CE-Chirps, the artifact threshold was detected at 10 dB nHL. The artifact morphology for the 500 Hz CE-Chirp was burst-like.

The ASSR measurement on the patient simulator showed false positive ASSR thresholds caused by the artifacts at 65 dB nHL ASSR stimulus intensity for 500 Hz, 45 dB nHL for 1000 Hz, 35 dB nHL for 2000 Hz, and 0 dB nHL for 4000 Hz (see Figure 17.7).

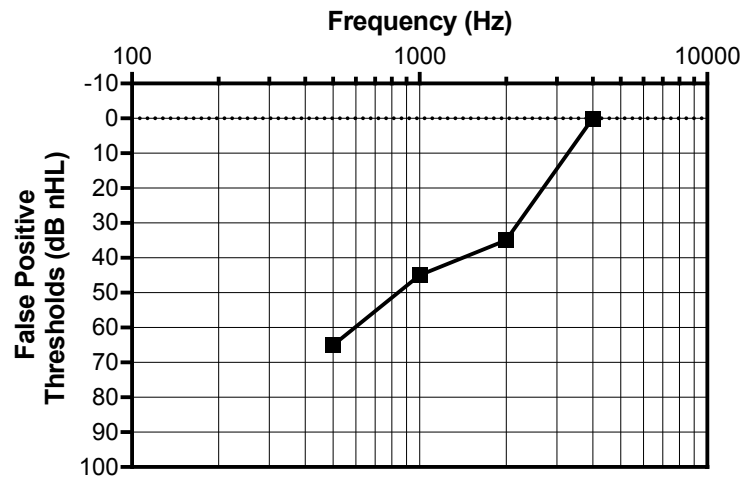


FIGURE 17.7. False positive ASSR thresholds by an AP404 audio processor with an insert earphone sound tube measured on a patient simulator.

17.3. Discussion

The input-output function measurements revealed that the dynamic range was dependent on frequency and amplification programming of the audio processor. The ABR stimulus intensity at which saturation occurred varied between 35 dB nHL and 45 dB nHL. The limitation has to be considered during the recording of ABR evoked potentials using this set-up. However, according to the hypothesis in the clinical study that the ABR threshold directly corresponds to the magnitude of coupling dissipation, a dynamic range of 35 dB is sufficient, as a coupling dissipation of less than 20 dB should be achieved to ensure adequate audiological outcome. In some conditions, the output level could not be recorded due to signal noise for low ABR stimulus intensities. Thus, it remains unclear from the technical measurements alone, if there was also a lower limit to the dynamic range. However, the data from the clinical study have shown that VSB-ABR thresholds of 0 dB nHL could be recorded. Therefore, it can be assumed that no lower limit of the set-up exists and that the limitations were attributed to the recording technique in this study. The upper limit varied with different audio processor programming settings. It can be assumed that the upper limit is attributed to limitations of the audio processor itself rather than to limitation of the implant-in-the-box which was used to measure the output level.

It was further observed that the output voltage measured from the AP404 with the sound tube was frequency dependent following a high-pass characteristic. The maximum difference was 17 dB between the output of a 500 Hz and a 2000 Hz CE-Chirp at an ABR stimulus intensity of 30 dB nHL. By the data alone it cannot be distinguished whether this behavior was caused by the sound tube or the audio processor itself. It is well known that sound tubes do show high-pass filter characteristics. However, these should be compensated for in the calibration data of the insert earphones in the Eclipse. The consequence for the clinical recording situation is that the lower frequency components of the broadband CE-Chirp are transmitted at significantly lower levels than the higher frequencies. By using the broadband stimulus alone, no statement about the coupling dissipation for the different frequencies can be made. However, the frequency dependent output behavior makes interpretation even more complicated. When an ABR threshold to a broadband stimulus is detected at 20 dB nHL, it could be interpreted as suboptimal coupling while

this is actually only true for the high frequencies. Coupling dissipation could still be in an acceptable range for the low frequencies but the output was not high enough, i. e., 17 dB lower at 500 Hz than at 2000 Hz, so that the coupling dissipation could still be just slightly worse (larger) than 3 dB ($20\text{ dB} - 17\text{ dB} = 3\text{ dB}$) at 500 Hz. Thus, coupling dissipation will less likely be detected for the low frequencies but is actually much more likely to occur for the low frequencies than for the high frequencies. The determination of coupling dissipation at the low frequencies therefore requires alternative stimuli.

Another important result for the interpretation of the clinical study data is the difference between the output and the saturation levels for various amplification settings of the audio processor. In the clinical study, the AP404 was always programmed according to the patient's BC hearing thresholds using the DSL I/O fitting formula and deactivating the output limitation and compression. With output limitation deactivated, the saturation levels would be expected to be at the MPO level for all settings. While the settings were adjusted in the preoperative programming of the audio processor for linear signal transmission and amplification, the prescription rules are still in place and work accordingly. However, as discussed above, the dynamic range is at least 35 dB which is sufficient for the estimation of the magnitude of coupling dissipation and the output limitation is not crucial in this case. It was also observed that the output difference between the 0 dB HL and 20 dB HL BC threshold amplification and between the 20 dB HL and 40 dB HL BC threshold amplification was 13 dB and 11 dB. Thus, the actual amplification changes of the AP404 did not match the differences between BC thresholds of 20 dB which were the basis for amplification settings. The applied DSL I/O prescription rule must also be considered in this case. The data from the clinical study still support the hypothesis that the ABR threshold equals the magnitude of coupling dissipation, but the amplification of the audio processor compensating for the hearing loss (amplifying the signals by 20 dB for hearing loss of 20 dB HL) is based on the DSL I/O formula.

It was observed that the delay by the AP404 with the sound tube was dependent on frequency with smaller delay times for higher frequencies. The results are in line with the findings of Cebulla et al. (2017) who reported frequency specific delay for their set-up consisting of a Samba audio processor and the MiniTek wireless streamer. While the total delay times differed for this set-up, the delay time function resembled to the results reported by Cebulla et al. The broadband CE-Chirp emerged as a click-like stimulus at the FMT with a delay of approximately 2 ms. For the recording of the transient potentials, this information about the delay is crucial when interpreting the response latencies. However, this was not done in the clinical study but may be of interest in future studies. It can be assumed that the delay is caused by the audio processor and implant itself, because the delay caused by the sound tube should be compensated for in the calibration of the insert earphones in the Eclipse system as can be seen in clinical routine ABR recordings with insert earphones stimulation. The click-like morphology of the stimulus is important for interpretation of the results as well. It must be assumed that VSB evoked ABRs measured in this set-up are responses to rather high frequencies of 2000 Hz and 4000 Hz, so that the information about coupling dissipation at 500 Hz cannot be obtained in this set-up. Thus, the determination of coupling dissipation at 500 Hz requires alternative stimuli. A modification of the chirp signal according to the concept described by Cebulla et al. (2017) could solve the problem.

The artifacts arising from electrical crosstalk when recording ABRs in VSB patients to stimulation by the AP404 with the sound tube of an insert earphone attached to its microphone have been shown to be present even at low ABR stimulus intensities. However,

this does not affect the feasibility of the method, because the response's wave V, which is normally observed to identify the threshold, was not covered by the artifact. In fact, the artifact can serve as an integrity control for the set-up itself as its presence verifies the correct audio processor placement over the implant. However, the artifact was not as present in the actual recordings of the clinical study.

It was also shown that an ASSR measurement in this set-up lead to false positive threshold results between 65 dB nHL up to 0 dB nHL, because the artifacts were misinterpreted by the system as a response. Thus, recording of ASSRs in VSB patients using an AP404 audio processor with a sound tube attached to its microphone for signal transmission is not feasible. The limitations of the experimental set-up and the implications for interpretation of the results were discussed in the previous Chapter 16. However, the use of the same set-up makes the results between the different set-ups for VSB evoked potential measurements comparable.

17.4. Conclusions

The technical investigations in this study have shown the general feasibility of using an AP404 audio processor with the sound tube of insert earphones attached to its microphone to transmit the stimuli in VSB evoked ABR measurements. A limitation of the maximum output was observed. However, this is not crucial for the assessment of coupling dissipation, as the desired range of coupling dissipation is within the limit. The output of the AP404 was further shown to follow a high-pass characteristic which has to be considered for interpretation of intraoperative findings. Coupling dissipation at the low frequencies might not be detected. The technical measurements also showed that the signal transmission was frequency dependent with low frequencies transmitted at significantly larger delay times. The broadband CE-Chirp therefore emerged as a click-like stimulus at the FMT with a delay of approximately 2 ms. Thus, care should be taken when response latencies are evaluated and the determination of coupling dissipation at 500 Hz requires alternative stimuli. Another very important observation from the technical measurements was that the described set-up is not feasible for recording of ASSRs in VSB patients, because the false positive responses due to artifacts occurred at very low stimulus intensities.

Investigating the Technical Principles of the Vibrogram

18.1. Materials and Methods

18.1.1. Vibrogram Input-Output Function of Samba Hi and Samba Lo

The input-output function of the vibrogram measurement was recorded for a Samba Hi and a Samba Lo audio processor. The audio processor was connected to the computer as during a regular clinical vibrogram measurement using the programming connection cable. Symfit fitting software within Connexx software was used to set the audio processor to the vibrogram settings provided as a template in the software and to present sinusoidal (pure tone) stimuli. The output voltage amplitude of the implant-in-the-box was recorded with an Infinii Vision 200 X-Series oscilloscope for all available vibrogram stimulus intensities between 15 dB and 105 dB and for all available frequencies, i. e., 500 Hz, 750 Hz, 1000 Hz, 1500 Hz, 2000 Hz, 3000 Hz, 4000 Hz, and 6000 Hz. The frequency specific amplification used for the vibrogram test was read and plotted from the fitting software for comparison.

18.1.2. Vibrogram Input-Output Function of Audio Processors of the Same Type

In order to investigate the difference between audio processors of the same type, the input-output function was measured in the same manner as described in the previous section for two Samba Hi and two Samba Lo audio processors at 500 Hz, 1000 Hz, 2000 Hz, and 4000 Hz. The difference between the output was calculated for each vibrogram stimulus intensity.

18.1.3. Vibrogram Input-Output Function for Varying Skin Flap Thickness

The influence of skin flap thickness on the transmitted voltage level was investigated by measuring the transmitted voltage level using the implant-in-the-box and the oscilloscope for skin flap thicknesses between 0 mm and 10 mm. This range includes the typical skin flap thickness of patients with implantable hearing devices between 3 mm and 9 mm (Raine et al., 2007). To mimic the skin flap, stacks of paper as non-conductive material were placed between the implant-in-the-box and the audio processor. The measurement was conducted using a Samba Hi audio processor and recording the transmitted voltage for 1000 Hz and 4000 Hz at a vibrogram stimulus intensity of 70 dB.

18.1.4. Inherent Noise of Samba Hi and Samba Lo

The inherent noise of the Samba Hi and Samba Lo audio processors was measured qualitatively in a sound proof cabin. The audio processors were programmed according to the vibrogram measurement setting and positioned on the implant-in-the-box. HDA205¹

¹Sennheiser electronic, Wedemark, Germany

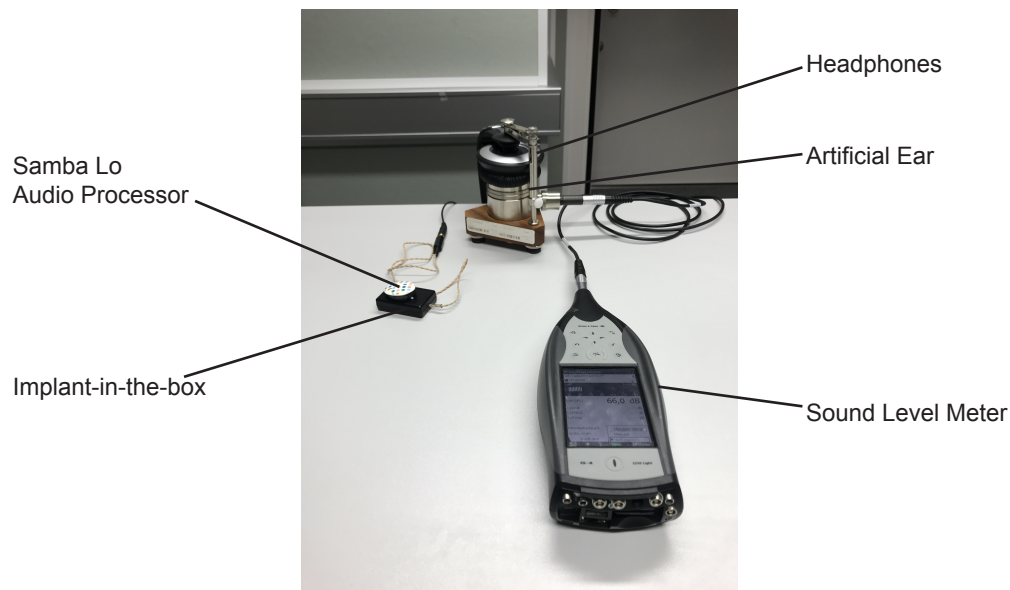


FIGURE 18.1. Experimental set-up for the qualitative measurement of the audio processor's inherent noise. The Samba Hi or Samba Lo was positioned on an implant-in-the-box as the receiver. HDA205 headphones were used to make the signal audible. The sound pressure level was measured on an artificial ear with a sound level meter.

headphones were connected to the implant-in-the-box and placed on a 4152 artificial ear². The output was measured by a 2250 Light³ sound level meter using A-frequency weighting and fast time-weighting. The set-up is shown in Figure 18.1.

18.2. Results

18.2.1. Vibrogram Input-Output Function of Samba Hi and Samba Lo

Figure 18.2 shows the output voltage as a function of vibrogram stimulus intensity for a Samba Hi and a Samba Lo audio processor. For the Samba Hi, the output level increased linearly and by the same magnitude as the vibrogram stimulus intensity. For the Samba Lo, the output level increased linearly as well but only up to 75 dB vibrogram stimulus intensity for 500 Hz, 80 dB for 6000 Hz, and 85 dB for the other test frequencies, respectively. Saturation was reached for higher vibrogram stimulus intensities. Comparing the output for each test frequency before reaching saturation, i. e., for vibrogram stimulus intensities up to 75 dB, the difference between the Samba Hi and the Samba Lo audio processor was very small varying between -1.2 dB (higher output by Samba Lo) and 4.6 dB (higher output by Samba Hi).

It can be seen from Figure 18.2 that the output varied with vibrogram stimulus frequency. This frequency dependent output is illustrated in Figure 18.3 for the Samba Hi and Lo audio processors and a vibrogram stimulus intensity of 70 dB. The output had a minimum at 1000 Hz and increased towards lower and higher frequencies. The vibrogram amplification settings as used in the fitting software during vibrogram measurements followed the same frequency dependency as shown in Figure 18.4. The minimum amplification was 32 dB

²Brüel & Kjær Sound & Vibration Measurement A/S, Nærum, Denmark

³Brüel & Kjær Sound & Vibration Measurement A/S, Nærum, Denmark

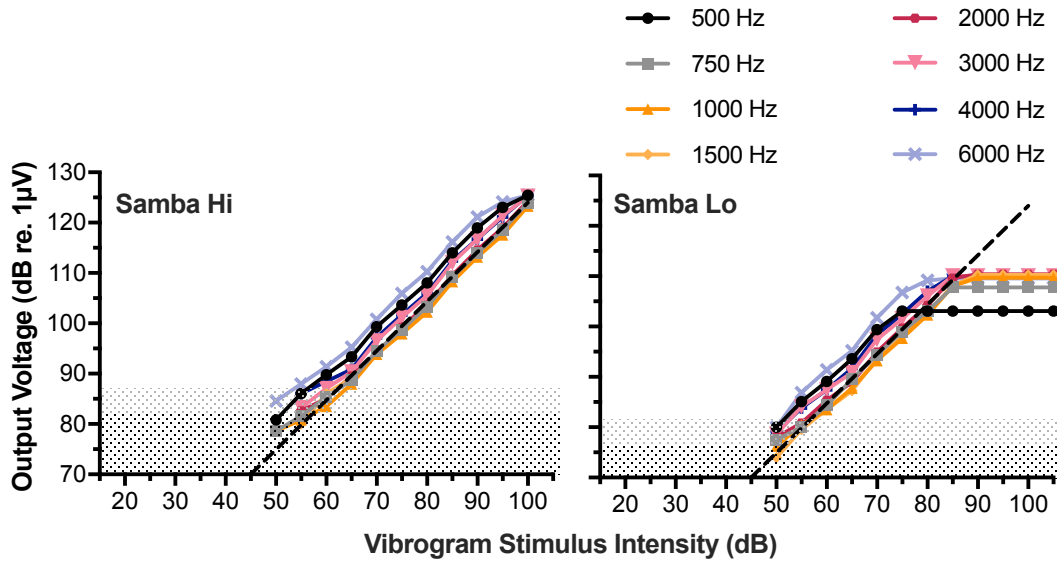


FIGURE 18.2. Vibrogram input-output function of Samba Hi and Samba Lo audio processors measured with the implant-in-the-box. The dashed line illustrates a linear function with a slope of 1 dB VL/1 dB. The dotted area represents the (frequency dependent) noise floor. For the Samba Lo audio processor, saturation of the output level occurred frequency dependent between 75 dB and 85 dB vibrogram stimulus intensity.

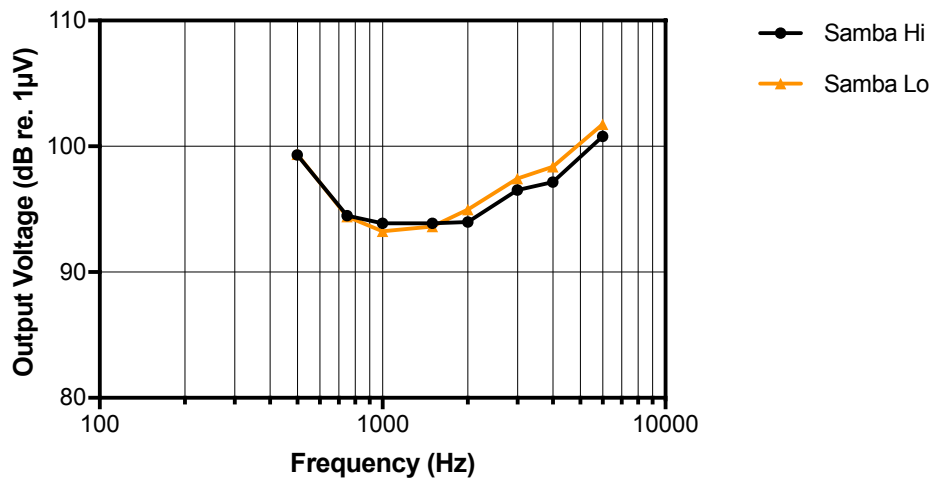


FIGURE 18.3. Output level as a function of vibrogram stimulus frequency measured for Samba Hi and Lo audio processors at a vibrogram stimulus intensity of 70 dB. For a constant vibrogram stimulus intensity, the output had a minimum around 1000 Hz and increased towards lower and higher frequencies.

at 1250 Hz for the Samba Lo and 18 dB at 1250 Hz for the Samba Hi. Towards lower and higher frequencies, the amplification increased.

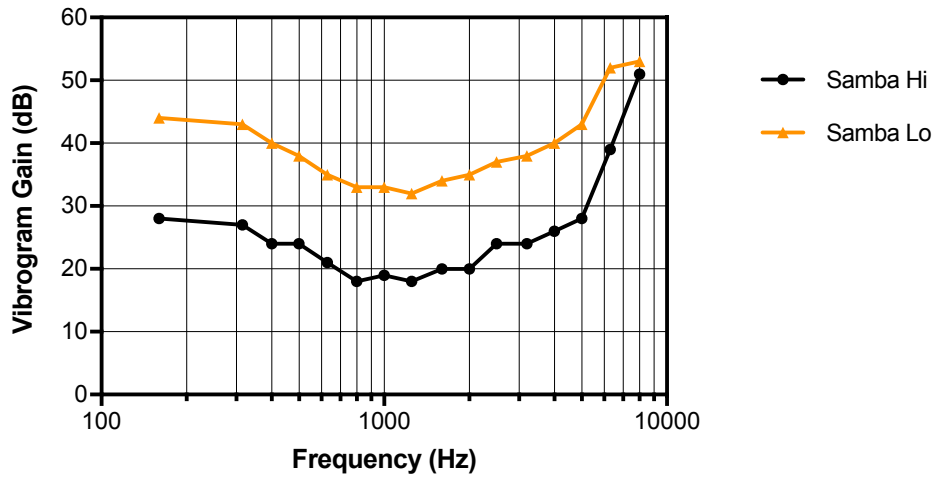


FIGURE 18.4. Vibrogram gain settings for Samba Hi and Samba Lo audio processors as used in the fitting software during the vibrogram measurement. The gain had a minimum at 1250 Hz and increased towards lower and higher frequencies.

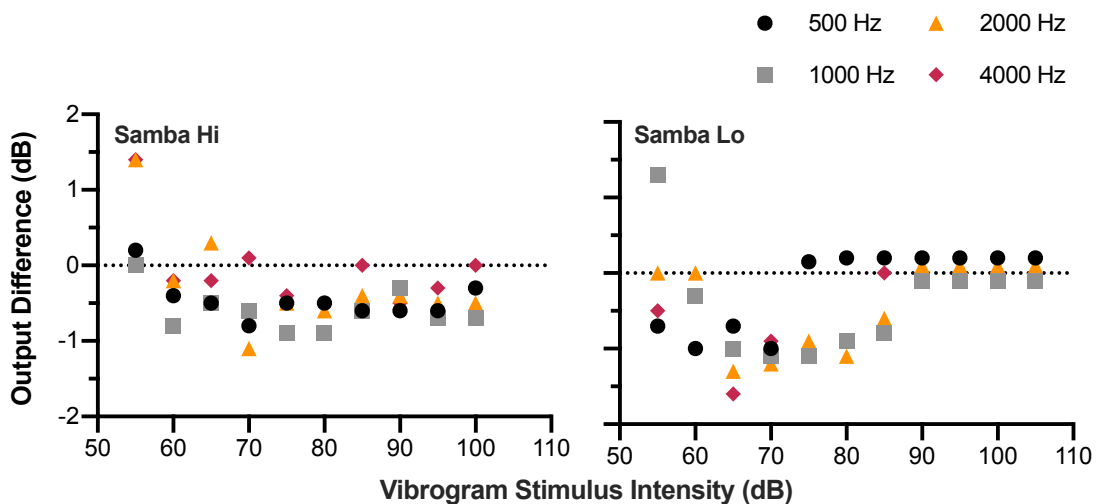


FIGURE 18.5. Vibrogram output difference between two Samba Hi and two Samba Lo audio processors. The differences were below 2 dB for both types of audio processors at all vibrogram stimulus intensities and frequencies.

18.2.2. Vibrogram Input-Output Function of Audio Processors of the Same Type

The difference between the output of two Samba Hi and two Samba Lo audio processors is shown for various vibrogram stimulus intensities in Figure 18.5. The absolute differences were very small with a maximum of 1.4 dB at 4000 Hz and 55 dB vibrogram stimulus intensity for the Samba Hi comparison and 1.6 dB at 4000 Hz and 65 dB vibrogram stimulus intensity for the Samba Lo comparison. For the Samba Lo comparison, the difference between the audio processors was constant when saturation was reached.

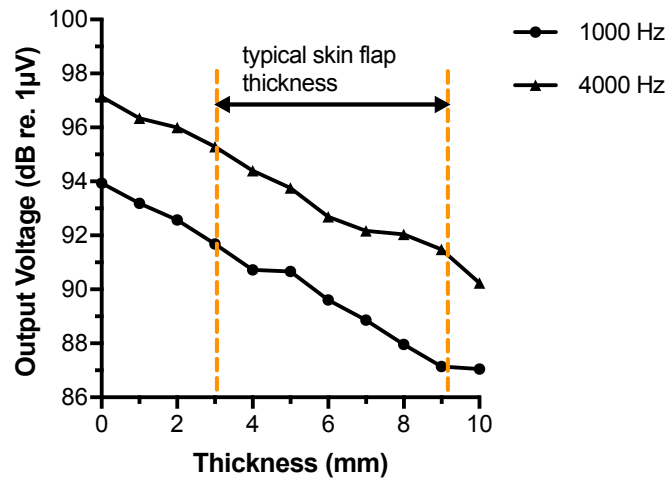


FIGURE 18.6. Vibrogram output for skin flap thicknesses between 0 mm and 10 mm measured for 1000 Hz and 4000 Hz at a vibrogram stimulus intensity of 70 dB. The vertical orange lines mark the clinically typical skin flap thicknesses between 3 mm and 9 mm. The output decreased linearly with increasing distance between the transmitter and receiver coil.

18.2.3. Vibrogram Input-Output Function for Varying Skin Flap Thickness

The influence of the distance between the transmitter and receiver coil, i. e., the skin flap thickness, on the transmitted voltage is shown in Figure 18.6 for vibrogram frequencies of 1000 Hz and 4000 Hz at a stimulus intensity of 70 dB. The output decreased linearly with increasing distance. The output difference between 3 mm and 9 mm, i. e., for typical skin flap thicknesses, was 4.5 dB for 1000 Hz and 3.8 dB for 4000 Hz.

18.2.4. Inherent Noise of Samba Hi and Samba Lo

The ambient sound pressure in the sound proof booth was 20 dB SPL. With the Samba Lo, the noise recorded with the implant-in-the-box was only 0.7 dB above the ambient sound pressure at 20.7 dB SPL. For the Samba Hi, the noise was 34.3 dB SPL. The inherent noise produced by the Samba Hi audio processor in the vibrogram setting was therefore 13.6 dB higher than for the Samba Lo.

18.3. Discussion

Since the underlying technical specifications of the vibrogram measurement procedure were not published by the manufacturer, the data obtained from the measurements presented in this study are the only available data. However, it is crucial to investigate the technical details of the vibrogram measurement procedure, because the vibrogram thresholds are the substantial basis for the clinical studies presented in Parts 2 and 3. Linearity, output difference between the Samba Hi and Samba Lo audio processors as well as audio processors of the same type and the influence of the skin flap thickness are of particular interest.

The results of the input-output function measurements have shown that the output level for both audio processors increased linearly with increasing vibrogram stimulus intensity. However, saturation occurred with the Samba Lo audio processor at 75 dB vibrogram stimulus intensity for 500 Hz, 80 dB for 6000 Hz, and 85 dB for the other test frequencies.

Thus, the output level did not increase for higher vibrogram stimulus intensities even though the vibrogram stimulus intensities were active and selectable in the software. This could have significant consequences for the measurement of vibrogram thresholds and the assessment of coupling dissipation in patients. While the audiologist must assume that the output level increases linearly up to the maximum available stimulus intensity, this is not realized when the Samba Lo audio processor is connected. Therefore, the vibrogram threshold could be considerably overestimated as being higher than the measurement limit while it is actually only higher than the saturation stimulus intensity.

The results from the input-output measurement also revealed that the audio processors' output voltage was dependent on vibrogram stimulus frequency with a minimum at 1000 Hz and higher output voltage for lower and higher frequencies. Thus, higher voltage is transmitted to the FMT at low and high frequencies to achieve hearing levels for a certain vibrogram stimulus intensity. On the one hand, this reflects the FMT resonance characteristics with its resonance frequency around 1000 Hz. For lower and higher frequencies higher voltage is needed to achieve the same vibration amplitude. On the other hand, this also reflects the threshold of normal hearing (ISO 389-1:2017) showing that higher sound pressure levels are necessary at frequencies lower and higher than 1000 Hz to reach auditory perception. This theory is supported by the fact that the amplification parameters which underly the vibrogram measurements and which are saved in the software showed the same frequency dependent pattern as the output measured from the audio processors directly and the RETSPL values themselves (see Figure 18.4). The observed frequency dependent output of the audio processors in the vibrogram mode might therefore be a combination of the two relations, the FMT's frequency response and the frequency dependent threshold of normal hearing, defining the calibration paradigm of the vibrogram measurement.

The difference between two audio processors of the same type was calculated as the difference between the input-output functions from two Samba Hi and two Samba Lo audio processors at 500 Hz, 1000 Hz, 2000 Hz, and 4000 Hz and were shown to be very small. The differences were below 2 dB for all vibrogram stimulus intensities. Thus, it can be assumed that the output of audio processors of the same kind is very consistent and comparable so that differences in vibrogram thresholds due to variable audio processor outputs cannot be expected. This provides the basis for qualitative data collection in different centers and for comparing results of different studies.

The technical investigations of this study also addressed the question of the influence by the distance between the audio processor's transmitter and the implant's receiver coil, i. e., the influence of the skin flap thickness. As discussed briefly before in Chapter 16, the design of radio frequency links for power and signal transmission in auditory implants is a complex problem and many factors have to be considered and optimized. The results from this study were obtained in a simplified experimental set-up and can only be used to qualitatively assess the influence of skin flap thickness during vibrogram measurements. However, the set-up can be considered to give adequate results on the magnitude of output differences depending on coil spacing. It was found that the output difference between the minimum and maximum skin flap thickness usually observed in patients was 4.5 dB for 1000 Hz. This is less than the 5 dB uncertainty of psychoacoustic threshold measurements in general and therefore not relevant for vibrogram threshold measurements. In the clinical studies, the error introduced by skin flap thickness was a systematic error cancelling within a patient data set, because it applied during the intraoperative as well as the postoperative measurement. The variation due to skin flap thickness would only be relevant in terms of coupling dissipation, as the vibrogram threshold is then related to the BC thresholds.

However, due to its small absolute magnitude it is irrelevant in typical clinical conditions. Caution is only necessary in cases of massive swelling over the implant as could be the case in very short-term revision surgeries.

The measurement of the audio processors' inherent noise as it was done in this study was only qualitative, as the signal was measured by the implant-in-the-box and headphones. However, the measurements allow for a relative comparison between the Samba Hi and Samba Lo. It was revealed that the Samba Hi's noise was considerably higher compared to the Samba Lo by 13.6 dB. This result is supported by the results of the input-output functions illustrated in Figure 18.2 where the noise floor was substantially higher for the Samba Hi compared to Samba Lo. While the Samba Lo has been shown to have a limited output during the vibrogram measurement which can lead to overestimation of thresholds, the Samba Hi's inherent noise can lead to unintended masking of thresholds in patients with good coupling and low BC thresholds close to the threshold of normal hearing or the inherent noise level. In practice, this would also cause overestimation of the vibrogram thresholds since the true thresholds would be masked.

18.4. Conclusions

The investigations of the technical principles of the vibrogram revealed relations crucial for the measurement of vibrogram thresholds in clinical practice and for the interpretation of the clinical study results in this thesis. It was revealed that the output of the Samba Lo audio processor is limited to 75 dB vibrogram stimulus intensity at 500 Hz, 80 dB at 6000 Hz, and 85 dB at the other vibrogram frequencies. Nevertheless, higher vibrogram stimulus intensities are selectable in the software without warning despite the serious consequences for threshold measurements in patients. The inherent noise of the audio processors could not be quantified in this study but relative measurements showed that the noise for the Samba Hi was 13.6 dB higher than for the Samba Lo. This could lead to unintended masking during vibrogram threshold measurements with the Samba Hi in patients with good coupling and low BC thresholds. Thus, the dynamic range of the vibrogram measurement has a lower limit for the Samba Hi audio processor due to inherent noise but an upper limit for the Samba Lo audio processor due to limited output. This has to be considered by the examiner during testing of VSB patients. Up to the saturation level, a linear input-output function was observed and differences between the output of Samba Hi and Samba Lo were negligible. This also applies to output differences between audio processors of the same type. Moreover, the influence of skin flap thickness was found to be small and negligible for typical thicknesses between 3 mm and 9 mm.

Part 5

Discussing the Objective Measurement of the Floating Mass Transducer Coupling Dissipation

The problem of objective determination of the FMT coupling dissipation in VSB patients is very complex and requires not only a reliable clinical study but also a detailed technical investigation of experimental the set-up used to provide stimulation via the implanted VORP. In order to solve the problem the following questions have to be answered: How do we transmit the stimuli? How do we calibrate the set-up? What exactly do we measure, considering possible limitations?

The problem was approached in this thesis by using two different experimental set-ups and following two different calibration procedures. Stimuli were transmitted to provide stimulation via the implant by a MiniTek wireless streamer and a Samba audio processor in the first approach and by an AP404 with the sound tube of insert earphones attached to its microphone in the second approach. Besides the clinical results, both set-ups were investigated for their technical properties and all functions which are relevant for proper interpretation of the clinical data as well as for proper handling of the set-ups were examined. Further, the basis of all calculations and relations, the vibrogram, was examined to overcome missing technical documentation of the procedure and its calibration.

The results from the clinical studies showed that both the Samba and MiniTek and the AP404 with the insert earphone sound tube were feasible for signal transmission and therefore for providing stimulation via the implant for recording of VSB evoked AEPs. However, only the set-up with the AP404 proved feasible to quantify coupling dissipation. The calibration approach with this set-up was a direct and mechanical approach by eliminating additional factors such as a wireless streamer and using calibrated equipment, i. e., insert earphones (standard audiometric transducers). With the Samba and MiniTek, no significant correlation between the vibrogram and the thresholds measured in the experimental set-up was observed and the VSB evoked ASSR thresholds accumulated between 20 and 40 dB nHL. The calibration as initially intended was not possible. A standard (fixed) programming of the Samba to maximum amplification was chosen in this approach aiming for the deduction of calibration factors. A direct calibration as with the AP404 was not possible due to the unknown transmission of the MiniTek. Thus, the calibration approach was very different for the two methods with the more direct calibration proving advantageous.

The reasons for the failure of the ASSR method could not be identified in detail. The accumulation of the VSB evoked ASSR thresholds suggested the existence of upper and lower limits, i. e., a limited dynamic range. However, the upper stimulation limit identified by the measurement of the input-output function was not in line with the upper limit of data accumulation. The lower stimulation limit seems to be the more important factor, since the relationship between the vibrogram and VSB evoked ASSR thresholds indicated that the measurement of lower ASSR thresholds is a prerequisite in order for the calibration approach to work. Figure 7.1 and Equation (8) show that very high vibrogram thresholds correspond to medium VSB evoked ASSR thresholds and medium vibrogram thresholds correspond to low ASSR thresholds. With the lower limit, the calibration approach in this method was not feasible. It was assumed that the lower limit is due to inherent noise of the Samba Hi audio processor. The noise level could not be quantified but was qualitatively examined and shown to be considerably higher than in a Samba Lo audio processor (see Chapter 18). The fixed uniform setting of the Samba Hi audio processor did not fit the individual requirements in all patients and low ASSR thresholds in the set-up were probably masked by inherent noise of the audio processor so that the calibration failed.

A lower limit could not be identified with the other set-up, the AP404 with the insert earphone sound tube. VSB evoked ABR thresholds as low as 0 dB nHL could be measured in the clinical study. However, an upper limit does exist and was found to be dependent on frequency and programming of the AP404 as shown by the input-output function. Nevertheless, this set-up proved feasible in the clinical study. The upper stimulation limit around 35 dB nHL ABR stimulus intensity was not crucial, as VSB evoked ABR thresholds directly corresponded to the 3PTA coupling dissipation and values lower than 20 dB are aimed at in clinical conditions.

The output of the Samba Hi and the AP404 saturated at the same level of 187 dB VL. This suggests that the upper limit in the Samba and MiniTek set-up was not necessarily caused by the MiniTek, as it was not higher in the AP404 set-up without a wireless streamer. However, the stimulus intensities at which saturation occurred were different in the two set-ups. With the Samba and MiniTek it was at 55 dB nHL ASSR stimulus intensity and with the AP404 with the insert earphones it was between 35 dB nHL and 45 dB nHL ABR stimulus intensity, depending on stimulus frequency and programming of the AP404. The different results show that the limitation cannot be attributed to the measurement method, i.e, the recording of the output voltage with the implant-in-the-box. Measurements are most likely not quantitative but this method gives reliable qualitative/relative results. The reasons for the different stimulus intensities at which saturation occurred remain unknown. Considering that the stimulus intensity transmitted by the MiniTek is unknown and the stimulus intensity at the AP404 microphone membrane is potentially higher due to neglect of the 2 cm^3 cavity of an acoustic coupler normally used for calibration (compare discussion in Part 3), the comparison of saturation stimulus intensities for the two different set-ups is difficult and does not lead to a better understanding of the technical properties. It is rather important to know the stimulus intensities at which saturation occurs for the individual method and consider saturation during AEP recording.

It was also observed, that the output of the AP404 with the attached insert earphone sound tube was frequency dependent. For the Samba and MiniTek, the output was independent of frequency. While this comparison is between audio processors of different types, it still supports the theory that this behavior was not caused by the AP404 itself but rather by the sound tube. The tube acts as a mechanical filter with a high-pass characteristic. This is not desirable but considering that calibration of the set-up with Samba and MiniTek was not possible, this technical drawback of the AP404 with the sound tube is a minor limitation of the method. However, this is another reason to exclude 500 Hz from the analysis in the clinical study.

The Samba and MiniTek are technically superior with respect to artifacts and false negative responses. For the AP404, the artifacts were recorded with the audio processor programmed to maximum amplification to identify the maximum possible artifacts. The same setting of AP404 and Samba (maximum amplification) makes the results comparable. The artifacts from the AP404 with the insert earphones were considerably higher in amplitude and artifact thresholds were lower compared to Samba and MiniTek. This resulted in false positive thresholds at stimulus intensities as low as 0 dB nHL with the AP404 when ASSRs were recorded using a patient simulator. The reasons for this different behavior are unknown but the consequence is that ASSRs cannot be recorded with the AP404 set-up.

The frequency dependent output of the AP404 with the sound tube and the signal transmission characteristics have shown that alternative stimuli are necessary to determine the coupling dissipation at 500 Hz. Clinically, the broad distribution of coupling dissipation

(see Figure 12.3) has shown that this would be highly desirable. As discussed before, the approach of Cebulla et al. (2017) is feasible for designing chirp stimuli specific to the signal chains, i. e., the individual experimental set-up for recording VSB evoked AEP. Signal transmission is not crucial for the ASSR, as the automated analysis is done in the frequency domain. Nevertheless, improved stimuli could enhance the signal to noise ratio and improve accuracy. However, for ABR recordings, where the analysis is done by the examiner, an improved signal to noise ratio would help substantially to identify wave V and therefore determine the response threshold (see clinical results of Cebulla et al.).

The results of Chapter 18 are the only available data about the technical properties of Samba Hi and Samba Lo audio processors with respect to the vibrogram measurements. The linearity of the vibrogram could be confirmed here and output differences between Samba Hi and Lo were shown to be small. However, the output limit for the Samba Lo at approximately 85 dB vibrogram stimulus intensity was observed in this study. This is not obvious for audiologists using the software. In the study with the Samba and MiniTek set-up, a Samba Hi was used for vibrogram measurements. The disadvantage with this was the inherent noise of the audio processor so that in the study with the AP404 with a sound tube, a Samba Lo was used for vibrogram measurements. This is principally advantageous to avoid masking of thresholds in patients with relatively good hearing, i. e., BC thresholds close to the noise level and good coupling. However, the procedure can only be used without the risk of false negative results when the output limit is known.

The findings of the technical examinations and the clinical studies with two different set-ups give a better understanding of the complex problem of objective determination of the VSB coupling dissipation. However, further research is required to solve the following challenges. Stimulus transmission has to be improved to allow for the determination of coupling dissipation at 500 Hz. A telemetry function should be integrated in the set-up to exclude false negative results due to inappropriate positioning of the audio processor over the implant. The system should also compensate for transmission loss due to the distance between transmitter and receiver coil. The approach with the AP404 experimental set-up has been shown to be promising and the results from the technical investigations support this conclusion but the existing limitations and drawbacks have to be solved. An experimental study using temporal bone specimens could be conducted to confirm the exact output levels of an experimental set-up by measuring ossicle vibrations by laser doppler vibrometry.

Part 6

Thesis Conclusions

Determining the coupling dissipation of the FMT in patients treated with a VSB middle ear implant became possible after implementation of the vibrogram procedure in the fitting software by the manufacturer. The vibrogram became the basis for the calculation of coupling dissipation. It is now a widely accepted concept for audio processor programming as well as clinical follow-up and quality control. Since coupling dissipation has a strong impact on audiological outcome with the VSB, an objective measurement especially for intraoperative applications is highly desirable. Even though many different approaches have been followed in the past, an objective procedure was not available yet. While custom-made set-ups were reported in the literature, the calibration of the set-ups remained an open question and some measurements were therefore only relative. This thesis aimed to develop a feasible method for the objective quantification of the FMT coupling dissipation by investigating two different methods and considering their technical properties with respect to possible limitations.

ASSR measurements using a Samba audio processor programmed to maximum amplification and a MiniTek wireless streamer for signal transmission have been shown to be feasible for integrity control, since the method was applicable in all patients of the clinical study, but not for quantification of coupling dissipation. No significant correlation between the VSB evoked ASSR thresholds in this set-up could be found except at 4000 Hz. The lower limit of dynamic range due to inherent noise of the audio processor is believed to have caused the accumulation of the threshold data and make calibration of the set-up impossible. Another technical drawback of the method was the limited transmission distance of the MiniTek.

Using an AP404 audio processor programmed to the patient's BC thresholds with the sound tube of insert earphones connected to the single microphone aperture and recording ABRs has been shown to be feasible for measuring coupling dissipation within the accuracy of recording ABRs as a method in general. VSB evoked ABR thresholds have been shown to be a direct indicator for the 3PTA coupling dissipation. Technical drawbacks were the signal transmission with frequency-specific delay times leading to deformation of the original input signals and frequency dependent output of the set-up so that 500 Hz had to be excluded from the analysis. Automated analysis as by ASSR was not possible with this set-up due to stimulation artifacts leading to false positive results.

The linearity of the vibrogram as a basis for all calculations was verified in this thesis. Measurements also revealed limited output of the Samba Lo audio processor which is essential to consider in all vibrogram tests and all future studies.

The results from this thesis have shown that considering advantages and disadvantages of both methods, the AP404 with the attached sound tube has proven to be a simple and robust technical solution which can be used by any audiologist. The method has the potential to help improving quality control during vibroplasty surgery. The objective determination of coupling dissipation with this method can help the surgeon while positioning the FMT or FMT-coupler assembly and can therefore help to avoid revision surgeries.

Future research is necessary to address the technical drawbacks of the method. Signal transmission should be improved by creating set-up specific stimuli which compensate for the frequency-specific delay times in the signal chain. This could provide a solution to determine the coupling dissipation at 500 Hz which would be highly desirable. Future research should also aim at a direct electrical input to an audio processor to develop a set-up similar to the set-ups used in intraoperative electrophysiological testing with cochlear implants. This set-up should also include a telemetry function to ensure proper signal transmission to the implant and avoid false negative results. In a measurement audio

processor of this kind, the chip should be removed so that programming algorithms, i. e., prescription rules, can be bypassed providing a direct and linear signal transmission. The output should be calibrated in temporal bone specimens by measuring ossicle vibrations using laser doppler vibrometry and calibration should be confirmed in a clinical experimental study.

List of Tables

Table 7.1 Patient Characteristics ASSR Study	35
Table 12.1 Patient Characteristics ABR Study	52

List of Figures

Figure 1.1	Human Ear Diagram	6
Figure 2.1	The Central Auditory Pathway and ABR Response	12
Figure 3.1	Vibrant Soundbridge in Situ	15
Figure 3.2	Standard Vibroplasty Couplers	17
Figure 3.3	Vibrogram of a Fictitious Patient	19
Figure 6.1	Experimental Set-Up Using Samba and MiniTek	32
Figure 7.1	BC, Vibrogram, VSB-ASSR _{subj.} , and VSB-ASSR Thresholds	36
Figure 7.2	Relation between VSB-ASSR _{subj.} and VSB-ASSR Thresholds	37
Figure 7.3	Relation between Vibrogram and VSB-ASSR Thresholds	38
Figure 11.1	Experimental Set-Up Using an AP404 Audio Processor with a Sound Tube	47
Figure 12.1	Example for Intraoperative VSB evoked ABR	53
Figure 12.2	Pre- and Postoperative BC Thresholds	53
Figure 12.3	Frequency specific Coupling Dissipation	54
Figure 12.4	Analysis of Intraoperative VSB-ABR and 3PTA Coupling Dissipation ...	55
Figure 12.5	3PTA Coupling Dissipation as Function of the Intraoperative VSB-ABR Subdivided by Coupler	56
Figure 16.1	Set-Up for Visualization of Artifacts from Samba Hi and MiniTek	68
Figure 16.2	Input-Output Function of Samba Hi and MiniTek	69
Figure 16.3	Wireless Signal Transmission Distance of the MiniTek	69
Figure 16.4	Electrical Artifacts from Samba Hi and MiniTek	71
Figure 16.5	False Positive ASSR Thresholds by Samba Hi and MiniTek	72
Figure 17.1	Experimental Implant for Signal Recording	76
Figure 17.2	Set-Up for Visualization of Artifacts from AP404 with Sound Tube	76
Figure 17.3	Input-Output Function of AP404 with Sound Tube	77
Figure 17.4	Input-Output Function of AP404 with Sound Tube for Different Audio Processor Settings	78
Figure 17.5	Signal Transmission of AP404 with Sound Tube and FMT	79
Figure 17.6	Electrical Artifacts from AP404 with Sound Tube	80
Figure 17.7	False Positive ASSR Thresholds by AP404 with Sound Tube	81
Figure 18.1	Set-up for Measurement of Inherent Noise	86

Figure 18.2 Vibrogram Input-Output Function of Samba Hi and Samba Lo.....	87
Figure 18.3 Frequency Dependence of Samba Hi and Samba Lo Vibrogram Input-Output Function.....	87
Figure 18.4 Vibrogram Gain Settings for Samba Hi and Samba Lo	88
Figure 18.5 Vibrogram Output Difference Between Audio Processors of the Same Type	88
Figure 18.6 Vibrogram Output for Varying Skin Flap Thickness.....	89

Bibliography

- Alzheimer, C. Somatoviszzerale Sensibilität. In Speckmann, E., Hescheler, J., and Köhling, R., editors, *Physiologie*. Urban & Fischer, Munich, 5th edition, 2008.
- Ball, G. R., Pombo, A. C., Julian, C. A., Jaeger, E. M., Dietz, T. G., and Katz, B. H. Dual coil floating mass transducers, 1999. URL <https://www.google.ch/patents/US5897486>.
- Bargen, G. A. Chirp-evoked auditory brainstem response in children: A review. *American Journal of Audiology*, 24:573–583, 2015. doi: 10.1044/2015_AJA-15-0016.
- Beleites, T., Bornitz, M., Neudert, M., and Zahnert, T. Die Vibrant Soundbridge als aktives Implantat in der Mittelohrchirurgie. *HNO*, 62:509–519, 2014. doi: 10.1007/s00106-014-2884-7.
- Beltrame, A. M., Martini, A., Prosser, S., Giarbini, N., and Streitberger, C. Coupling the Vibrant Soundbridge to cochlea round window: Auditory results in patients with mixed hearing loss. *Otology & Neurotology*, 30:194–201, 2009. doi: 10.1097/mao.0b013e318180a495.
- Beutner, D., Delb, W., Frenzel, H., Hoppe, U., Hüttenbrink, K. B., Mlynski, R., Limberger, A., Schönweiler, R., Schwab, B., Todt, I., Walger, M., Wesarg, T., Zahnert, T., and Zeh, R. Guideline “implantable hearing aids”– short version: German s2k guideline of the working group of german-speaking audiologists, neurotologists and otologists (ADANO), of the german society of oto-rhino- laryngology, head and neck surgery (DGHNO) in collaboration with the german society of audiology (DGA), the german society of phoniatics and pediatric audiology (DGPP), and patient representatives. *HNO*, 66:71–76, 2018. doi: 10.1007/s00106-018-0533-2.
- Bille, J. and Schlegel, W., editors. *Medizinische Physik*. Springer, Berlin, 1st edition, 1999.
- Boenheim, K., Pok, S.-M., Schloegel, M., and Filzmoser, P. Active middle ear implant compared with open-fit hearing aid in sloping high-frequency sensorineural hearing loss. *Otology & Neurotology*, 31:424–429, 2010. doi: 10.1097/MAO.0b013e3181cabd42.
- Brkic, F. F., Riss, D., Auinger, A., Zoerner, B., Arnoldner, C., Baumgartner, W.-D., Gstoettner, W., and Vyskocil, E. Long-term outcome of hearing rehabilitation with an active middle ear implant. *The Laryngoscope*, 129:477–481, 2019. doi: 10.1002/lary.27513.
- Brooke, R. E., Brennan, S. K., and Stevens, J. C. Bone conduction auditory steady state response: Investigations into reducing artifact. *Ear and Hearing*, 30:23–30, 2009. doi: 10.1097/AUD.0b013e31819144bd.
- Burkard, R. F., editor. *Auditory evoked potentials: Basic principles and clinical application*. Lippincott Williams & Wilkins, Philadelphia, Pa., 2007.

- Butler, C. L., Thavaneswaran, P., and Lee, I. H. Efficacy of the active middle-ear implant in patients with sensorineural hearing loss. *The Journal of Laryngology & Otology*, 127: 8–16, 2013. doi: 10.1017/S0022215113001151.
- Byrne, D. and Tonisson, W. Selecting the gain of hearing aids for persons with sensorineural hearing impairments. *Scandinavian Audiology*, 5:51–59, 1976. doi: 10.3109/01050397609043095.
- Byrne, D., Dillon, H., Ching, T., Katsch, R., and Keidser, G. NAL-NL1 procedure for fitting nonlinear hearing aids: Characteristics and comparisons with other procedures. *Journal of the American Academy of Audiology*, 12:37–51, 2001.
- Békésy, G. v. *Experiments in hearing*. McGraw-Hill, New York, 1960.
- Canale, A., Dagna, F., Cassandro, C., Giordano, P., Caranzano, F., Lacilla, M., and Albera, R. Oval and round window vibroplasty: a comparison of hearing results, risks and failures. *European Archives of Oto-Rhino-Laryngology*, 271:2637–2640, 2014. doi: 10.1007/s00405-013-2752-1.
- Cebulla, M., Stürzebecher, E., and Elberling, C. Objective detection of auditory steady-state responses: Comparison of one-sample and q-sample tests. *Journal of the American Academy of Audiology*, 17:93–103, 2006. doi: 10.3766/jaaa.17.2.3.
- Cebulla, M., Geiger, U., Hagen, R., and Radeloff, A. Device optimised chirp stimulus for abr measurements with an active middle ear implant. *International Journal of Audiology*, 56:607–611, 2017. doi: 10.1080/14992027.2017.1314558.
- Chittka, L. and Brockmann, A. Perception Space – The Final Frontier, February 2009. CC BY 2.5.
- Cho, S.-W., Han, K.-H., Jang, H.-K., Chang, S., Jung, H., and Lee, J. Auditory brainstem responses to CE-chirp stimuli for normal ears and those with sensorineural hearing loss. *International Journal of Audiology*, 54:700–704, 2015. doi: 10.3109/14992027.2015.1043148.
- Colletti, V., Soli, S. D., Carner, M., and Colletti, L. Treatment of mixed hearing losses via implantation of a vibratory transducer on the round window. *International Journal of Audiology*, 45:600–608, 2006. doi: 10.1080/14992020600840903.
- Colletti, V., Mandala, M., and Colletti, L. Electrocochleography in round window Vibrant Soundbridge implantation. *Otolaryngology – Head and Neck Surgery*, 146:633–640, 2012. doi: 10.1177/0194599811430808.
- Cornelisse, L. E., Seewald, R. C., and Jamieson, D. G. The input/output formula: A theoretical approach to the fitting of personal amplification devices. *The Journal of the Acoustical Society of America*, 97:1854–1864, 1995. doi: 10.1121/1.412980.
- Dau, T., Wegner, O., Mellert, V., and Kollmeier, B. Auditory brainstem responses with optimized chirp signals compensating basilar-membrane dispersion. *The Journal of the Acoustical Society of America*, 107:1530–1540, 2000. doi: 10.1121/1.428438.
- Dunn, F., Hartmann, W., Campbell, D., Fletcher, N., and Rossing, T. *Handbook of Acoustics*. Springer Verlag, Berlin, 2nd edition, 2015.
- Eggermont, J. Electric and magnetic fields of synchronous neural activity. In Burkard, R. F., editor, *Auditory evoked potentials*, pages 73–101. Lippincott Williams & Wilkins,

Philadelphia, Pa., 2007.

- Elberling, C. and Don, M. A direct approach for the design of chirp stimuli used for the recording of auditory brainstem responses. *Journal of the American Academy of Audiology*, 128:2955–2964, 2010. doi: 10.1121/1.3489111.
- Elberling, C., Don, M., Cebulla, M., and Stürzebecher, E. Auditory steady-state responses to chirp stimuli based on cochlear traveling wave delay. *Journal of the American Academy of Audiology*, 122:2772–2785, 2007. doi: 10.1121/1.2783985.
- Fedtke, T. and Hensel, J. Determination of peak-to-peak equivalent reference equivalent threshold sound pressure levels for an audiometric headphone, for ten different test signals of short duration: Report. Physikalisch-Technische Bundesanstalt, 2008.
- Fedtke, T. and Richter, U. Reference zero for the calibration of air-conduction audiometric equipment using tone bursts as test signals. *International Journal of Audiology*, 46:1–10, 2007. doi: 10.1080/14992020500060230.
- Fisch, U., Cremers, W. R. J., Lenarz, T., Weber, B., Babighian, G., Uziel, A. S., Proops, D. W., O'Connor, A. F., Charachon, R., Helms, J., and Fraysse, B. Clinical experience with the Vibrant Soundbridge implant device. *Otology & Neurotology*, 22:962–972, 2001. doi: 10.1097/00129492-200111000-00042.
- Fröhlich, L., Rahne, T., Plontke, S. K., Oberhoffner, T., Dziemba, O., Gadyuchko, M., Hoth, S., Mir-Salim, P., and Müller, A. Intraoperative recording of auditory brainstem responses for monitoring of floating mass transducer coupling efficacy during revision surgery — proof of concept. *Otology & Neurotology*, 41:e168–e171, 2019. doi: 10.1097/MAO.0000000000002511.
- Geiger, U., Radeloff, A., Hagen, R., and Cebulla, M. Intraoperative estimation of the coupling efficiency and clinical outcomes of the Vibrant Soundbridge active middle ear implant using auditory brainstem response measurements. *American Journal of Audiology*, 28:553–559, 2019. doi: 10.1044/2019_AJA-18-0066.
- Ghoncheh, M., Lenarz, T., and Maier, H. A precision driver device for intraoperative stimulation of a bone conduction implant. *Scientific Reports*, 10:1797, 2020. doi: 10.1038/s41598-020-58512-7.
- Gorga, M. P., Neely, S. T., Hoover, B. M., Dierking, D. M., Beauchaine, K. L., and Manning, C. Determining the upper limits of stimulation for auditory steady-state response measurements. *Ear and Hearing*, 25:302–307, 2004. doi: 10.1097/01.AUD.0000130801.96611.6B.
- Gorga, M., Johnson, T., Kaminski, J., Beauchaine, K., Garner, C., and Neely, S. Using a combination of click- and tone burst-evoked auditory brainstem response measurements to estimate pure-tone thresholds. *Ear and Hearing*, 27:60–74, 2006. doi: 10.1097/01.aud.0000194511.14740.9c.
- Gøtsche-Rasmussen, K., Poulsen, T., and Eberling, C. Reference hearing threshold levels for chirp signals delivered by an ER-3A insert earphone. *International Journal of Audiology*, 51:794–799, 2012. doi: 10.3109/14992027.2012.705901.
- Hall, J. *Introduction to Audiology Today*. Pearson, New York, 1st edition, 2013.

- Herdman, A. T. and Stapells, D. R. Auditory steady-state response thresholds of adults with sensorineural hearing impairments: Umbrales de las respuestas auditivas de estado estable en adultos con hipoacusia sensorineural. *International Journal of Audiology*, 42: 237–248, 2009. doi: 10.3109/14992020309078343.
- Hochmair, E. S. System optimization for improved accuracy in transcutaneous signal and power transmission. *IEEE Transactions on Biomedical Engineering*, BME-31:177–186, 1984. doi: 10.1109/TBME.1984.325404.
- Hoth, S. Medizinische Akustik und Audiologie. In Bille, J. and Schlegel, W., editors, *Medizinische Physik*. Springer, Berlin, 1st edition, 1999.
- Hoth, S. Audiometrie – Die Untersuchung des Gehörs und seine technische Versorgung. In Kramme, R., editor, *Medizintechnik*. Springer, Heidelberg, 3rd edition, 2007.
- Hoth, S. and Lenarz, T. *Elektrische Reaktionsaudiometrie*. Springer, Berlin, 1994.
- Hoth, S., Mühler, R., Neumann, K., and Walger, M. *Objektive Audiometrie im Kindesalter*. Springer Verlag, Berlin, Heidelberg, 2015.
- Huber, A. M., Mlynski, R., Muller, J., Dillier, N., Holzmann, D., Wolframm, M. D., and Hagen, R. A new vibroplasty coupling technique as a treatment for conductive and mixed hearing losses: A report of 4 cases. *Otology & Neurotology*, 33:613–617, 2012. doi: 10.1097/MAO.0b013e31824bae6e.
- IEC 60645-3:2007. Electroacoustics - audiometric equipment - part 3: Test signals of short duration. IEC, Geneva.
- ISO 389-1:2017. Acoustics - Reference zero for the calibration of audiometric equipment - Part 1: Reference equivalent threshold sound pressure levels for pure tones and supra-aural earphones. ISO, Geneva.
- ISO 389-3:2016. Acoustics - Reference zero for the calibration of audiometric equipment - Part 3: Reference equivalent threshold vibratory force levels for pure tones and bone vibrators. ISO, Geneva.
- ISO 389-6:2007. Acoustics - reference zero for the calibration of audiometric equipment - part 6: Reference threshold of hearing for test signals of short duration. ISO, Geneva.
- ISO 8253-1:1989. Acoustics - Audiometric test methods - Part 1: Pure-tone air and bone conduction audiometry. ISO, Geneva.
- Jenderka, K.-V. and Fedtke, T. Hörschwellen für die objektive Audiometrie. *PTB Mitteilungen*, 117:23–26, 2007.
- Keidser, G., Dillon, H., Flax, M., Ching, T., and Brewer, S. The NAL-NL2 prescription procedure. *Audiology Research*, 1:88–90, 2011. doi: 10.4081/audiores.2011.e24.
- Klinke, R. Hören und Sprechen: Kommunikation des Menschen. In Klinke, R., Pape, H.-C., Kurtz, A., and Silbernagl, S., editors, *Physiologie*. Thieme, Stuttgart, 6th edition, 2010.
- Korczak, P., Smart, J., Delgado, R., Strobel, T. M., and Bradford, C. Auditory steady-state responses. *Journal of the American Academy of Audiology*, 23:146–170, 2012. doi: 10.3766/jaaa.23.3.3.
- Lee, H.-J., Lee, J. M., Choi, J. Y., and Jung, J. Evaluation of maximal speech intelligibility with Vibrant Soundbridge in patients with sensorineural hearing loss. *Otology &*

- Neurotology*, 38:1246–1250, 2017. doi: 10.1097/MAO.0000000000001537.
- Lehnhardt, E. and Laszig, R. *Praxis der Audiometrie*. Thieme, Stuttgart, 8th edition, 2001.
- Lynch, P. and Jaffe, C. Human brain coronal section, December 2016. CC BY 2.5.
- Mandala, M., Colletti, L., and Colletti, V. Treatment of the atretic ear with round window Vibrant Soundbridge implantation in infants and children: Electrocochleography and audiologic outcomes. *Otology & Neurotology*, 32:1250–1255, 2011. doi: 10.1097/MAO.0b013e31822e9513.
- Marino, R., Lampacher, P., Dittrich, G., Tavora-Vieira, D., Kuthubutheen, J., and Rajan, G. P. Does coupling and positioning in vibroplasty matter? A prospective cohort study. *Otology & Neurotology*, 36:1223–1230, 2015. doi: 10.1097/MAO.0000000000000790.
- McCreery, R., Kaminski, J., Beauchaine, K., Lenzen, N., Simms, K., and Gorga, M. The impact of degree of hearing loss on auditory brainstem response predictions of behavioral thresholds. *Ear and Hearing*, 36:309–319, 2015. doi: 10.1097/AUD.0000000000000120.
- Mlynski, R., Mueller, J., and Hagen, R. Surgical approaches to position the Vibrant Soundbridge in conductive and mixed hearing loss. *Operative Techniques in Otolaryngology-Head and Neck Surgery*, 21, 2010. doi: 10.1016/j.otot.2010.10.006.
- Mlynski, R., Dalhoff, E., Heyd, A., Wildenstein, D., Hagen, R., Gummer, A. W., and Schraven, S. P. Reinforced active middle ear implant fixation in incus vibroplasty. *Ear and Hearing*, 36:72–81, 2015a. doi: 10.1097/AUD.0000000000000078.
- Mlynski, R., Dalhoff, E., Heyd, A., Wildenstein, D., Rak, K., Radeloff, A., Hagen, R., Gummer, A. W., and Schraven, S. P. Standardized active middle-ear implant coupling to the short incus process. *Otology & Neurotology*, 36:1390–1398, 2015b. doi: 10.1097/MAO.0000000000000822.
- Mühler, R. Zur Terminologie der stationären Potenziale des auditorischen Systems. *HNO*, 60:421–426, 2012. doi: 10.1007/s00106-011-2382-0.
- Mühler, R., Ziese, M., and Hoth, S. Patientensimulatoren zur Überprüfung von FAEP-Systemen. *Zeitschrift für Audiologie*, 53:158–160, 2014.
- Müller, A., Mir-Salim, P., Zellhuber, N., Helbig, R., Bloching, M., Schmidt, T., Koscielny, S., Dziemba, O. C., Plontke, S. K., and Rahne, T. Influence of floating-mass transducer coupling efficiency for active middle-ear implants on speech recognition. *Otology & Neurotology*, 38:809–814, 2017. doi: 10.1097/MAO.0000000000001412.
- Oliver, D. and Fakler, B. Auditorisches System. In Speckmann, E., Hescheler, J., and Köhling, R., editors, *Physiologie*. Urban & Fischer, Munich, 5th edition, 2008.
- Ozdek, A., Karacay, M., Saylam, G., Tatar, E., Aygener, N., and Korkmaz, M. H. Comparison of pure tone audiometry and auditory steady-state responses in subjects with normal hearing and hearing loss. *European Archives of Oto-Rhino-Laryngology*, 267: 43–49, 2010. doi: 10.1007/s00405-009-1014-8.
- Park, Y. A., Kong, T. H., Chang, J. S., and Seo, Y. J. Importance of adhesiolysis in revision surgery for Vibrant Soundbridge device failures at the short incus process. *European Archives of Oto-Rhino-Laryngology*, 274:3867–3873, 2017. doi: 10.1007/s00405-017-4715-4.

- Picton, T. W. and John, S. M. Avoiding electromagnetic artifacts when recording auditory steady-state responses. *Journal of the American Academy of Audiology*, 15:541–554, 2004. doi: 10.3766/jaaa.15.8.2.
- Picton, T. Audiometry using auditory steady-state responses. In Burkard, R. F., editor, *Auditory evoked potentials*, pages 441–459. Lippincott Williams & Wilkins, Philadelphia, Pa., 2007.
- Radeloff, A., Shehata-Dieler, W., Rak, K., Scherzed, A., Tolsdorff, B., Hagen, R., Mueller, J., and Mlynski, R. Intraoperative monitoring of active middle ear implant function in patients with normal and pathologic middle ears. *Otology & Neurotology*, 32:104–107, 2011. doi: 10.1097/MAO.0b013e3181fcf167.
- Rahne, T. Physikalisch-audiologische Grundlagen implantierbarer Hörsysteme: Über Energieübertragung, Ankopplung und Ausgangsleistung. *HNO*, 2019. doi: 10.1007/s00106-019-00776-1.
- Rahne, T. and Plontke, S. K. Apparative Therapie bei kombiniertem Hörverlust: Ein audiologischer Vergleich aktueller Hörsysteme. *HNO*, 64:91–100, 2016. doi: 10.1007/s00106-015-0087-5.
- Rahne, T., Skarzynski, P. H., Hagen, R., Radeloff, A., Lassaletta, L., Barbara, M., Plontke, S. K., and Mlynski, R. A retrospective European multicenter analysis of the functional outcomes after active middle ear implant surgery using the third generation vibroplasty couplers. *European Archives of Oto-Rhino-Laryngology*, 2020, in press.
- Raine, C. H., Lee, C. A., Strachan, D. R., Totten, C. T., and Khan, S. Skin flap thickness in cochlear implant patients — a prospective study. *Cochlear Implants International*, 8: 148–157, 2007. doi: 10.1179/cim.2007.8.3.148.
- Richter, U. and Fedtke, T. Reference zero for the calibration of audiometric equipment using clicks as test signals. *International Journal of Audiology*, 44:478–487, 2005. doi: 10.1080/14992020500060230.
- Roger, A. and Thornton, D. Instrumentation and recording parameters. In Burkard, R. F., editor, *Auditory evoked potentials*, pages 73–101. Lippincott Williams & Wilkins, Philadelphia, Pa., 2007.
- Schraven, S. P., Gromann, W., Rak, K., Shehata-Dieler, W., Hagen, R., and Mlynski, R. Long-term stability of the active middle-ear implant with floating-mass transducer technology: A single-center study. *Otology & Neurotology*, 37:252–266, 2016. doi: 10.1097/MAO.0000000000000943.
- Skarzynski, H., Olszewski, L., Skarzynski, P. H., Lorens, A., Piotrowska, A., Porowski, M., Mrowka, M., and Pilka, A. Direct round window stimulation with the Med-El Vibrant Soundbridge: 5 years of experience using a technique without interposed fascia. *European Archives of Oto-Rhino-Laryngology*, 271:477–482, 2014. doi: 10.1007/s00405-013-2432-1.
- Small, S. A. and Stapells, D. R. Artfactual responses when recording auditory steady-state responses. *Ear and Hearing*, 25:611–623, 2004. doi: 10.1097/00003446-200412000-00009.
- Snik, A., Noten, J., and Cremers, C. Gain and maximum output of two electromagnetic middle ear implants: Are real ear measurements helpful? *Journal of the American Academy of Audiology*, 15:249–257, 2004. doi: 10.3766/jaaa.15.3.7.

- Snik, A. F. M. and Cremers, C. W. R. J. Vibrant semi-implantable hearing device with digital sound processing: Effective gain and speech perception. *Archives of Otolaryngology-Head & Neck Surgery*, 127:1433–1437, 2001. doi: 10.1001/archotol.127.12.1433.
- Spiegel, J. L., Kutsch, L., Jakob, M., Weiss, B. G., Canis, M., and Ihler, F. Long-term stability and functional outcome of an active middle ear implant regarding different coupling sites. *Otology & Neurotology*, 41:60–67, 2020. doi: 10.1097/MAO.0000000000002418.
- Stenfelt, S. Acoustic and physiologic aspects of bone conduction hearing. *Oto-Rhino-Laryngology*, 71:10–21, 2011. doi: 10.1159/000323574.
- Stenfelt, S. and Goode, R. Bone-Conducted Sound: Physiological and Clinical Aspects. *Otology & Neurotology*, 26:1245–1261, 2005. doi: 10.1097/01.mao.0000187236.10842.d5.
- Swanepoel, D. W., Ebrahim, S., Friedland, P., Swanepoel, A., and Pottas, L. Auditory steady-state responses to bone conduction stimuli in children with hearing loss. *International Journal of Pediatric Otorhinolaryngology*, 72:1861–1871, 2008. doi: 10.1016/j.ijporl.2008.09.017.
- Taghavi, H., Håkansson, B., and Reinfeldt, S. Analysis and design of RF power and data link using amplitude modulation of class-E for a novel bone conduction implant. *IEEE Transactions on Biomedical Engineering*, 59:3050–3059, 2012a. doi: 10.1109/TBME.2012.2213252.
- Taghavi, H., Håkansson, B., and Reinfeldt, S. A novel bone conduction implant - analog radio frequency data and power link design. In *Biomedical Engineering / 765: Telehealth / 766: Assistive Technologies*, Innsbruck, Austria, 2012b. ACTAPRESS. doi: 10.2316/P.2012.764-054.
- Todt, I. Vibrant Soundbridge. In de Souza, C. and Joshi, S., editors, *Implantable Hearing Devices*, pages 231–239. Plural Publishing, San Diego, 2019.
- Todt, I., Seidl, R. O., Gross, M., and Ernst, A. Comparison of different Vibrant Soundbridge audioprocessors with conventional hearing aids. *Otology & Neurotology*, 23:669–673, 2002. doi: 10.1097/00129492-200209000-00012.
- Truy, E., Philibert, B., and Collet, L. Vibrant Soundbridge versus conventional hearing aid in sensorineural high-frequency hearing loss: A prospective study. *Otology & Neurotology*, 29:684–687, 2008. doi: 10.1097/MAO.0b013e31817156df.
- Tysome, J. R., Moorthy, R., Lee, A., Jiang, D., and Fitzgerald O’Connor, A. Systematic review of middle ear implants: Do they improve hearing as much as conventional hearing aids? *Yearbook of Otolaryngology-Head and Neck Surgery*, 31:131–134, 2011. doi: 10.1016/j.yoto.2011.03.106.
- Ulrich, J. and Hoffmann, E. *Hörakustik: Theorie und Praxis*. DOZ Verlag, Heidelberg, 2nd edition, 2011.
- Uziel, A., Mondain, M., Hagen, P., Dejean, F., and Doucet, G. Rehabilitation for high-frequency sensorineural hearing impairment in adults with the Symphonix Vibrant Soundbridge: A comparative study. *Otology & Neurotology*, 24:775–783, 2003. doi: 10.1097/00129492-200309000-00015.
- Veit, I. *Technische Akustik*. Vogel, Würzburg, 4th edition, 1988.

- Verhaegen, V. J. O., Mulder, J. J. S., Noten, J. F. P., Luijten, B. M. A., Cremers, C. W. R. J., and Snik, A. F. M. Intraoperative auditory steady state response measurements during Vibrant Soundbridge middle ear implantation in patients with mixed hearing loss: Preliminary results. *Otology & Neurotology*, 31:1365–1368, 2010. doi: 10.1097/MAO.0b013e3181f0c612.
- Wang, D., Zhao, S., Zhang, Q., Li, Y., Ma, X., and Ren, R. Vibrant Soundbridge combined with auricle reconstruction for bilateral congenital aural atresia. *International Journal of Pediatric Otorhinolaryngology*, 86:240–245, 2016. doi: 10.1016/j.ijporl.2016.05.006.
- Zwartenkot, J. W., Hashemi, J., and Snik, A. F. M. Active middle ear implantation for patients with sensorineural hearing loss and external otitis: Long-term outcome in patient satisfaction. *Otology & Neurotology*, 34:855–961, 2013. doi: 10.1097/MAO.0b013e31828f47c2.
- Zwartenkot, J. W., Snik, A. F. M., Mylanus, E. A. M., and Mulder, J. J. S. Amplification options for patients with mixed hearing loss. *Otology & Neurotology*, 35:221–226, 2014. doi: 10.1097/MAO.0000000000000258.
- Zwartenkot, J. W., Mulder, J. J. S., Snik, A. F. M., Cremers, C. W. R. J., and Mylanus, E. A. M. Active middle ear implantation: Long-term medical and technical follow-up, implant survival, and complications. *Otology & Neurotology*, 37:513–519, 2016. doi: 10.1097/MAO.0000000000001015.

Comments

- Parts of this thesis have been presented as oral and/or poster presentations at national and international conferences. An invited talk has been given at the annual conference of the DGA (Deutsche Gesellschaft für Audiologie) in Heidelberg 2019.
- Scientific papers about the studies included in this thesis have been published in international journals (see list of publications for details).

Eigenständigkeitserklärung

Hiermit erkläre ich, dass ich die vorliegende Arbeit selbstständig und ohne unzulässige Hilfe Dritter verfasst und nur die angegebenen Quellen und Hilfsmittel verwendet habe. Die aus fremden Quellen direkt oder indirekt übernommenen Daten, Fakten oder Konzepte sind als solche kenntlich gemacht.

Die Arbeit wurde bisher in gleicher oder ähnlicher Form keiner anderen Prüfungskommission vorgelegt.

Halle (Saale), 15.12.2020

Laura Fröhlich

Laura Fröhlich

Curriculum Vitae

Personal Details

Date of birth December 9, 1991
Place of birth Soest, Germany

Professional Experience

since 11/2016 **University hospital Halle, Department of Otorhinolaryngology, Head and Neck Surgery, Research Associate**, Mapping of cochlear implants and other implantable hearing aids, research in auditory evoked potentials, bone conduction hearing and vestibular diagnostics.

Education

11/2016 **Beginning of Advanced Vocational Education for Certification in Medical Physics**, *Deutsche Gesellschaft für Medizinische Physik (DGMP)*, Specialization: clinical audiology.

University

04/2017–12/2020 **PhD**, *Martin Luther University Halle-Wittenberg and University hospital Halle*.

Topic of thesis: „Bridging the Gap – Brainstem Evoked Potential Measurements in Patients with Active Middle Ear Implants“

10/2014–10/2016 **Master of Science (grade: 1.2)**, *Martin Luther University Halle-Wittenberg*, Discipline: Medical Physics, Audiology.

Topic of thesis: „Vibrotactile Thresholds and Bone-conduction Hearing Thresholds: A Comparison of Transducers“ (*grade: 1.0*)

10/2011–09/2014 **Bachelor of Science (grade: 2.0)**, *Martin Luther University Halle-Wittenberg*, Discipline: Medical Physics.

Topic of thesis: „Untersuchung von Nanoporen in dielektrischen low-k Schichten (english: Characterization of porous low k dielectric layers)“ (*grade: 1.1*)

School

08/2002–07/2011 **A-level (grade: 1.5)**, *Aldegrever-Gymnasium Soest*, Advanced courses: Physics, English.

09–12/2008 **High School, New Brunswick, Canada**, *Leo Hayes High School*, Courses: Mathematics, Geography, English, Environmental Science, Arts.

Research Stays and Internships

- 08/2019–
11/2019 **University of Sydney, Vestibular Research Laboratory, Sydney, Australia**, *Research stay*, „Bone conducted vibration and VEMPs – the effect of skull location on the otolithic stimulus“, three months.
- 10/2015 **Chalmers University of Technology, Department of Signals and Systems, Gothenburg, Sweden**, *Research stay*, „Investigation of MRI induced change of the electroacoustic properties in bone conduction hearing implants“, three weeks.
- 02/2015 **University hospital Halle, Department of Otorhinolaryngology, Head and Neck Surgery**, *Internship audiology*, „The effect of contralateral and ipsilateral masking on the ASSR threshold in normal hearing subjects“, three weeks.
- 10/2010 **St. Marien-Hospital, Department of Radiation Therapy, Hamm**, *Internship (voluntary)*, one week.

Honors and Awards

- 12/2019 **Best Poster Award, Co-author**, *OSSEO Conference, Miami*, BC Stimulated VEMP in Patients with Vestibular Schwannoma using B250, Fredén Jansson, K.J., Reinfeldt, S., Håkansson, B., Fröhlich, L., Rahne, T.
- 2019 **Toni-Haid-Reisestipendium (travel grant)**, *Arbeitsgemeinschaft Deutschsprachiger Audiologen, Neurootologen und Otologen (ADANO)*.
- 01/2018 **Anton-Wilhelm-Amo-Preis**, *Martin Luther University Halle-Wittenberg*, Best Master's thesis of the MLU.
- 02/2017 **Nachwuchs-Forschungspreis (junior scientist award)**, *Deutsche Gesellschaft für Audiologie (DGA)*.
- 05/2016 **Vortragspreis (conference presentation award)**, *Spanisch-Deutsche Gesellschaft für Hals-Nasen-Ohrenheilkunde, Kopf- und Hals-Chirurgie (SDGHNO)*.

Halle (Saale), 15.12.2020

Laura Fröhlich

List of Publications

Publications in Peer Reviewed National and International Journals

- 2020 **Fröhlich, L.**, Curthoys, I.S., Kösling, S., Rahne, T., Plontke, S.K. Cervical and Ocular Vestibular-Evoked Myogenic Potentials in Patients With Intracochlear Schwannomas. *Frontiers in Neurology*, 11:549817.
- 2020 Plontke, S.K., Caye-Thomasen, P., Strauss, C., Kösling, S., Götze, G., Siebolts, U., Vordermark, D., Wagner, L., **Fröhlich, L.**, Rahne, T. Management of transmodiolar and transmacular cochleovestibular schwannomas with and without hearing rehabilitation with cochlear implants. *HNO*, online ahead of print.
- 2020 **Fröhlich, L.**, Rahne, T., Plontke, S.K., Oberhoffner, T., Dahl, R., Mlynski, R., Dziemba, O., Aristeidou, A., Gadyuchko, M., Koscielny, S., Hoth, S., Kropp, M.H., Mir-Salim, P., Müller, A. Intraoperative Quantification of Floating Mass Transducer Coupling Quality in Vibrant Soundbridge Middle Ear Implants – A Multicenter Study. *European Archives of Oto-Rhino-Laryngology*, online ahead of print.
- 2020 Plontke, S.K., **Fröhlich, L.**, Cozma, S., Koitschev, A., Reimann, K., Weiß, R.M., Götze, G., Seiwert, I., Kösling, S., Rahne, T. Hearing rehabilitation after subtotal cochleoectomy using a new, perimodiolar malleable, cochlear implant electrode array: a preliminary report. *European Archives of Oto-Rhino-Laryngology*, online ahead of print.
- 2020 **Fröhlich, L.**, Plontke, S.K., Rahne, T. A Quantitative Approach for the Objective Assessment of Coupling Efficiency for an Active Middle Ear Implant by recording Auditory Steady-State Responses. *Otology & Neurotology*, 41:e906-e911.
- 2020 Wagner, L., Plontke, S.K., **Fröhlich, L.**, Rahne, T. Reduced spread of electric field after surgical removal of intracochlear schwannoma and cochlear implantation. *Otology & Neurotology*, 41:e1297-e1303.
- 2020 Plontke, S.K., **Fröhlich, L.**, Wagner, L., Kösling, S., Götze, G., Siebolts, U., Liebau, A., Rahne, T. How much cochlea do you need for cochlea implantation?. *Otology & Neurotology*, 41:694-703.
- 2019 **Fröhlich, L.**, Rahne, T., Plontke, S.K., Oberhoffner, T., Dziemba, O., Gadyuchko, M., Hoth, S., Mir-Salim, P., and Müller, A. Intraoperative Recording of Auditory Brainstem Responses for Monitoring of Floating Mass Transducer Coupling Efficacy During Revision Surgery – Proof of Concept. *Otology & Neurotology*, 41:e168-e171.

- 2019 Wagner, L., Hönig, E., **Fröhlich, L.**, Plontke, S.K., Rahne, T. Optimal retention force of audio processor magnets. *Otology & Neurotology*, 40:e482–e487.
- 2019 Rahne, T., Hocke, T., Strauß, C., Kösling, S., **Fröhlich, L.**, Plontke, S.K. Perioperative recording of cochlear implant evoked brain stem responses after removal of the intralabyrinthine portion of a vestibular schwannoma in a patient with NF2. *Otology & Neurotology*, 40:e20–e24.
- 2018 **Fröhlich, L.**, Plontke, S.K., Rahne, T. Influence of transducer types on bone conduction hearing thresholds. *PloS one*, 13:e0195233.
- 2017 Fredén Jansson, K.J., Håkansson, B., Reinfeldt, S., **Fröhlich, L.**, Rahne, T. Vibrotactile Thresholds on the Mastoid and Forehead Position of Deaf Patients Using Radioear B71 and B81. *Ear and Hearing*, 38:714–723.